LOW FREQUENCY INTERMOLECULAR AND INTERIONIC VIBRATIONS

By MICHAEL JOHN FRENCH.

A thesis submitted for the

DEGREE OF DOCTOR OF PHILOSOPHY

in the University of London

Department of Chemistry,

Imperial College of Science and Technology,

London, S. W. 7.

August, 1967.

ABSTRACT

The factors affecting the optical design of far infra-red spectrometers for use in the 10 to 400 cm^{-1} region of the spectrum are discussed with particular reference to the problems associated with the observation of broad, weak absorption bands, such as those expected from the interionic interaction of ions in solution

The far infra-red double beam spectrometer, the design and construction of which is described, is the first far infra-red double beam instrument to employ large area gratings and an Ebert-Fastie monochromator and as such should show about a five-fold increase in signal to noise ratio, at a given slit width, compared to that achieved with previous double beam spectrometers operating in this region of the spectrum. The design and problems associated with the electronics, filtering and calibration of the instrument are also described.

The low frequency interionic vibrations of a series of tetraphenylboron salts were investigated in a range of polar solvents. The absorption frequency was not sensitive to the nature of the solvent and this is adduced as evidence of the absence of strong ion-solvent interaction. The observed vibration frequencies indicate almost identical force constants for the interionic vibration of the potassium, sodium, ammonium and ammonium D_4 salts and a slightly higher value for the lithium salts. This suggests that there is little change in the interionic potential between the five salts and this observation may be rationalised on the basis of a Morse type potential function.

The observed variations of molar extinction coefficient with solvent, total ion concentration and cationic radius are shown to be consistent with a variation in the proportion of ions that are actually present as ion pairs as measured by thermodynamic and conductiometric methods.

ACKNOWLEDGEMENTS

The author wishes to express his sincere thanks to his supervisor, Dr. J. L. Wood, for his constant encouragement and advice throughout the course of this work.

The author would also like to thank those who have advised on the design and construction of the spectrometer, especially Dr. D. E. H. Jones in the electronic field and Mr. H. G. Cobley on the mechanical side. Thanks are also due to his colleagues in the laboratory for many stimulating and helpful discussions.

Financial assistance from the Science Research Council, both by means of a grant for the construction of the spectrometer and the award of a Research Studentship, is gratefully acknowledged.

CONTENTS

INTRODUCTION

Over the last decade interest in far infra-red spectroscopy in general, and interest in chemical far infra-red spectroscopy in particular, has expanded dramatically. This is reflected not only in the large increase in the number of papers on this topic appearing in the literature - from around 20 per annum in the mid fifties to 35 per annum in the early sixties to nearly 100 each year at present - but also in their increasing attention to the elucidation of chemical problems rather than concentration on the physical problems of instrumentation and technique.

A bibliography of all published material relating to far infra-red spectroscopy was compiled in 1962 by Palik (1). In the same year a review article by Wilkinson et al (2) appeared and in the following year one by Wood (3). Recently an excellent review on chemical far infra-red spectroscopy has been published by Jakobsen et al (4).

This increasing application of the technique to chemical problems must be due, in part, to the appearance of three commercial double beam far infra-red spectrometers: the Perkin Elmer 301 (5) which operates from 666 to 33 cm^{-1}; the Beckmann IR 11 (6) which operates from 800 to 33 cm^{-1} and a Japanese instrument described by Yoshinaga (7) which covers the range 500 to 60 cm^{-1}. These instruments have relatively small gratings, area 41 cm^{2}, and consequently lower energy throughput and resolution than has been achieved with single beam instruments, for example that of Kneubuhl (8). Nevertheless, these commercial double beam spectrometers and prototype single beam instruments are adequate for the elucidation of problems associated not noly with low frequency vibration fundamentals, particularly torsional oscillations, but also with hydrogen bonding, charge transfer and crystal spectra. The absorption bands associated with these phenomena are characterised by a relatively narrow bandwidth; typically less than 15 wavenumbers.

Far less progress has been made in the study of weak low frequency absorptions arising between poorly quantised energy levels where the bandwidths encountered are frequently in the region of 100 wavenumbers. Typical of this type of absorption is the polar interaction arising between the molecules of a highly polar liquid first reported by Jakobsen and Brasch (9) and the interionic interaction between the dissolved ions in a polar liquid first reported by Evans and Lo (10). The observation of weak, broad bands is particularly difficult in the far infra-red with a grating spectrometer since the mode of filtering employed (Section 1:5:5) results in an undulatory change in energy throughput with frequency. The ability to detect broad, weak absorptions is dependent on the linearity of the 100% transmission line (i.e. the ratio plot with no sample in either beam). Although this would appear to be an important factor in the performance it is not explicitly stated by any author in his discussion on the three double beam far infra-red instruments mentioned above. From the spectra presented and from the subsequent experience on the present instrument (Section 3:5) a linearity greater than 5% over the range 60 to 200 cm^{-1} cannot be expected. This effectively makes the positive observation of absorption bands having bandwidths greater than 100 cm^{-1} and whose peak absorption is less than 10% extremely difficult.

The most straight-forward method, therefore, of observing broad, weak absorptions would appear to be to increase the pathlength or concentration of the absorbing medium until the absorption rises above 10%. Even in the case of pure liquids this approach is defeated to a certain extent by the increasing overall attenuation of the liquid and in the case of solute absorptions other factors present difficulties:

1) The solubility of the solute in the solvent is frequently reached and no further increase in concentration is possible.
2) If the path length of the saturated solution is increased, then

attenuation of the radiation by the solvent is also increased. It will be seen later (Section 4:3:1) that in the case of absorption by interionic species in solution the main factor rendering the observation of the interionic stretching vibration so difficult is the absorption caused by the solvent. These problems may be most readily overcome by a double beam spectrometer in which solvent absorption may be compensated for in each beam and by a spectrometer with the highest possible energy throughput. This not only maximises the signal to noise ratio at a given slit width but also enables strongly absorbing samples to be investigated at viable slit widths of the order of 8 to 10 wavenumbers. It was therefore decided to construct a double beam vacuum grating spectrometer with a large energy throughput for the study of broad, weak absorptions in the far infra-red.

It might be asked, in view of the increasing interest in interferometric methods in this region of the spectrum (11), why a grating spectrometer rather than an interferometer was chosen?
In a two beam interferometer the interference pattern, or interferogram, $I(\Delta)$, for monochromatic energy of frequency, ν, and path differnce, Δ, is (12)

$$I(\Delta) = S(0) \left| \frac{1}{2} + \cos 2\pi\nu\Delta \right|$$

For an arbitrary spectral input, $S(\nu)$,

$$I(\Delta) = \int_0^\infty S(\nu) \left| \frac{1}{2} + \cos 2\pi\nu\Delta \right| d\nu$$

Application of the Fourier-integral theorem for the even function $I(\Delta)$ gives the desired spectrum in terms of the measured parameters $I(\Delta)$ and $I(0)$

$$S(\nu) = 4\int_0^\infty \left| I(\Delta) - \tfrac{1}{2} I(0) \right| \cos 2\pi\nu\Delta \, d\nu \qquad \text{Equation 1}$$

In general the interferogram is measured as a function of the path difference and the spectrum computed from equation 1 by analog or digital means. Superficially the interferometer would appear to have a number of advantages.
1) With an interferometer the whole spectral range of interest is incident on the detector at one time rather than the single resolution width as is the case with a grating spectrometer. Since spectroscopy is detector noise limited in the far infra-red due to low source energies, the signal to noise ratio is much greater with an interferometer than with a

grating spectrometer: this is the Fellget advantage(12).

2) The smallest spectral interval that can be resolved by an interferometer is $1/d_{max}$, where d_{max} is the maximum path difference to which the interferogram is measured. Therefore, to double the resolution the interferogram must be taken to twice the path difference, which thus doubles the measuring time. To double the resolution of a grating spectrometer it is necessary to halve the slit width which reduces the energy throughput to one quarter. If detector noise predominates it takes 16 times as long to obtain a spectrum with the same signal to noise ratio as before.

3) Since a single beam splitter may be used in an interferometer to cover the range 40 to 200 cm^{-1} the energy throughput has a less undulatory nature than with a grating spectrometer.

Despite these apparent advantages of an interferometer, a spectrometer was preferred for the following reasons:

In the description of the spectrometer that follows it will be frequently observed that a basic principle of the design was to ensure that it was capable of producing accurate and reliable results when operated in a routine manner by chemists whose main interest lies in the spectra produced rather than the instrument producing them. In several respects an interferometer is inferior to a grating spectrometer for this type of work.

1) Most chemists are familiar with the use of a grating spectrometer whereas the operation of an interferometer, which appears to require some finesse to avoid the observation of spurious bands, would be a novel technique.

2) For speculative, non routine work the various sample parameters such as thickness, concentration, etc. must be optimised empirically. This is straight-forward in a spectrometer where the sample may be inserted in the beam and the percentage absorption at that frequency observed: if this does not provide sufficient information a fast scan across the region of interest is always possible. With an interferometer, however,

no information on the absorption can be obtained until the interferogram has been produced, which may take from 10 to 600 minutes, and very little information can be obtained until the Fourier Transform of the interferogram has been computed, which may take from 5 to 3,000 minutes depending on the computing facilities available in the particular laboratory.

Apart from these essentially practical difficulties, the double beam grating spectrometer has the absolute advantage of being able to measure directly the ratio of the absorption in two different samples, thus permitting the absolute calculation of extinction coefficients, etc. The interferometer as at present developed, on the other hand, can only operate in an analagous manner to a single beam spectrometer, deriving percentage absorptions from the ratio of two successive Fourier transformed interferograms, the accuracy of this procedure being limited by the stability of the instrument parameters, such as source energy, detector sensitivity, etc.

The published comparisons of interferometers and grating spectometers have concentrated on the question of the ultimate resolution available rather than the possibility of observing broad, weak absorption bands. On the question of resolution, however, there appears to be a very slight superiority claimed for the interferometer, 0.05 cm^{-1} at 40 cm^{-1} (14) as against 0.1 cm^{-1} at 40 cm^{-1} for the best grating instruments (15).

Although a number of reviews of far infra-red spectroscopy and descriptions of far infra-red spectrometers have been published, none of these discuss in detail the factors affecting the design of a far infra-red spectrometer. The first chapter of this thesis will, therefore, be a comprehensive survey of the present state of development of far infra-red spectroscopic techniques and the factors affecting the design of the spectrometer whose construction is discussed in the

succeeding chapter. After a brief review of the operation and performance of this instrument the remaining chapters will be devoted to a discussion of the low frequency interionic vibrations observed in tetraphenylboron salts.

1) FACTORS AFFECTING THE OPTICAL DESIGN OF A FAR INFRA-RED SPECTROMETER

1:1) SOURCE

The practice of far infra-red spectroscopy would be revolutionised by the discovery of a coherent tunable source. Laser technology has advanced in the last two to three years to such an extent that it is now possible to produce a coherent output at almost any far infra-red frequency either directly (16) or by a combination of the stimulated Raman and non-linear optical effects (17). Little progress has been made, however, on the problem of tuning the laser output: the most successful method so far has been the utilisation of the Zeeman effect to separate the energy levels from which the stimulated emission is occurring. By applying an axial magnetic field of 1,800 Gauss to a neon laser Brunet (18) was able to shift the 1298 cm^{-1} emission by $\pm$ 1 cm^{-1}. He used a continuous variation of the magnetic field to make a high resolution study of the ν_4 absorption of methane with a resolution of 0.001 cm^{-1} in this two wavenumber region.

Lasers are, however, of little practical use in the design of far infra-red spectrometers at present and recourse to thermal sources is inevitable. Although some early workers used a Globar because of its high emission above 200 cm^{-1}, the high pressure mercury arc is now almost universally used due to its superior performance below 50 cm^{-1} (19). At high frequencies, above 100 cm^{-1}, the radiation is almost entirely from the heated envelope acting as a grey body, whereas below 50 cm^{-1} bremstrahlung radiation from the arc predominates (20). Papoular (21) has measured the effective temperature of a high pressure mercury arc on a Boltzmann interferometer calibrated with an 800°C black body furnace and found that above 40 cm^{-1} the apparent temperature was constant at about 1500°K whereas below 40 cm^{-1} it rose steadily to reach 3000°K at 10 cm^{-1}. Cano and Mattioli (22) in a similar experiment showed that below 25 cm^{-1} the lamp emission is actually independent of frequency as would be expected for the emission from an optically thin plasma. Since in the

Rayleigh-Jeans approximation the energy of a black body is proportional to ν^2 this low frequency plasma emission accounts for the rise in the effective temperature of the mercury arc below 50 cm^{-1} and for its consequent superiority to the Globar. The present spectrometer, therefore, utilises a Phillips MBL/U 125 watt high pressure mercury arc.

1:2) MONOCHROMATOR

Strong (23) has calculated the energy throughput, E, of a spectrometer whose resolving power is limited, not by diffraction blurring of the spectrum, but either by the available source energy or by the inadequacy of the detector sensitivity. To simplify the calculation it was assumed that the source emitted according to the Rayleigh-Jeans approximation, i.e.

$B_\lambda = B_o\Theta/\lambda^4$ watts. cm^{-2}. steradians-cm^{-1}.

Where Θ = effective temperature of the source

B_o = emissivity of constant of source

If the dispersive element has a cross sectional area,A, and a dispersion, $d\theta/d\lambda$, then the energy reaching the detector is given by:

$E = B_o T\Theta (s A/F) d\theta/d\lambda \Delta\nu^2$ EQUATION 1:1

Where s = length of the slit

F = focal length of the collimated beam

$\Delta\nu$ = wavenumber band passed by the exit slit

T = total transmission efficiency of instrument

B_o and Θ are dependent on the properties of the source: the design of the monochromator must, therefore, concentrate on maximising the remaining variables in order to maximise the energy throughput at a given spectral resolution.

In a grating instrument the cross-sectional area of the grating,A, can only be increased within the limits imposed by availability and expense. In the present instrument six inch square gratings were chosen, being

the largest of the required line spacing that were readily available in the United Kingdom. Even these led to a sizeable instrument requiring fifty square feet of floor space and a sixteen cubic foot evacuable chamber. Even if larger gratings had been available the greatly increased cost of the instrument might have prevented their use.

The transmission efficiency of the surface aluminised mirrors normally used is already very high in the far infra-red and any effort put into increasing the transmission efficiency, T, will have only a marginal effect in increasing the energy throughput.

The ratio s/F is, however, largely at the discretion of the designer and one possibility is to build a monochromator with a very short focal length. McCubbin and Sinton (24) adopted this approach with an f/1 monochromator which achieved a resolution of one wavenumber in the 100 to 14 cm^{-1} region. This approach has several disadvantages, however, in that it requires severly curved mirrors, it requires critical positioning of the optical components and the very fast beam creates serious difficulties in the introduction of samples.

An alternative approach to maximising the s/F ratio is to increase s by using very long slits but this normally introduces severe problems of abberation and vignetting. These may be overcome by the use of the Ebert-Fastie monochromator (25). The basic optical design is shown in Figure 1:1.

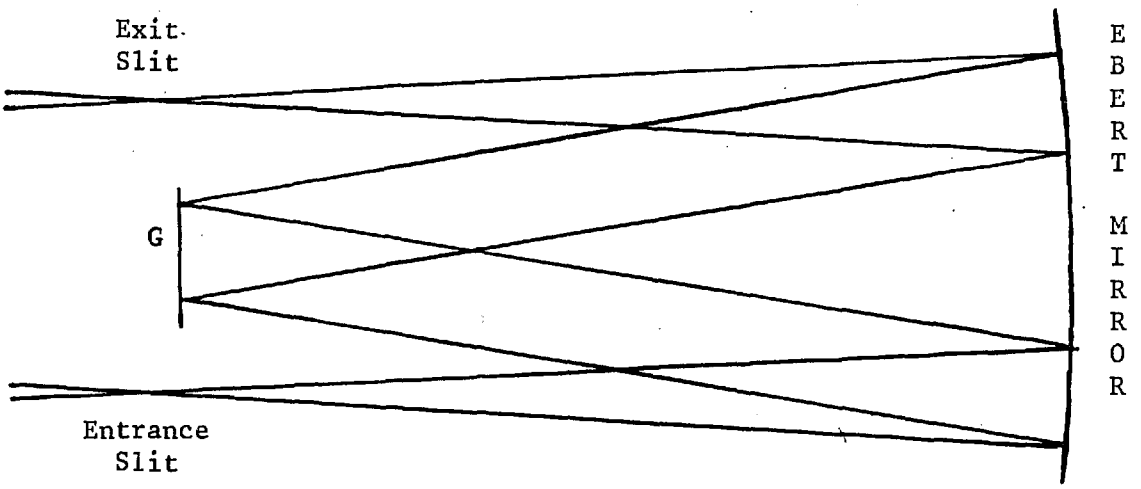

Figure 1:1 The Ebert - Fastie Monochromator

Light from the entrance slit, S_1, which is in the focal plane of the spherical mirror, M, strikes the mirror and is reflected onto the grating, G, as a parallel beam. Light is diffracted back onto the other half of the spherical mirror and is focussed onto the exit slit, S_2, which is also in the focal plane of the mirror. The slits are equidistant from the mirror axis which is also the centre point of the grating. It will be observed that the Ebert-Fastie system is only a special case of the Czerny-Turner system (26) in which two reflecting areas have co-incident centres of curvature. The symmetrical arrangement of the slits with respect to the grating eliminates for any slit length all aberrations except astigmatism and this may also be reduced to negligible proportions if the slits, instead of being straight, are curved about the axis of the spherical mirror. Curved slits also remove a third factor normally limiting resolution when long straight slits are used, that of wavelength error due to the spread of frequencies along the length of the slits.

This possibility, of using long curved slits to increase the energy throughput at a given slit width without a concomitant reduction in the resolution due to aberration or wavelength error, has resulted in a preference for the Ebert-Fastie and Czerny-Turner monochromators in high resolution single beam instruments. Examples are the spectrometers of Kneubuhl, Moser and Steffen (8); Bell and Barnes (27); Moller et al. (28); Rusell and Strauss (29) and Hunt et al. (30).

The Littrow mount, Figure 1:2, has also been used in high resolution single beam far infra-red spectrometers (31). This suffers from the disadvantage that the slit height is limited to about one centimetre by aberration effects.

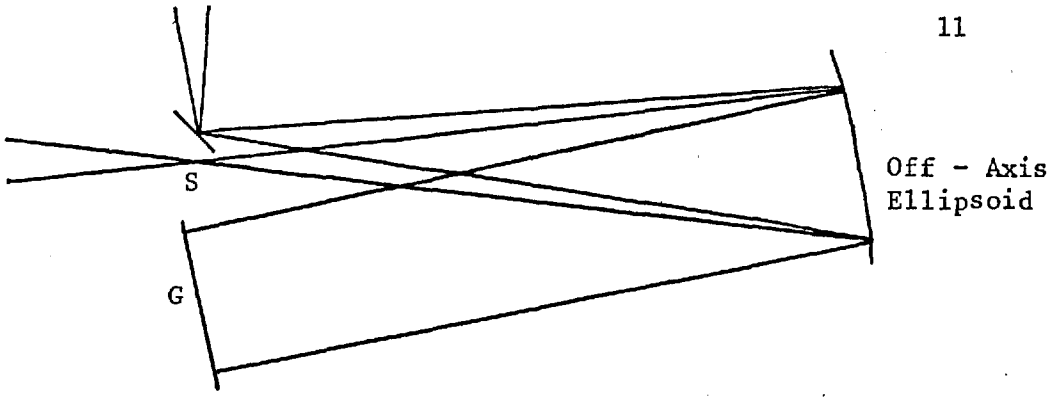

Figure 1:2 The Littrow Monochromator

A third type of monochromator that has also been used in the far infra-red is the Pfund monochromator shown in Figure 1:3

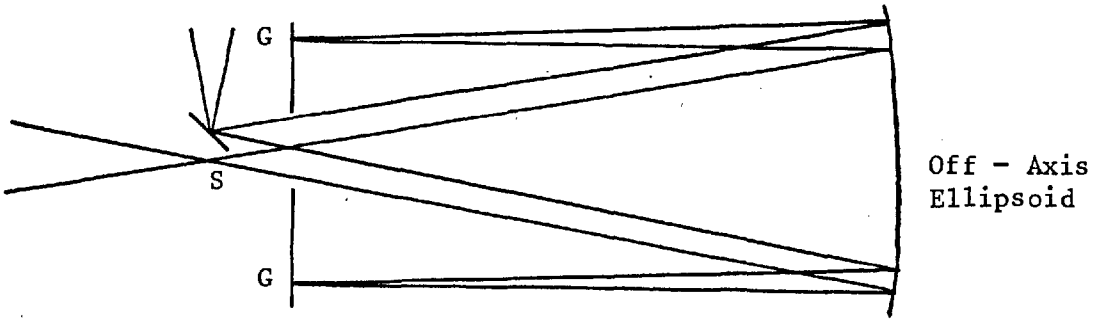

Figure 1:3 The Pfund Monochromator

A very high performance spectrometer using a double pass Pfund monochromator has been build by Yarslavsky et al. (32) which achieved a resolution of 0.3 to 0.5 cm^{-1} in the 500 to 20 cm^{-1} region. Recently the Pfund system was adopted by Richards (33) due to the ease with which a dispersion grating spectrometer of this type may be converted to a Lamellar Grating interferometer for comparative tests. As with the Littrow system, the Pfund monochromator is limited to slit heights of about one centimetre.

In addition to the high energy throughput at a given spectral resolution achievable with an Ebert-Fastie monochromator by the use of long, curved slits it also has several practical advantages. The use of large gratings necessitates the use of large monochromator mirrors and whereas the Pfund and Littrow systems require off axis parabaloids, the Ebert-Fastie system uses only the cheaper and more readily available spherical mirrors. The symmetrical arrangement of the Ebert-Fastie monochromator also makes it

very easy to enclose in a cylindrical tank for evacuation to remove water vapour absorption.

Although the optical and practical advantages of the Ebert-Fastie monochromator have generally been recognised in the design of high resolution single beam spectrometers it is interesting to note that the three double beam instruments reported in the literature (5,6,7) have all been designed about a Littrow monochromator. This is almost certainly due to the fact that these spectrometers were designed for commerical manufacture where an important factor influencing the design is the cost of the gratings, since four to six are required to cover the entire infra-red region. Large gratings, i.e. greater than 50 cm^2 would be prohibitively expensive and all, in fact, use 41 cm^2 Bausch and Laumb Replica gratings. These gratings may be completely illuminated by a monochromator having, for example, an f/4 aperture and a 25 cm focal length; for a 1 cm slit the s/F ratio is then 1/25.

The present instrument, however, utilises 225 cm^2 gratings and an f/4 monochromator therefore requires a 60 cm focal length mirror to fully illuminate the grating. With a Pfund or Littrow monochromator where the slit height is limited to 1 cm, this effectively limits the s/F ratio that can be obtained to 1/60: with an Ebert system where 10 cm slits are quite feasible the s/F ratio can be raised to 1/6. The use of large area gratings, therefore, necessarily implies the use of the Ebert-Fastie monochromator if full advantage is to be taken of the extra energy diffracted from the grating.

1:3 IMAGE TRANSFORMER

We have seen in the previous section that the highest energy throughput at a given spectral resolution is obtained by maximising the ratio of slit height to the focal length of the monochromator. This may be achieved by the use of the Ebert-Fastie system in which aberration in the monochromator optics places no limit on the length of the slit which may be

used. A practical difficulty occurs, however, in that, if full use is to be made of the grating area, all radiation emitted from the exit slit of the monochromator must be condensed onto the detector window. It will be shown below that far infra-red detectors normally have areas of a few square millimetres in order to reduce their intrinsic noise levels. An important factor in the choice of the Golay detector for use in this instrument was its relatively large window area, about 20 mm^2, and its large acceptance angle, aperture ratio f/1. Nevertheless, the condensation of the elongated slit image of the Ebert monochromator onto the circular window of the Golay detector presents severe problems. This may be eased by employing an image transformer (34) to reform the elongated slit image into a more nearly circular shape. This not only assists in condensing the image onto the detector but, as will be shown below, results in an increase in the signal to noise ratio of the instrument at a given spectral resolution.

If the exit slit image of height S is directly condensed onto a detector window of height, h, then h and S are related by

$S = h\, f_m / f_d$

Where f_m = aperture of monochromator

f_d = aperture of detector

In the Ebert-Fastie monochromator the aperture of the monochromator, f_m, is related to the focal length of the Ebert mirror, F, and the width of the grating, $A^{\frac{1}{2}}$, see Figure 2:6, by

$f_m = F/A^{\frac{1}{2}}$ and therefore,

$S = hF/f_d\, A^{\frac{1}{2}}$.

Consequently Equation 1:1 for the energy throughput of the spectrometer may be expressed in the form

$$E = k\, h\, A^{\frac{1}{2}} \Delta\nu^2 / f_d \qquad \text{EQUATION 1:3}$$

where k is a constant dependent on the properties of the source and grating.

Hence for a given resolution the energy throughput is limited by the

linear dimensions of the detector window, h. Since the window is normally circular, whereas the slit image width is about one tenth of its height the effective linear dimension of the window may be increased by slicing the exit slit image to form a series of n parallel images as in Figure 1:4

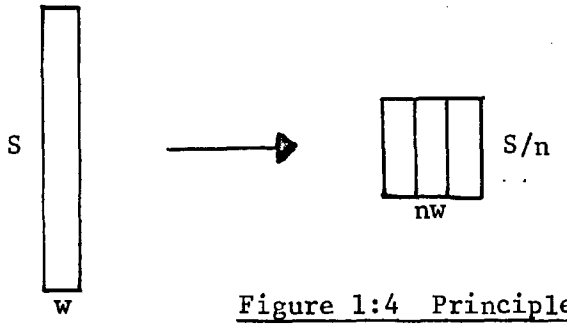

Figure 1:4 Principle of the Image Transformer

The relationship between the detector window height and the slit height is now

$$S = h\,Fn / f_d\,A^{\frac{1}{2}} \qquad \text{EQUATION 1:4}$$

$$\text{and } E = kh\,A^{\frac{1}{2}}\,n\Delta\nu^2 / f_d \qquad \text{EQUATION 1:5}$$

Since the noise level in the Golay detector is effectively dependent only on the dimensions of the window, the effect of cutting the beam into n slices is to increase both the signal and the signal to noise ratio, n fold at constant spectral resolution. In practical terms, it is possible to condense an n fold faster beam onto a given detector, thus increasing the energy throughput as given by Equation 1:1 by a factor of n through reducing the focal length of the monochromator to 1/n th of its previous value.

The limitation to this approach is that the maximum slit width usable is governed, as can be seen from Figure 1:4, by the necessity of producing a square image, i.e.

$$n\,w \not> S / n$$

$$\text{i.e. } w_{max} = S / n^2 \qquad \text{EQUATION 1:6}$$

The relationship between the slit width in wavenumbers, $\Delta\nu$, and the slit width in centimetres, w, is given by Strong (23)

$$\Delta\nu = w \,/\, F\,\lambda^2 d\theta/d\lambda \qquad \text{EQUATION 1:7}$$

and the focal length of the monochromator is given by Equation 1:2

$$F = S\, f_d\, A^{\frac{1}{2}}/h\, n \qquad \text{EQUATION 1:8}$$

Inserting the values of equations 1:6, 7 and 8 into Equation 1:1 the energy throughput at the maximum usable slit is then given by Equation 1 as

$$E_{max} = (B_o\, T\, \Theta\, h^3 / d\theta/d\lambda\lambda^4\, f_d^3\, A^{\frac{1}{2}}\ )\ (1/n) \qquad \text{EQUATION 1:9}$$

That is, for a given source - detector - grating system, the energy throughput at maximum slit is inversely proportional to the number of slices taken. The practical results of these equations for a typical system are collected in Table 1:1.

The choice of the number of slices to take is therefore a compromise between the increase in the signal to noise ratio to be obtained at constant spectral resolution from taking a large number of slices, Equation 1:5, and the decrease in the maximum energy available that this causes, Equation 1:9. This loss of energy throughput is critical in the far infra-red and it was decided to take only three slices as this appeared to offer the best compromise. Practically this gives a convenient length of about 70 cm. for the focal length of the monochromator and a convenient aperture of about f/4 for the main optics of the instrument. This may be easily condensed onto the Golay window by a single optical element such as an off-axis ellipsoid or a Greenler image reducer.

The actual physical slicing of the beam was performed by a slicer of the type described by Benesch and Strong (34). In a previous single beam instrument built in this laboratory (35) an exceedingly complex beam slicer, based on that used in the Cary Raman Spectrometer (36), was employed due to a lack of space and to the lower number of optical

TABLE 1:1

FACTORS AFFECTING THE OPTIMUM TRANSFORMATION OF THE EXIT SLIT IMAGE

Number of Slices		1	3	5
Signal to noise ratio at constant resolution	Eqn. 1:5	7.5k	22.5k	37.5k
Maximum slit width	Eqn. 1:6	7.00cm	0.78cm	0.28cm
Focal length of monochromator	Eqn. 1:8	210 cm	70 cm	42 cm
Resolution at maximum slit width	Eqn. 1:7	$5.8cm^{-1}$	$1.92cm^{-1}$	$1.16cm^{-1}$
Energy at maximum slit width	Eqn. 1:5	254k	85k	51k
Aperture of monochromator	Eqn. 1:4	14	4.6	2.8

Detector window height $h = 0.5cm$

Grating side $A^{\frac{1}{2}} = 15cm$

Aperture of detector $f_d = 1$

Slit height $S = 7cm$

For $\theta = 30^{\circ}$ and $d = 1/100$ $\lambda^2 d\theta/d\lambda = \frac{1}{\sqrt{3}\ 100}$

elements required. Where space permits the physically simpler Benesch and Strong type is to be preferred, the additional number of optical elements required, two in the case of a beam slicer taking three slices having little effect on the transmission efficiency of the instrument. This type has the advantage over a third possible form of beam slicer, a multiple light pipe of preserving the reformed exit slit image in a single focal plane.

1:4) DOUBLE BEAM OPTICS

Three systems have been used in the past to provide the two beams of radiation required in a double beam spectrometer : these are the twin beam, double beam and split aperture systems.

1:4:1) Twin Beam System In this system two entirely separate beams are provided from the source to some point past the sample - reference space where they are alternatively passed through the entrance slit of the monochromator. This is the most common system in the infra-red, although it may be criticised on the grounds that the two beams are receiving radiation from slightly different areas of the source. This method is only applicable where the sample - reference area immediately follows the source since division of the beams can only occur at the source.

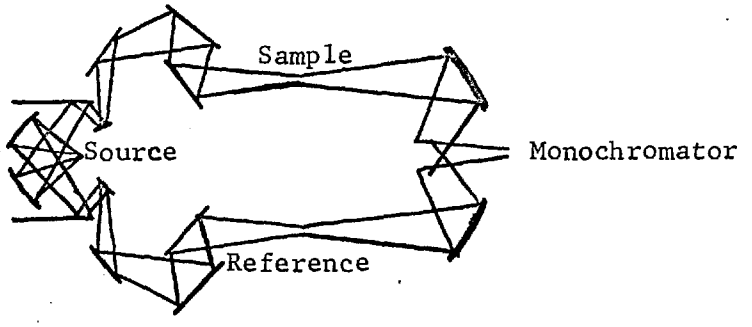

Figure 1:5 The Twin Beam Optics of the Perkin - Elmer 301

In the present instrument the pratical advantages of illuminating the entrance slit of the Ebert monochromator directly by a twofold magnification of the source and reformation of the image into a more nearly circular shape before the sample - reference space were felt sufficient to eliminate this system. The twin beam system was used by Helms (5) in the Perkin Elmer

301 Far Infra-red Spectrometer where the choice of a Littrow monochromator removed one of the serious disadvantages of its use.

1:4:2 Double Beam System In this system the single beam from the source is alternatively directed through the sample and reference areas by means of a pair of reciprocatory mirrors or by a rotating mirror sector. After passage through the sample-reference area the two beams are recombined into a single beam by a second mirror driven in synchronisation with the first.

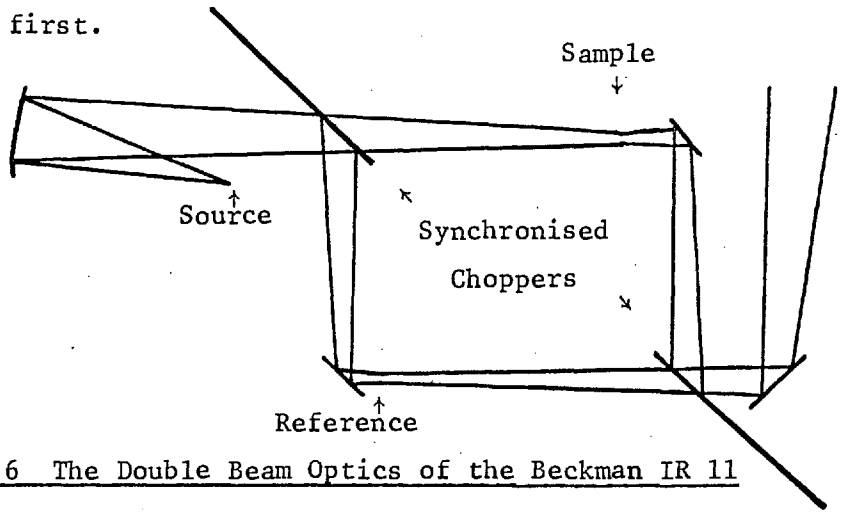

Figure 1:6 The Double Beam Optics of the Beckman IR 11

This is a very flexible system and was used by Beckmann (6) and Yoshinaga (7) in their far infra-red spectrometers and is ideally suited to the present instrument.

1:4:3 Split aperture system This was first suggested by Savitzky and Halford (37). In this system the two beams are formed from the upper and lower halves of the slit image respectively and after passage through the sample-reference space may be recombined to give the original image. In order to extract the ratio of the beam intensities it is necessary to modulate the two beams, while separate, so that one beam has a phase lag, usually 90^{o}, with respect to the other. It is desirable in the far infra-red to modulate the radiation with a crystal chopper to aid the filtering and a split aperture system therefore requires the construction of two crystal choppers to run 90^{o} out of phase with one another. This appeared

to be an unnecessary complication without any certain advantage and so was rejected for this instrument. It might be possible to design a split aperture system in conjunction with an Ebert monochromator, but without an image transformer, recombining the beams directly into a light cone in front of the detector where the slightly different trajectories of the two beams would not be important. This does not, however, appear to have ever been attempted.

1:5 FILTERING

1:5:1 Nature of the Problem The grating is not a complete monochromator by itself since when the angle of rotation of the grating is such that the diffracted image on the exit slit has a frequency of ν in the first order, then the second at 2ν, and generally the n^{th} order at $n\nu$, will also be falling on the exit slit. Thus to produce pure radiation at the first order frequency these higher orders must be eliminated by a filtering technique.

1:5:2 Magnitude of the Problem The magnitude of the problem may be illustrated by considering a black body source at $1300^{o}K$ radiating according to Planck's Law and being dispersed by an ideal echelette grating ruled with 71 lines to the centimetre and blazed at 21^{o}. When used at its blase angle the first order radiation will have a frequency of 100 cm^{-1}. Since the dispersion increases directly with the order number, the spectral interval passing through the exit slit is proportional to 1/n: the radiant power reaching the detector in each order will, therefore, be proportional to the ratio of the radiant power of the source at the order frequency to the order number. Arbitrarily setting the first order frequency to unity the relative intensities in the higher orders have been calculated by Oetjen et al. (38). The results of this calculation are shown in Table 1:2:1. By integration of a suitable function derived from Planck's Law, Oetjen estimated that the relative intensity of the first order to the higher order was $5x10^{-6}$.

Consequently if the spectral purity in the first order is to exceed 99% then the higher order radiation must be attenuated by a factor of about 10^7.

TABLE 1:2

RELATIVE INTENSITIES OF ENERGY IN THE VARIOUS ORDERS DIFFRACTED BY AN IDEAL ECHELETTE GRATING

Spectral Region	Order of Spectrum	Relative Intensity
100 cm^{-1}	1	1
200	2	8
300	3	24
400	4	54
500	5	99
600	6	161
700	7	241
800 - 1000	8 - 10	1371
1100 - 1400	11 - 14	3870
1500 - 2500	15 - 25	25100
2600 - 10,000	26 - 100	145000
100 - 10,000	1 - 100	175000

Above the seventh order the intensity is calculated by considering a spectral interval 3 microns wide about the diffraction frequency.

1:5:3 Use of the Grating as a Filter The calculation in Section 1:5:2 was of the radiation diffracted from a grating at its blaze angle. White (39) has shown that for a well machined echelette grating up to 98% of the radiation falling on the grating will be diffracted into the order which causes the diffracted angle to lie closest to the blaze angle. Since the angular width of the blaze radiation is inversely proportional to the order number, the higher order radiation will be preferentially concentrated in the blaze direction. (An example of this is shown in Figure 3:6:1) Consequently the elimination of higher orders becomes less acute as the grating is rotated away from its blaze position and the calculation in section 1:5:2 represents, therefore, the worst possible filtering conditions for the elimination of higher orders.

By considering the half width of the spectral distribution of intensity of the diffracted beam Murzin and Demshina (40) have given the usable range of a grating as

$$\tan\theta_1 = 0.694 \tan \theta_{b1}$$

$$\tan \theta_2 = 1.805 \tan \theta_{b1}$$

Where θ_1 = lower limit on the angle of rotation of the grating

θ_2 = upper limit on the angle of rotation of the grating

θ_{b1} = blaze angle

Therefore, a grating blazed at 30° may be used at angles of rotation between 22° and 46° and a grating blazed at 10° from 7.5° to 19°. It is imperative, therefore, with a grating blazed at 30°, if a large potentially useful of the grating is not to be wasted, to scan through the blaze. On the other hand, with a grating blazed at 10° the portion giving frequencies above the blaze frequency may be abandoned and the grating used solely below the blaze angle, thus avoiding the need for severe filtering as the grating passes through its blaze position. In

this instrument the majority of the gratings are blazed at 27° and are successfully used at angles of rotation between 15 ° and 40°. The two coarsest gratings, however, are blazed at 10° and due to the more difficult filtering conditions encountered at low frequencies are used only at angles of rotation greater than their blaze angles.

1:5:4 Optical Chopper To facilitate amplification and the elimination of zero drifting all detectors at present employed in the far infra-red are designed to respond only to a chopped A.C. signal. In single beam machines this necessitates the introduction of a chopper to modulate the light at a suitable frequency dependent on the type of detector in use, e.g. 10 cps for a Golay. (In a double beam machine, however, the modulation may be effected by the switching of the radiation between the sample and reference beams.) The necessity in single beam machines to insert a chopper has for a long time (41) been utilised as an additional means of filtering the radiation. If the chopper is composed of a material opaque only to far infra-red radiation but transparent to higher frequencies, the A.C. Signal received by the detector will be due only to the low frequency radiation to which the chopper is opaque. Suitable materials for the chopper are NaCl, which is opaque below 550 cm^{-1}; KBr opaque below 400 cm^{-1} and CsI opaque below 225 cm^{-1} (31).

The use of a crystal chopper is almost universal in single beam instruments and it was considered that this represented an important element in the filtering and, although double beam instruments have been built on the optical null principle which precludes the use of a crystal chopper (7), it was considered desirable to choose a double beam chopping system which permitted the use of a crystal chopper. A novel filter/chopper using wire mesh rather than crystals has been described by Bell and Drasky (42).

1:5:5 Reststrahlen filters Crystalline materials reflect efficiently only radiation which is close in frequency to their crystal lattice vibrations. This property may be used to isolate far infra-red

radiation of narrow bandwidth, about 30 cm^{-1}., with high spectral purity. Radiation close to the crystal lattice frequency, reststrahlen frequency, is reflected with a peak reflectivity of 0.9 to 0.95 whereas the majority of the remaining radiation is absorbed by the crystal and only a small proportion reflected. Further rejection of the unwanted radiation may be achieved by utilising the fact that if the angle of incidence is close to the Brewster angle, then the unwanted radiation after reflection will be strongly polarised perpendicular to the plane of incidence, whereas the reststrahlen reflected radiation will be unpolarised. Consequently very high discrimination against the unwanted radiation can be achieved, with only slight attenuation of the reststrahlen reflected radiation, by the insertion of a second crystal whose plane of incidence to the radiation is perpendicular with respect to the plane of incidence of the first crystal. The effect on all radiation apart from that close to the reststrahlen frequency of these two 'crossed' reststrahlen crystals will be similar to the effect of two 'crossed' Nicol prisms in the visible. Table 1:3 gives the reststrahlen frequencies of some selected crystals. (43,44).

TABLE 1:3 SOME SELECTED RESTSTRAHLEN MAXIMA

Crystal	Lif	$CaCO_3$	CaF_2	NaF	BaF_2	NaCl	KCl	KBr
Reststrahlen maximum	380	340	305	280	220	190	160	120

Crystal	KI	CsBr	CsI	TlCl	TlBr	TlI	KRS-5
Reststrahlen maximum	110	80	70	72	65	59	85 cm^{-1}

An interesting development of reststrahlen filters in the 300 to 500 cm^{-1} region, which may result in an improvement in far infra-red reststrahlen filters, is the coating of the filter surface with a thin interference film of a non-absorbing material. For example Turner et al. (45) found

that the magnesium oxide reststrahlen band centred on 450 cm^{-1} could be made appreciably more rectangular by coating the surface with a thin film of lead chloride.

1:5:6 Transmission filters 1) Crystal quartz: the opacity of crystal quartz in the 2000 to 250 cm^{-1} region has been known since 1897 (46). Consequently this has frequently been used to isolate radiation of frequency less than 250 cm^{-1}; 1 mm thickness being sufficient to ensure almost complete opacity between 5 and 40 microns. Berreman (47) has recently reported that the cut-on point for crystal quartz may be lowered to 180 cm^{-1} by deposition of a thin, 1.3 $mg.cm^{-2}$, layer of BaF_2, SrF_2 or CuF_2 on the surface of the quartz. Fused quartz has a distinctly lower cut-on at about 100 cm^{-1} and has been employed as a far infra-red filter.

2) Polythene embedded reststrahlen filters: these were first reported by Yoshinaga (48) and have attracted much interest subsequently as a convenient method of eliminating short wave radiation. It was observed that when powdered reststrahlen crystals were dispersed in polythene sheets at about 10% concentration complete absorption occurred at the reststrahlen frequency when the sheets were about 3 mm thick. Typical examples for LiF, NaCl and TlCl are shown in Figure 1:7

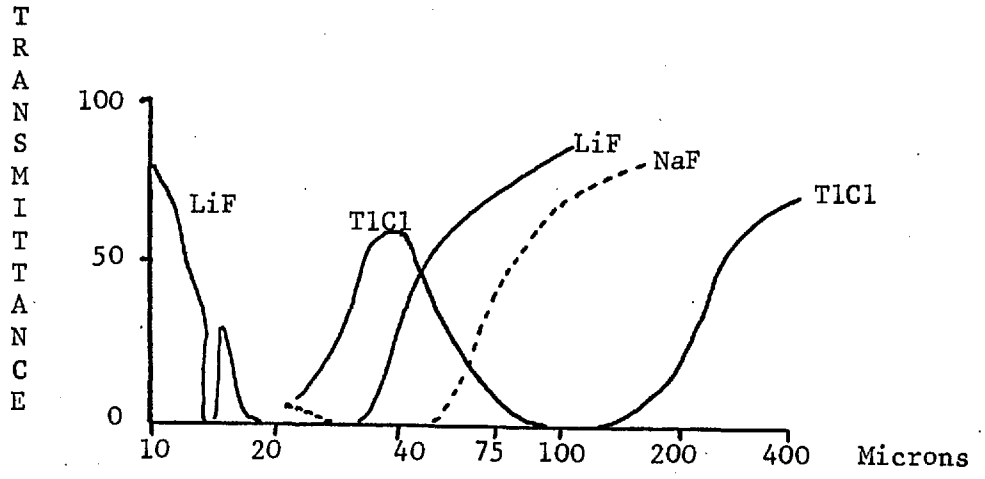

Figure 1:7 Transmittance of some reststrahlen crystals in polythene

The thallium chloride curve shows a second effect wheich becomes important at higher frequencies, namely light scattering by the powdered crystal. This is particularly pronounced in the case of thallium salts where the indices of refraction are high compared with that for polythene. Yoshinaga investigated the transmission of about 20 crystals embedded in polythene and by a suitable combination of crystals was able to produce a series of filters which were opaque from 800 cm^{-1} to their cut-on point which varied from 400 cm^{-1} for a BeO-ZnO combination to 50 cm^{-1} for a filter composed of TlCl, TlI and NaF. The high frequency radiation, greater than 800 cm^{-1} is attenuated by scattering within the filter and by the use of other forms of filter.

Manley and Williams (49) investigated the 50 cm^{-1} cut-on filter of Yoshinaga and found that the claim to complete opacity in the 100 cm^{-1} to 300 cm^{-1} region was not justified. In order to improve these filters they investigated various metal oxides and halides and on the basis of these measurements suggested a further set of 12 filters for the 500 to 66 cm^{-1} region.

The performance of these filters is affected by the concentration and by the particle size. In order to obtain the sharpest cut-on it is desirable to use the lowest concentration and the thinnest sample which will give complete opacity in the reststrahlen absorption region. About 35% crystal and 3mm thickness appears optimum. A scattering maximum occurs at a wavelength approximately half the particle diameter. It is clearly desirable that this absorption due to the physical scattering should reinforce the selective absorption of the crystals at their reststrahlen maximum. Thus the average size of the particles should be half the reststrahlen cut-off wavelength together with a few particles less than half this wavelength to scatter shortwave radiation.

1:5:7 Scatter Filters We have seen that very small particles embedded in polythene preferentially scatter short wave radiation. Their scattering is proportional to $d^3/_\lambda 4$, by Rayleigh's Law, and it is this scattering

from carbon particles which makes black polythene an effective high frequency filter. The scattering phenomenon may also be used as a high frequency reflection filter by using roughened aluminium plates in the place of plane mirrors. The degree of roughness required appears, in general, to be arrived at empirically but some indication may be obtained from the work of Bennett and Porteus (50), who showed that the specular reflectance of a rough surface, R_s, was related to the reflectance of a perfectly smooth surface, R_o, by

$$R_s = R_o \exp\ (- 4\pi\sigma/\lambda)^2$$

where σ = Root Mean Square surface roughness

λ = Wavelength

An indication of the σ values produced on a ground glass surface when they are abraded by emery powder of known particle size is given, from which approximate values for the reflectance of aluminium plates abraded with emery powder may be calculated.

1:5:8 Echelette Grating Filters White (39) first suggested the use of an echelette grating to eliminate unwanted high frequency radiation. For a grating, illuminated almost normally, the majority of the radiation goes into the order that causes the diffracted angle to lie closest to the blaze angle. The zero order spectrum is, therefore, specularly reflected whereas the higher orders, which are spread out over wide angular ranges, contain all the high frequency radiation. If the optical path is designed to accept only light that is specularly reflected from the grating and not diffracted light at the blaze angle the grating will act as a filtering element.

In the far-infra-red the echelette may be used either in reflection or in transmission. In reflection, the gratings are normally ruled on a metal base and, although they need not reach the perfection of the dis-

persing grating, a high quality is required and this has restricted their use. Despite this, Yoshinaga (51) ruled no less than twenty reflection filter gratings with spacings from 30 to 750 microns. When used in transmission a polythene replica from a hot former is adequate (52) and this results in a very cheap form of filter. Moller (28) has compared the efficiency of transmission and reflection filter gratings and found that four reflection gratings or two transmission gratings in series are sufficient to reduce the high frequency radiation at λ/d less than 0.2 to zero, while attenuating, by no more than 40%, the low frequency radiation at λ/d greater than 1.0. The cut-on frequency may, therefore, be selected at will by varying the grating spacing, d. The cut-ons of typical sets of echelette grating filters are shown in Figure 1:8

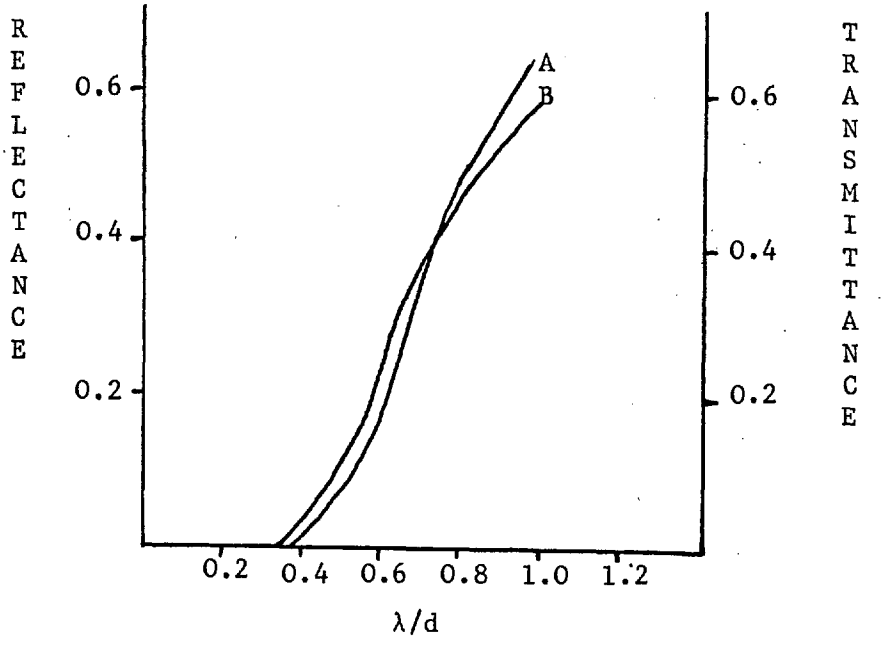

Figure 1:8 Cut - on Wavelengths of Some Typical Echelette Grating Filters

A. Two Transmission Filter Gratings

B. Four Reflection Filter Gratings

A secondary effect of the use of an echelette to eliminate the high frequency radiation may be to polarise the low frequency radiation. Hadni (53) has shown that only if the plane of incidence is perpendicular to the principal section of a reflection grating is polarization negligible: on the other hand, Moller (54) was unable to observe any appreciable polarization by a transmission grating irrespective of whether the grooves were orientated towards or away from the slit or parallel or vertical to the planes of incidence. Richards (33) has suggested cutting grooves orthogonally on both sides of the polythene to be certain of eliminating polarization effects. Transmission filter gratings are especially useful below 40 wavenumbers where no reststrahlen transmission filters have yet been produced.

1:5:9 Metal Mesh Filters 1) Reflection meshes: the use of metal meshes as reflection filters in the far infra-red was first recommended by Yoshinaga et al. (55) as a result of its use as a beam splitter in a Fabry-Perot Interferometer (56). The results presented showed a highly discriminatory filter: for five different meshes with inter-wire spacings, d, varying from between 95 and 384 microns, they found less than 5% reflection for λ/d less than 1.5 rising to over 95% reflection for λ/d greater than 2.1. See Figure 1:9

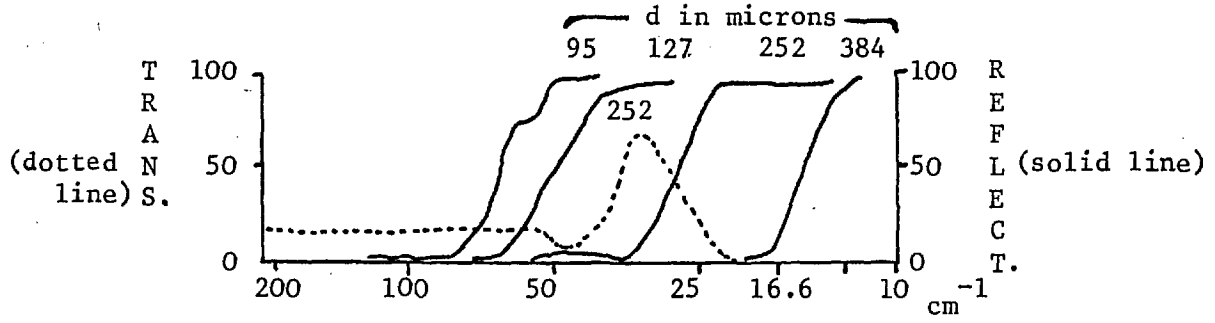

Figure 1:9 Reflection and Transmission Properties of some Wire Meshes

Several factors might be expected to affect the reflectivity of a wire mesh:

1) Form of grid. Two forms are readily available; firstly, woven wire meshes in which circular wires are woven into meshes and, secondly, electroformed meshes where the 'wires' are effectivly of rectangular cross-section. This will clearly influence the high frequency reflectivity of the mesh and, as expected, Vogel and Genzel (57) showed that the electroformed meshes had considerably greater reflectivity at high frequencies compared with woven wire meshes: typically 30% compared with 2%.

2) Angle of incidence. Yoshinaga (55) observed subsidiary maxima at $\lambda/d = 1$, and $\lambda/d = 1.8$ in the reflection curve when the angle of incidence was 52° but not when the angle of incidence was 15°. Vogel and Genzel have explained these on the basis of diffraction modes, these appear at:

$$\lambda = d\sin\alpha - \sin\beta_m / m$$

where α = angle of incidence

β = angle of diffraction

Diffraction is observed at grazing outgoing modes where $\beta_m = \pm \pi/2$. Hence, for an angle of incidence close to 0°, the first diffraction mode to appear approaching from long wavelengths will be at $\lambda/d = 1$: clearly this will not be observable in the reflection spectrum since the reflectance equals zero at this point.

For an angle of incidence of 45° the first diffraction mode to appear should be at $\lambda/d = 1.72$ for the vertical sublattice of the mesh. This agrees with the observations of Yoshinaga (55) and the more detailed study of Vogel and Genzel (57) using polarised radiation.

2) Transmission Meshes: since the sum of the reflection, transmission and diffraction losses of the mesh must be unity (neglecting the absorption and scattering losses which were shown by Renk and Genzel (56) to be less than 1%) the reflectance minimum at $\lambda/d = 1$ must be accompanied by a transmission maxima: this is shown in Figure 1:9) taken from the results of Yoshinaga (55).

This is particularly pronounced in the case of electroformed meshes and has been used as a far infra-red transmission filter by Moller (58), who mounted a reststrahlen transmission filter between two (d = 100 microns) electroformed meshes. This resulted in a bandpass filter having zero transmission at frequencies greater than 170 cm^{-1} or less than 50 cm^{-1} and 50% transmission at 110 cm^{-1}. This was used to observe spectra in the 140 to 70 cm^{-1} region using the second order of a grating blazed at 40 cm^{-1}.

3) Transmission reciprocal grid: In order to produce a combination filter having a bandpass at less than 100 cm^{-1}, Moller (58) investigated the properties of a reciprocal grid. This is a grid formed by evaporating aluminium onto a crystal quartz substrate using an electroformed metallic mesh as a mask. Moller's grid had d = 50 microns and showed about 5% transmission for λ/d less than 2 and increasing transmission at longer wavelengths., Two or three reciprocal grids in series is, therefore, the only way known at present to form an effective low frequency transmission filter. The relation of reciprocal grids to their complementary structure, the inductive grids or common meshes has been developed by Ulrich (59).

1:5:10 Other Filters 1) Transmission Filters: Alkali halides begin to transmit again below 60 cm^{-1}, for example 0.2 mm of KBr or NaCl has zero transmittance at 60 cm^{-1} but this has risen to 60% at 20 cm^{-1} (31) This effect was enhanced in the case of CsI by cooling to $4^{o}K$. At room temperatures 1 mm of CsI is completely opaque from 200 to 40 cm^{-1} but at $4^{o}K$ Hadni (60) found that the transmission cut-on very sharply from zero at 66 cm^{-1} to 100% at 40 cm^{-1}.

Slow cut-ons in the 100 to 50 cm^{-1} region are also shown by 2 mm samples of Irtrans 1 to 5 (61) and by 4.5 mm of monocrystalline silicon (62). 1 mm of magnesium oxide is completely opaque from 1000 to 110 cm^{-1} but the transmission rises to 50% at 40 cm^{-1} (19).

A low frequency transmission filter can be constructed by the application of frustrated total reflection. In the less dense medium of a totally reflecting boundary there exists an inhomogeneous plane wave: if a second dense medium is brought up to the boundary to a distance,d, the percentage of radiation entering the second medium and thus frustrating the total reflection will be proportional to the wavelength and the cut-on wavelength can be adjusted arbitrarily, by adjusting the distance apart,d, of the two denser media. The increase in transmittance is slow, i.e. from 1 to 60% in five octaves, but it might be useful as an efficient way to completely eliminate high frequency radiation (63).

1:6 DETECTORS

The mercury arc, though the best broad band far infra-red source available, provides very much less power in a given fractional bandwidth than do sources in other regions of the spectrum: detectors of the highest possible sensitivity are, therefore, required to obtain spectra of even moderate resolution. Of the many types experimented with in the past only the bolometer, semiconductor devices and the Golay pneumatic cell merit attention. A review of a selection of detectors falling within the first two categories has been made by Richards(64).

1:6:1 Bolometers

1) Superconducting bolometers: (65) This utilises the high temperature coefficient of resistance of a superconducting metal in the neighbourhood of its transition temperature. For example, Martin et al. (66) used an evaporated tin film a few square millimetres in area with a resistance of 50 ohms and (I/R) (dR/dT) of 10^2. deg^{-1} at 3.7°K. The bolometer area was $3mm^2$, and the overall response time 1.25 secs., the chopping frequency 10 cps and the Noise Equivalent Power for one cycle bandwidth (N.E.P.) was 1.2×10^{-12} watts. Hz^{-1}. Almost all the noise obtained with the superconducting bolometer had its origin in the

vacuum valve amplifier, as the first stage of amplification was by means of a transformer in the liquid helium bath, and the signal equivalent of the Johnson noise and temperature fluctuations of the bolometer were calculated to be two orders of magnitude less than the minimum detectable power.

2) Carbon Resistance Bolometers: As a result of the use of carbon resistors as thermometers at liquid helium temperatures Boyle and Rogers (67) developed a liquid helium cooled bolometer in which a thin, 0.25 mm, slice of a commercial carbon resistor served as the temperature sensitive element. The bolometer has a resistance of about 0.1 megohm and a temperature coefficient of resistance$(I/R)(dR/dT)$ of -2 at $2^{o}K$. The optimum time constant may be varied to suit the chopping frequency of the incident radiation by altering the specific heat and thermal conductance of the sample but a typical value is 10 msec. The N.E.P.is 1×10^{-11} watts.Hz^{-1} and in general carbon bolometers show current noise that is large compared with that from a good amplifier and thus are inferior to either superconducting or Germanium bolometers.

3) Germanium Bolometers: The first germanium bolometer was described by Low (68) and in a typical detector the sensitive area is a 4mm square of germanium about 0.25 mm thick. Due to the absence of current noise as encountered in the carbon bolometer, the inherent detector noise is divided almost equally between Johnson noise and phonon noise. The time constant may be varied from less than 10^{-5} secs. to several seconds but at a typical value of about 1 msec. the N.E.P. is 5×10^{-13} watts.Hz^{-1}. The action of the germanium bolometer is not well understood but appears to be due to the increased mobility of the electrons in the impurity conduction band (69). Thus it is necessary to add n or p type dopants to the germanium, as described in Section 1:6:2:1. Low (68) used gallium but greater temperature coefficients of resistance are obtainable with arsenic doping (70).

1:6:2 Semi-conductor Devices

1) Extrinsic semi-conductors: The low frequency threshold of intrinsic semi-conductors is determined by the energy gap between the valence and conduction bands. The relation between the energy gap,E, and the threshold frequency, , is

$$\nu = (E_{\text{in E.V.}} \times 10^{4}) / 1.23$$

Most elements and compounds investigated either have energy gaps greater than 0.2 E.V. corresponding to threshold frequencies of greater than 800 cm^{-1} or,alternatively, have negligibly small energy gaps. Since the impurity levels of a semi-conductor lie between the conduction and valence bands the energy required to form free charge carriers from the impurity levels is less than that required for intrinsic semi-conduction. The shallowest donor and acceptor levels in germanium are formed with antimony and boron. The free charge carrier together with the fixed core charge may be treated as a hydrogen atom embedded in the lattice and to a first approximation the ionization energy,e, and the Bohr radius,a, of the impurity centre are given by

$$e = 13.6(m^*/mk^2)\ \text{e.V} \qquad \text{EQUATION 1:10}$$

$$a = 5.29 \times 10^{-9}\ (m^*/m)k\ \text{cm.} \qquad \text{EQUATION 1:11}$$

where m^* = effective mass of electron

m = rest mass of electron

k = dielectric constant

When applied to germanium these give an ionization energy of 10^{-2} E.V. and a Bohr radius of 4.2×10^{-7}. This ionization energy corresponds to a photoconductive threshold frequency of 70 cm^{-1} and the Bohr radius to a maximum dopant concentration of about 10^{16} cm^{-3}. Higher dopant concentrations lead to a merging of the impurity levels with the conduction band and consequent metallic behaviour at low temperature as exemplified by the highly doped germanium bolometer. The ability of this detector

to respond to far infra-red radiation depends not on extrinsic photoconduction but on increased electron mobility. The germanium bolometer does not, therefore, show the low frequency threshold characteristic of extrinsic photoconductors.

A typical extrinsic semi-conductor far infra-red detector is the boron doped germanium detector of Shenker (71). This consists of a 2mm thick slice of germanium about 20 mm^2 in area with a boron dopant concentration of 10^{15} cm^{-3}. The response time is very fast, about 10 microseconds, and the N.E.P. is 5×10^{-12} watts.Hz^{-1}. The detector shows a low frequency threshold of about 70 cm^{-1} and the response is peaked at 100 cm^{-1}. Above this the response falls off, partly due to a decrease in the free carrier absorption but also as a result of the absorption of the crystal quartz window and the reduced efficiency of the light pipe conducting radiation to the detector.

2) Indium Anitmonide Photoconductive Detector: (73) The properties of this detector are sufficiently unique for it to merit separate consideration; the total behaviour of the InSb detector being the sum of several separate effects.

a) Extrinsic photoconduction: The effective mass of the electron in Indium Antimonide is about one-tenth its value in germanium. Application of Equations 1:10 and 1:11 to Indium Antimonide lead to an ionization energy of 10^{-3} E.V. and a threshold frequency of 10 cm^{-1}. The reduction in the effective mass reduces the Bohr radius to 5.7×10^{-6} indicating a maximum permissible dopant concentration of 10^{13} cm^{-3}. Unfortunately, the purest samples of Indium Antimonide obtainable have impurity concentrations greater than 10^{14} cm^{-3} and thus show only metallic properties at low temperatures.

b) Application of a small, 3-10KG magnetic field: When a sufficiently large magnetic field, greater than 3K Gauss, is applied to a semiconductor the conduction band will be split into a series of sub-bands or Landau levels. In the case of Indium Antimonide, even at dopant

concentrations of 5×10^{14} cm^{-3}, only the lowest Landau level is occupied and the metallic behaviour is destroyed, thus making extrinsic photoconduction possible.

c) Hot electron effects: It is well known that at low frequencies the free carriers in a semi-conductor absorb the radiation very efficiently but since the absorption involves only inter-band transitions this should not produce photoconductivity. When the temperature is sufficiently low, however, the absorbed radiation causes a change in the distribution of energy of the electrons in the band: this causes a change in mobility and a consequent change in conductivity. Since the absorption of radiation by the free carriers is optimal at low frequencies and falls of as ν^{-2} the Indium Antimonide detector is unique among photoconductive detectors in not showing a low frequency threshold.

Thus in a low field of 7 to 10 k Gauss the Indium Antimonide detector shows photoconductive behaviour due to both extrinsic semi-conductivity and to hot electron effects. There is no evidence for a low frequency threshold but the spectral response is peaked at 10 cm^{-1} and has fallen by an order of magnitude at 100 cm^{-1} owing to the decrease in free carrier absorption with frequency.

d) Operation in large, greater than 10 k Gauss, magnetic field: When magnetic fields of greater than 10 k Gauss are applied the low frequency extrinsic semiconductivity is reduced and is replaced by a narrow peak in the photoconductive response corresponding to the cyclotron resonance frequency ν_c. This frequency, due to the motion of the electrons in orbits perpendicular to the applied magnetic field, is given by

$$\nu_c = eB / 2\pi m^*$$

Where B = magnetic flux density.

Thus the cyclotron resonance frequency is dependent on the applied magnetic field, for example, it occurs at 110 cm^{-1} for an applied field of 14 k Gauss and at 390 cm^{-1} for a field of 76 k Gauss. Since the peak

has a band width of about 10% at $4^{o}K$ and 5% at $2^{o}K$ the Indium Antimonide detector used with a large magnetic field constitutes a narrow band tunable far infra-red detector.

1:6:3 The Golay Pneumatic Detector

The Golay detector (74,75) is a room temperature thermal detector and is consequently limited by the $300^{o}K$ radiation on the 9 mm^{2} window to the N.E.P. of 5×10^{-12} watts.Hz^{-1}, for a chopping frequency of 10Hz. The fact that the Golay cell has been refined to give an N.E.P. of 5×10^{-11} watts.Hz^{-1} is remarkable considering its basically simple concept.

The salient features of the Golay cell are shown in Figure 1:11 (76)

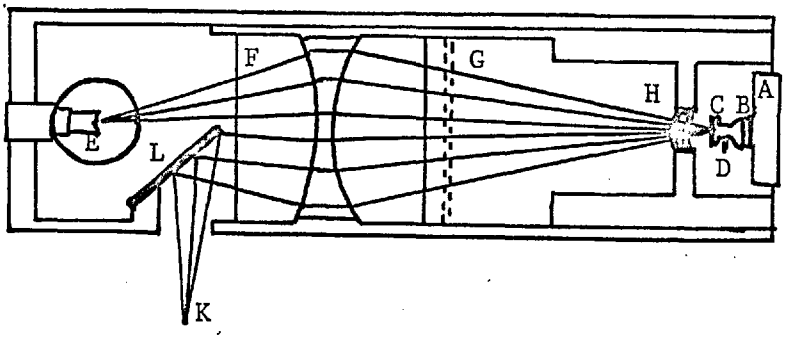

A. Detector window
B. Absorbing Membrane
C. Flexible Mirror
D. Bleed to the Ballast
E. Exciting Lamp
F. Condensing Lens
G. Line Grid
H. Meniscus Lens
K. Photocell
L. Plane Mirror

Figure 1.11 Schematic diagram of the Golay Cell

Radiation from the exciting lamp is allowed to pass through the line screen and is focussed on the flexible mirror: the light reflected from the mirror passes through the line screen on return and is focussed on

the photocell: the focussing is such that with the flexible mirror flat no light reaches the photocell, the clear portions of the line screen on the lamp side corresponding to opaque portions on the photocell side. Radiation entering the front window, which may be of diamond, crystal quartz or potassium bromide, is absorbed by the collodion-aluminium membrane at the front of the cell. This results in an increase in the kinetic energy of the gas in the cell which causes the flexible mirror to distort and the reflected light from the exciting lamp then passes the line screen and reaches the photocell.

The response time is limited by the mechanical flexibility of the mirror membrane and is normally about 100 msec. This is entirely dependent on the nature of the membrane and would be expected to vary widely from detector to detector. Potter and Eisenman (77) found a gain of 2.5 in the detectivity of a Golay detector for operation at 20 cps compared with the normal operating frequency of 10 cps. Unfortunately, it is not normally possible to investigate the frequency response of the specific Golay in use.

1:6:4 Choice of Detector

Table 1:4 shows the main features of the far infra-red detectors described. Four main criteria govern the choice of detector: response time, detectivity, spectral response and convenience.

1) Response time: For the observation of transient phenomena, for example, plasma discharges, an exceptionally fast response time, of the order of one microsecond, is imperative. For a normal absorption spectrometer there is no advantage in using a fast detector.

2) Detectivity: On the basis of their N.E.P. there is little to choose between a germanium bolometer, a superconducting bolometer, a boron doped germanium photoconductor or the Indium Antimonide detector. The similar detectivity of these detectors and their three to four fold superiority over the carbon bolometer has been confirmed experimentally by Richards (64,75). Few comparisons between liquid helium cooled

TABLE 1:4 PROPERTIES OF SOME TYPICAL DETECTORS

Detector	Carbon Bolometer	Germanium Bolometer	Super-conducting Bolometer	InSb (7 k Gauss)	InSb 14-76 k Gauss	Boron doped Germanium	Golay
Operating temperature	2.1°K	2.15°K	3.7°K	1.8°K	4.0°K	4.0°K	300°K
Spectral response	Flat	Flat	Flat	1-100 cm^{-1}	Variable $_{-1}$ 90-110 cm at 14k Gauss	50-150 cm^{-1}	Flat
Response time in seconds	10^{-2}	10^{-3}	10^{-2}	2×10^{-7}	1.0×10^{-7}	10^{-5}	10^{-1}
Area in mm^2	20	15	3	5	25	20	20
Resistance in ohms	30 K	140 K	50	1 - 5 K	1 - 5 K		
(I/R)(dR/dT)	-2	-4	100				
N.E.P.wattsHz^{-1}	1.0×10^{-11}	5×10^{-13}	1.2×10^{-12}	5×10^{-12}	1.5×10^{-11}	5.0×10^{-12}	2.0×10^{-10}

detectors and the Golay cell have been made under truly identical conditions but Martin et al. (66) established a forty-fold improvement in the signal to noise ratio for their superconducting bolometer over a Golay cell and similar results have been found by Putley (73).

3) Spectral Response: The Golay cell and the bolometers have an essentially flat spectral response whereas the semi-conductive devices tend to have a peaked response. In addition any liquid helium cooled device requires a relatively large, transparent window which will withstand a vacuum: this normally implies a crystal quartz window which effectively sets an upper frequency limit of 200 cm^{-1} for the operation of the detector. The Golay detector, however, needing only a 5mm diameter window, may be fitted with a diamond window and used at any frequency.

4) Convenience: For routine spectroscopic use the slightly lower detectivity of the Golay cell compared with the other detectors is greatly outweighed by the fact that it does not require cooling with liquid helium. Apart from this it has several other advantages in that it is possible to use it above 200 cm^{-1} when fitted with a diamond window, it is readily available as a commercial instrument (the only other commercially available far infra-red detectors are the Mullard Indium Antimonide detector and a Germanium Bolometer from Texas Instruments) and owing to its large window area and large angle of acceptance the focussing and direction of the incident radiation is not critical. It is interesting to note that in a direct comparison of a Golay detector and a commercial liquid helium cooled germanium bolometer Jones et al. (78) obtained only a threefold increase in the signal to noise ratio for the cooled detector instead of the forty-fold increase predicted from the N.E.P. The only explanation of this discrepancy that could be offered was inadequate refinement of the optical system of the bolometer. This instrument, therefore, utilises a Unicam Golay detector fitted with a 5mm diamond window.

2) CONSTRUCTION OF A FAR INFRA-RED SPECTROMETER

2:1 MECHANICAL CONSTRUCTION

2:1:1 General Considerations

It has been shown in the previous section that the primary consideration in the design of this spectrometer was to achieve the highest possible energy throughput at a given spectral resolution. This necessitates the use of large gratings and an Ebert-Fastie monochromator. This spectrometer is, therefore, fundamentally different from the three previously described far infra-red double beam spectrometers in that they utilised relatively small gratings and a Littrow monochromator (5,6,7). As a result all three have a very similar basic optical design. In this instrument, however, quite different problems were encountered in the optical design and little guidance could be obtained from these Littrow instruments.

2:1:2 Order of Optical Components

It has been shown that six or seven basic components are required in the design of the spectrometer and an early decision that has to be made is "In what sequence should they occur in the optical path?"

It is convenient to illuminate the elongated monochromator slit directly with the elongated image of the source and to transform the exit slit image into a more nearly square image before the sample-reference space. This results in greater flexibility in the sample area where the square image is more amenable to the insertion of long path length gas cells, cryostats, etc. than an elongated image. The main filtering was placed after the sample space to help eliminate any spurious signal caused by emission from the sample. The optical scheme might, therefore, be represented in block diagram form as:

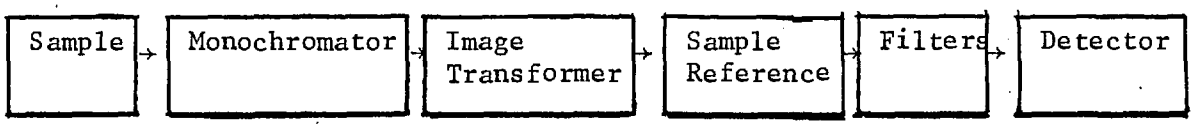

2:1:3 Vacuum Instrument

Because of intense water vapour absorption in the 10 to 350 cm^{-1} region it is essential to remove the atmospheric water vapour from the optical path either by evacuation or by flushing with dry gas. The latter method is generally agreed to be exceptionally tedious and unsatisfactory (7) and complete absence of water vapour absorption can only be achieved by evacuation.

2:1:4 Misalignment of the Optics on Evacuation

Previous workers (79) have experienced difficulties due to the misalignment of the optical path on evacuation as a result of mounting the optical components on the walls of vacuum tanks which distort on evacuation. To prevent this without the expense of providing a rigid vacuum tank it was decided to mount all the optical components on a central optical bench to be enclosed by a vacuum tank in which slight distortion on evacuation could be tolerated. It proved impossible, if reasonable flexibility in the sample - reference space was to be maintained, to use a single optical bench and the instrument was therefore designed around two benches, one containing the source, monochromator, image transformer and beam dividing optics and a second containing the beam recombining, filtering and detector optics. These two units are linked together by the sample and reference cells. Construction is simplified, and access to the components improved, if the optics are enclosed in four drums instead of a single one. This is illustrated in figures 2:1 and 2:2.

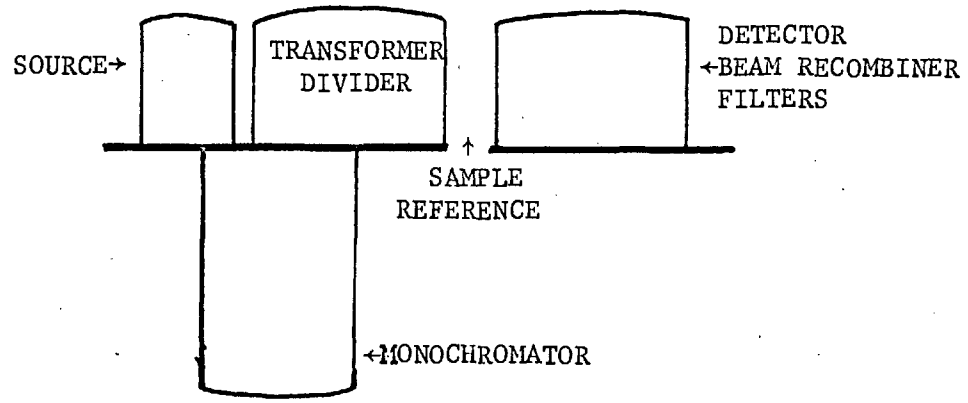

Figure 2:1 Plan of the Mechanical Construction of the Spectrometer

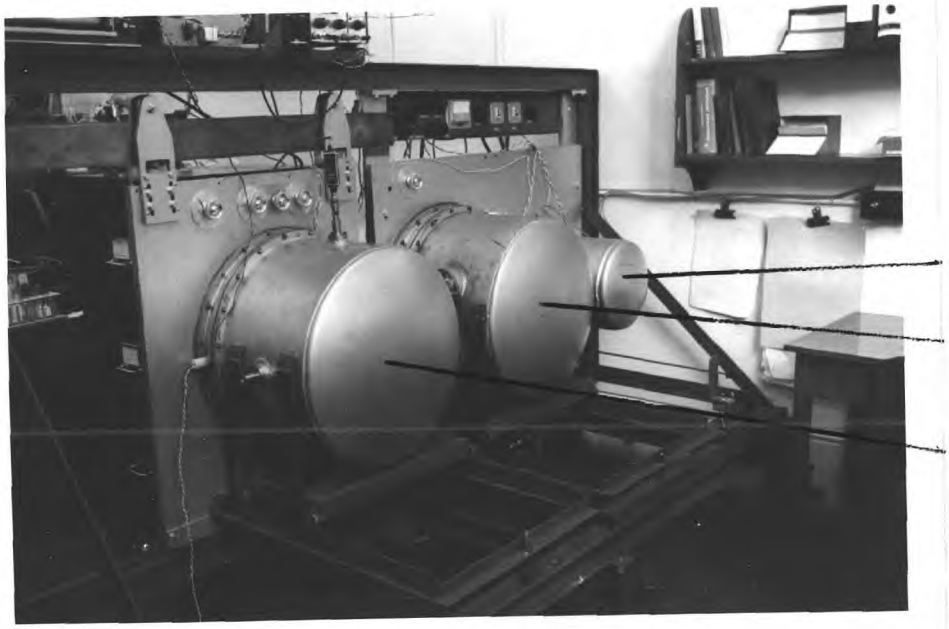

Figure 2:2 Spectrometer Elevation

The four drums and the two main plates were constructed by W. P. Butterfield, Engineers Ltd., of Shipley, Yorks. The principal dimensions of the drums and plates are given in Table 2:1 (All dimensions in inches).

TABLE 2:1 PRINCIPAL DIMENSIONS OF MAIN VACUUM DRUMS AND PLATES

	Main Plate	46 by 36 by 1	
	Detector Plate	30 by 36 by 1	
Drum	Source	Monochromator	Detector Image Transformer
Internal Diameter	12	20	22
Length, including collar	16	30	17
Thickness	$\frac{1}{8}$	$\frac{1}{8}$	$\frac{1}{8}$

2:1:5 Mechanical Construction

For easy insertion and removal of the sample and reference cells the detector bench is moveable with respect to the main bench. This is achieved by erecting the main bench vertical and hanging the detector plate from a beam on two roller bearings, as shown in Figure 2:2. The detector plate then rolls backwards and forwards in the plane of the main plate over a distance of about sixteen inches. The main plate and the beam for the detector plate are permanently bolted to a welded three inch rolled steel girder frame approximately eight feet square and five feet tall. In order to provide easy access to the optical components within, the drums are mounted on trolleys which roll on and off along rails, as shown in Figure 2:2. To allow the drums to be rolled back and forwards without having to disconnect any leads each drum is fitted with a two and a half inch brass collar which is semi-permanently bolted onto the mainplate. Copper pipes are soldered through the collar to provide the cooling water for the source and all electrical leads are taken out through standard B7G glass to metal seals bolted onto the collars and made leakproof with 'O' ring seals. All potential metal to metal seals are similarly rendered vacuum tight by the incorporation of 'O' ring seals into their construction.

The monochromator and source drums and the monochromator and image transformer drums are linked by two holes approximately 4 by $1\frac{3}{4}$ inches cut in the main plate: the slit cage assembly to be described in Section 2:2:3:3 fits over these holes. The image transformer and detector drums are linked by the sample and reference cells which bolt onto a pair of flanges on each drum. A polythene window is sandwiched between the flange and the cell so that the instrument may be evacuated independently of the sample and reference cells.

2:1:6 Evacuation

The monochromator and detector drums are each provided with a pair of standard B 19 taper cones for the insertion of vacuum takeout pipes and

Pirani guages. Evacuation is effected by a pair of Edwards ESC 150 rotary vacuum pipes in parallel connected to the instrument via oil traps. The vacuum piping is so arranged that both pumps or a single pump can be used to evacuate the whole instrument, or each section can be separately evacuated with its own pump. The Golay detector is extremely sensitive to low frequency mechanical vibration and although the relatively high frequency, around 300 cps, vibration caused by the rotation of the pump does not seriously interfere with the detector, considerable trouble was experienced from vibrations with a period of about one second caused by the two pumps 'beating' against each other. This was eliminated by mounting the pumps on anti-vibration mountings and ensuring that the vacuum pipes connecting the pumps to the instrument have the greatest possible flexibility.

Evacuation to 1mm, which is sufficient to remove the majority of the water vapour absorption, is effected in about ten minutes and continued pumping reduces the pressure, as recorded on a Pirani guage, to about 0.2mm in one hour: the equivalent McLeod guage pressure is about 0.04mm.

2:2 OPTICAL DESIGN AND CONSTRUCTION

2:2:1 General Considerations

In order to simplify the construction and reduce costs, all the mirrors, except the final condensing element which is an ellipsoid, are either plane or spherical mirrors. The plane mirrors were cut from a quarter inch sheet of Pilkington Float Glass and the spherical mirrors were manufactured either by the Optics Workshop, Physics Department, Imperial College or by Messrs. Gowllands, 176, Morlands Road, Croydon. The Ebert monochromator mirror was ground by the Ealing Optical Works, The Mall, London, W.5. All mirrors are aluminised on the front surface. The optical design is shown in Figure 2:3 and each component will be considered separately.

2:2:2 Source

2:2:2:1 Optical Design

The source used in this instrument is a Phillips MBL/U 125 watt high pressure mercury arc lamp. This lamp is particularly convenient owing to its compactness: the quartz envelope is about 4 cms. long and 1 cm. in diameter and the overall length of the lamp, including its SBC socket, is only 10.5 cms. The entrance slit of the monochromator is 7cm long and a twofold magnification of the source is, therefore, required to fill it. This is achieved with the optical scheme shown in Figure 2:4

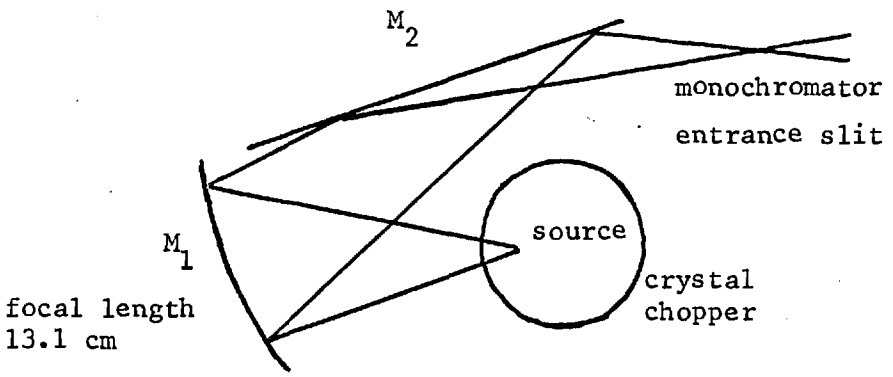

Figure 2:4 Optical Design of Source

The plane mirror, M_2, serves to laterally invert the aberration caused by the off-axis spherical mirror so that the image of the source is curved in the same direction as the slit. This is important only at wide slit widths and possibly when the low frequency radiation is arising from the arc rather than the quartz envelope.

The source may be run either uncooled (80) or cooled in a water jacket. In order to reduce radiative heating of the source drum and thus protect

SCALE 1 cm ≡ 2 inches

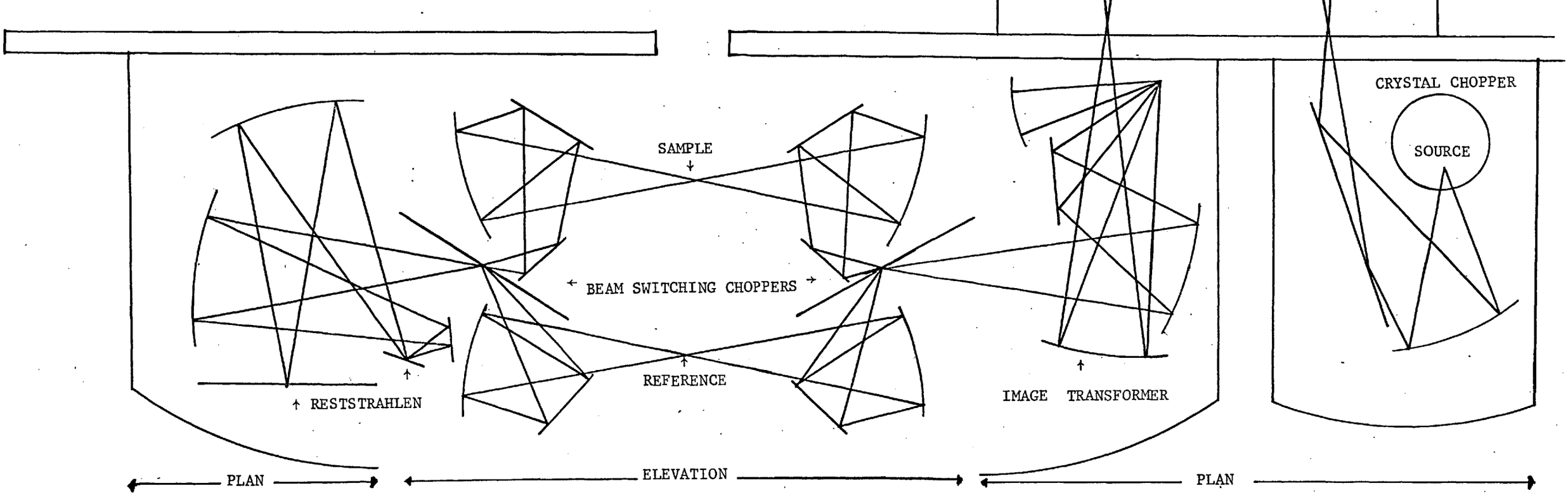

Figure 2:3 The Optical Design

the crystal chopper, a cooling jacket was utilised. This consists of two concentric brass cylinders soldered together through which water is circulated and with an aperture for the light to emerge. The lamp socket is screwed into the top of the housing and the lamp hangs within the two cylinders: the whole is suspended vertically. This is shown in Figure 2:5.

Figure 2:5 The Source and Crystal Chopper

Papoular (21) claims that water cooling of the mercury arc reduces long period fluctuations in its low frequency output. Cano and Matiolli (22) found it necessary to dimple the walls of the quartz envelope to prevent modulation of the spectrum at 2 cm^{-1} intervals due to interference effects. This has not been found necessary in the present instrument.

2:2:2:2 Effect of Placing a Spherical Mirror behind the Source

By a principle commonly referred to as the brightness gain theorem the photometric brightness of the image cannot exceed that of the object (81) and consequently the radiant flux through the spectrometer is limited to that accepted from the source. For an object of area,S, and photometric brightness,B, the total flux energy,E, is given by

$$E = \pi B S \sin^2\theta$$

where θ = angular semi aperture of the object

In particular the effect of placing a spherical mirror behind the source must, by the brightness gain theorem, be approached by considering its effect on the photometric brightness of the source,B, rather than claiming a doubling of the angular aperture of the system.

In the present instrument two cases may be distinguished:
1) Radiation to which the quartz envelope is opaque: this occurs in the 100 to 2,000 cm^{-1} region. In this case the photometric brightness is dependent on the effective black body temperature of the source. The placing of a mirror behind the source will, therefore, only cause the lamp to equilibrate at a slightly higher temperature with a consequent small increase in the photometric brightness.
2) Radiation to which the quartz envelope is transparent: this occurs in the region below 50 cm^{-1} and above 2,000 cm^{-1}. Below 50 cm^{-1} the effective increase in the photometric brightness will depend on the self absorption of the plasma. Many plasma experiments have been satisfactorily explained on the assumption that the plasma is optically thin and the self absorption small (21,82). Consequently an almost 100% increase in the photometric brightness of the plasma would be expected on placing a mirror behind the source. This was tested experimentally in a series of experiments with the inside of the water cooling jacket covered in soot and with it highly polished and gold plated (83). At 165 cm^{-1} the

polished lamp housing gave a 10% increase in signal over the blackened lamp housing. At 20 cm^{-1} the increase was 20%: if half the radiation at 20 cm^{-1} was arising from the arc then a 50% increase in signal would be expected, allowing for the poor quality of the spherical mirror inserted, the experimental increase appears to be in accord with the above analysis. This demonstrates the beneficial effect of polishing the back of the lamp housing.

2:2:2:3 Crystal Chopper

It has been shown (Section 1:5:4) that an important consideration in the choice of electronic chopping system was the desire to include an optical chopper formed from potassium bromide or caesium iodide crystals to act as a filter-modulator. In order to achieve a good optical waveform, it is necessary to chop the light near a focus. A convenient method is to mount the crystal chopper vertically around the source jacket, as shown in Figure 2:5. Although the chopper may be either an oscillatory or a reciprocatory one the former is to be preferred due to the reduction in vibration (84).

It has been shown (Section 1:6:3) that the Golay detector is most sensitive when the input signal is modulated at ten to twenty Hz. Since the radiation intensity on the Golay is a four level signal a suitable primary chopping frequency would be five Hz: this may be achieved with an ungeared twenty-four pole synchronous motor which revolves at 25/6 Hz. Since space is limited in the instrument only a very small motor may be accommodated but the starting torque required is large, about 10^4 gm.-cm^2. Experiments were initiated with Mullard stepping motors (type AU 5055/80) but these proved to have very poor starting characteristics under heavy loads. An ordinary synchronous motor (Mullard type AU 5100/02) incorporating a ratchet mechanism to assist starting was therefore utilised. The mechanical construction is greatly simplified if these motors are placed inside the vacuum drums but certain difficulties have been encountered in attempting to do this due

to arcing between the input terminals and the case. This was reduced by isolating the terminals from the case by a sheet of Paxolin but this was not entirely satisfactory and these motors are being progressively replaced by 110 volt motors (type AU 5100/03) which are less prone to arcing.

In order to present the detector with as good a waveform as possible the chopper consists of 180° of crystal and 180° open. A simpler electronic system would have resulted from having 90° of crystal alternating with 90° open but the optical waveform would have been considerably poorer. A further squareing of the waveform is achieved by mounting the chopper eccentrically with respect to the lamp: this is also shown in Figure 2:5. As a result of starting torque limitations the largest practical chopper was an 11 cm diameter octagon mounted on four adjacent sides with potassium bromide crystals $2\frac{3}{4}$ by $1\frac{3}{4}$ by $\frac{1}{8}$ inches and kinetically counterbalanced with lead weights. The centre of the octagon was placed $3\frac{1}{2}$ cm behind the centre of the lamp to give complete chopping of the exit beam for 155° and an interphase period of 50° in every cycle.

The density of caesium iodide is approximately 5/3 that of potassium bromide, consequently the diameter of the chopper had to be reduced for rotation by the same motor. The caesium iodide chopper is an 8 cm hexagon mounted concentrically with the source carrying three caesium iodide blades of the same dimensions as the potassium bromide ones. Despite the fact that with the caesium iodide chopper complete chopping is achieved for only 120° and the interphase period is increased to 120° no significant difference in performance from that obtained with potassium bromide has been noted.

It was noted that the caesium iodide chopper was quickly discoloured with a dark brown surface deposit whereas the potassium bromide one was not. This deposit was identified as elemental iodine. Other workers (70) have observed polymerisation on mirrors caused by radical formation

at the heated source from oil molecules back diffusing from the rotary pump: a similar explanation for this deposit is suggested.

2:2:3 Monochromator

2:2:3:1 Optical Design

The Ebert-Fastie monochromator was designed about the largest gratings ruled with the requisite number of lines readily available in the United Kingdom. These were six inch square replica gratings from the National Physical Laboratory ruled with 625 and 312.5 lines.inch^{-1}. Image slicing considerations (Section 1:3) show that for the detector in use a suitable aperture for the monochromator is f/3.5 with slits 7 cm high. With these factors decided the monochromator design is straightforward and the resultant system is shown in Figure 2:6.

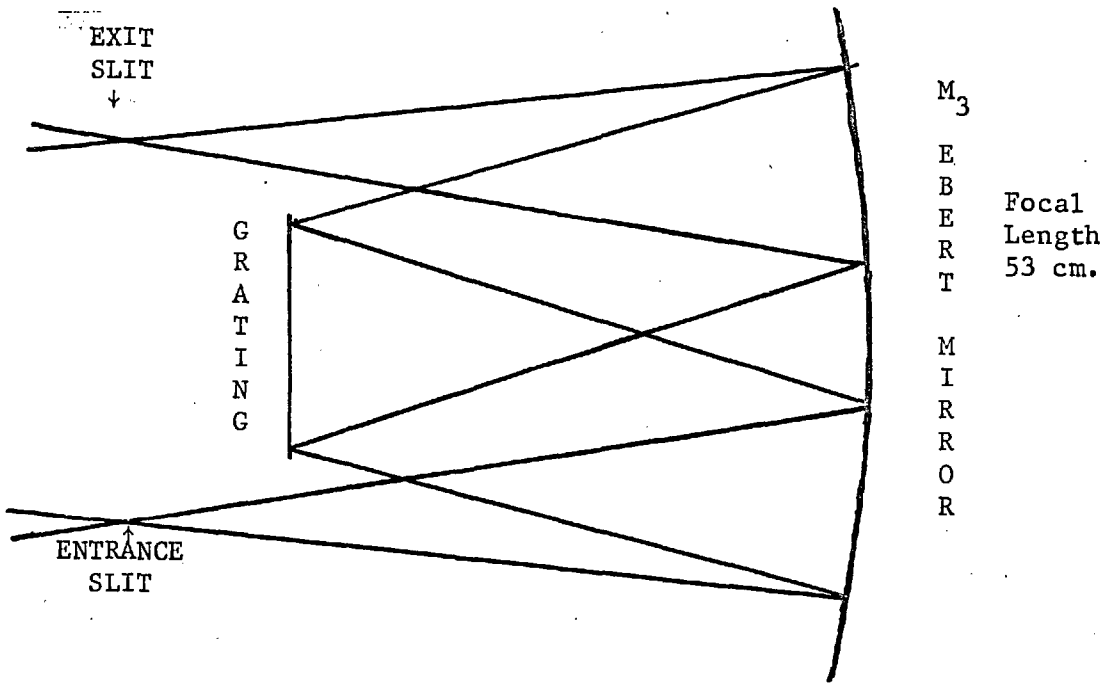

Figure 2:6 Optical Design of the Monochromator

2:3:2 Ebert Mirror

The Ebert mirror, M_3, has a focal length of 53 cm and is 45 cm in diameter. Since the top and bottom of the mirror receive no light from the grating they have been removed so that the mirror is only 20 cm wide. This reduces the weight that must be supported on a very long, 60 cm, cantilever from the main plate. The mirror is kinematically mounted so that its focal plane may be accurately adjusted to include the entrance and exit slits.

2:3:3 Slits

The slits, S_1 and S_2, are circularly curved about the axis of the Ebert mirror. In order to reduce the diameter of the Ebert mirror it is necessary to reduce the radius of the slits to a minimum while avoiding vignetting of the beam on the grating mount. The smallest practical radius in this case is five inches.

The five inch radius, three inch high slits were machined from stainless steel and mounted in tandem, i.e. the concave slit of one pair and the convex slit of the other pair were ganged together, as described by Taimsalu (85), so that the entrance and exit slits open together to equal slit widths while maintaining their centre points exactly five inches from the axis of the Ebert mirror. By a series of bevel gears and 'O' ring seals the control mechanism is brought to the front of the main plate where the slit opening may be adjusted from outside the drums. The opening mechanism is controlled by a 2BA threaded stainless steel rod with 31.4 threads to the inch. One turn, therefore, corresponds to an opening of 1.62 mm and the maximum opening of 7 and 50/360 turns to 11.5 mm. The subsequent optics are designed so that at the maximum slit width the window area and acceptance angle of the Golay are completely filled. In this limiting case no increase in the energy per spectral slit width can be obtained by varying the geometry or increasing the size of the monochromator.

2:2:3:4 Grating

One of the disadvantages of a wide-band grating spectrometer is the necessity of utilising a large number of gratings for optimum performance. This instrument uses five gratings to cover the range 400 to 10 cm^{-1}. A list of the gratings used is given in Table 2:2

TABLE 2:2 GRATINGS USED IN THIS INSTRUMENT

Grating	1	2	3	4	5
lines per inch	625	312.5	166	50	20
1/d in cm^{-1}	246	123.6	65.3	19.7	7.9
Blaze angle	27^{o}	27^{o}	26^{o}	10^{o}	10^{o}
Blaze frequency	$261cm^{-1}$	$138cm^{-1}$	$75cm^{-1}$	$56.8cm^{-1}$	$22.7cm^{-1}$
Usable range, see Section	$400-180cm^{-1}$	$200-90cm^{-1}$	$103-48cm^{-1}$	$80-30cm^{-1}$	$32-12cm^{-1}$
Experimentally usable range	$400-170cm^{-1}$	$220-90cm^{-1}$	$110-50cm^{-1}$	$55-15cm^{-1}$	$20-10cm^{-1}$

Gratings 1 and 2 are on loan from the National Physical Laboratory and are experimental Replica Gratings.

Gratings 3 and 4 were kindly ruled by the Royal Radar Establishment, Malvern, Worcs.

Grating 5 was ruled by the Chemistry Department Workshop, Imperial College.

It is not possible, with any simple design, to mount more than two gratings on a turntable so that the axis of rotation passes close to the plane of the grating face. Yoshinaga (7) mounted three gratings on a

prism turntable and did not report any difficulties with the peculiar scan involved. Despite this it was decided to mount only two gratings back to back on a single spindle so that the gratings were rotated about an axis very close to their groove plane. Having only two gratings on the turntable meant that a system had to be devised whereby the gratings could be readily exchanged without the need to recalibrate the instrument after every change. This was achieved by permanently fixing each grating in a brass box and providing each box with three tapered hardened steel pegs which located in holes with minimum clearance on the grating turntable. The position of each grating in its box was adjusted until the entrance slit image was accurately superimposed on the exit slit, the position of the grating in its box was then semi-permanently fixed by tightening four grub-screws. It has been found possible to insert and remove the gratings over a period of six months with no noticeable change in the calibration: the difference in the position of the grating is certainly less than 0.05 degrees. In order to permit the complete rotation of the grating turntable so as to bring either grating into the optical path, the axis of the mount is positioned 3.5 inches in front of the mainplate, as shown in Figure 2:3. The mounting is provided with a number of adjustment points so that the axis of rotation may be brought parallel to the slit plane to better than 0.005^{o} and coincident with the normal plane bisecting the slits to better than 1 mm.

2:2:3:5 Calibration

The grating turntable shaft carries a 360 tooth gearwheel by means of which the grating is rotated by a worm shaft through an 'O' ring seal from outside the drum. One revolution of the worm shaft, therefore, corresponds to a one degree rotation of the grating. In order to facilitate the calibration a fiduciary mark is made on the recording chart for every 0.2^{o} rotation of the grating. This is effected by mounting a five tooth cam on the worm shaft and causing a microswitch

(Burgess type CRI-KR) to discharge a capacitor through the recorder on being actuated by this cam. The circuit is shown in Figure 2:7

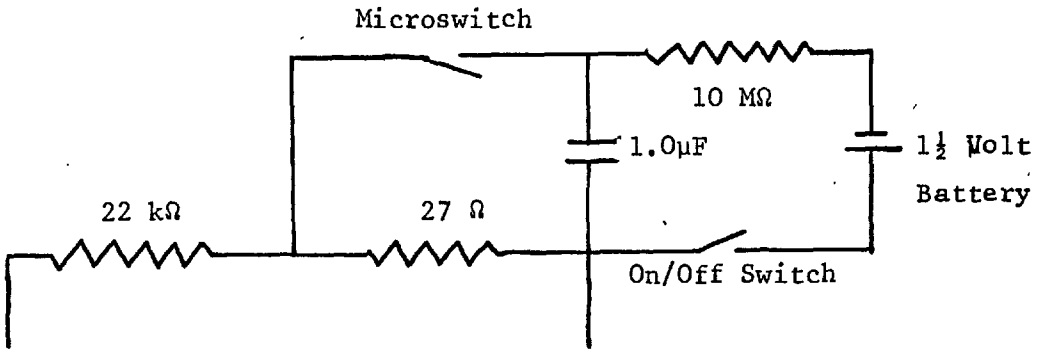

The worm shaft also carries a mechanical revolution counter (English Numbering Machines type 421/012) which records the rotation of the grating in degrees. In practice one tooth of the cam is absent, a gap therefore occurs at every fifth fiduciary mark, corresponding to one degree rotation of the grating, and the reading of the revolution counter is inserted on the chart manually.

2:2:3:6 Gearbox

To speed construction a commercial six speed gearbox from a Smiths Ultralette 5651 Recorder was purchased. This was supplied with a Smiths M25 Mark 1 3.5 watt synchronous motor which resulted in the output shaft of the gearbox rotating at $3\frac{3}{4}$, $7\frac{1}{2}$, 15, 30, 60 and 120 r.p.m. The gearbox was attached to the worm shaft of the grating through a 15 to 1 worm reduction gear. The grating therefore rotated at $\frac{1}{4}$, $\frac{1}{2}$, 1, 2, 4 and 8 degrees per minute. This corresponds to a scan rate of about $\frac{1}{2}$ to 16 wavenumbers per minute at 100 cm^{-1} and a delay of about 22 minutes when changing from one grating to the other on the turntable.

A D.P.D.T. switch enables the direction of rotation of the grating to be varied at will, the motor being a hysteresis one run with a phase

splitting capacitor.

The Golay detector is exceptionally sensitive to low frequency mechanical vibration and because of this the gearbox and motor were attached to the mainplate via an anti-vibration mounting formed from the moulded steel-rubber-steel sandwich from a B.M.C. 1100 shock absorber. To prevent the transmission of vibration through the grating drive shaft a rubber dog clutch was inserted between the gearbox and the 15 to 1 worm reduction gear.

2:2:4 Image Transformer

A Benesch and Strong (34) type image transformer was designed as shown in Figure 2:8

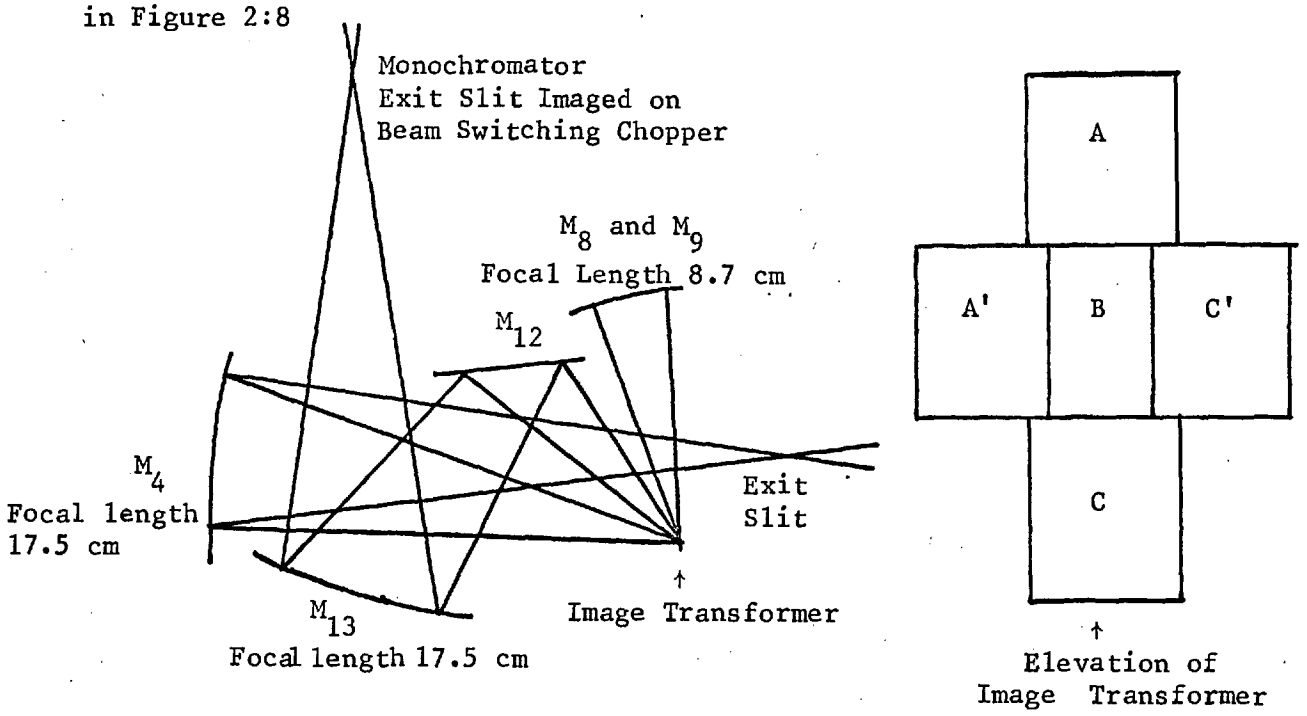

Figure 2:8 Optical Design of the Image Transformer

It should be noted that the aberration of the first spherical mirror, M_4, tends to straighten the curved slit image, thus presenting the image transformer with an essentially straight image.

The construction of the image transformer posed some practical problems since the mirrors were too small to mount in the normal kinetic mounts for easy adjustment. This was solved by raising the mainplate on a steel scaffold until it was almost horizontal, the five small mirrors required for the image transformer were then set in a bed of fast-setting putty and adjusted until correctly aligned. Their position was then fixed by flooding the edges of the assembly with Araldite. After allowing the Araldite to harden the excess was removed, the putty completely enclosed with Araldite to prevent outgassing, and the whole assembly re-aluminised.

Apart from a lack of flexibility for future adjustment this method is quite satisfactory. The plane mirror, M_{12}, is not an essential feature of the design but no design was found within the limits imposed by the drum which would eliminate this mirror without introducing large aberrations due to the highly off-axis use of the spherical mirrors.

2:2:5 Beam Switching

Two considerations prevented the use of the usual form of beam switching optics employed in most double beam instruments shown in Figure 1:6.
a) In order to preseve the optical waveform it is desirable to insert the chopper at an optical conjugate, i.e. focus of the slit.
b) It is desirable to have a second optical conjugate of the slit in the centre of the sample-reference space. This is especially necessary where the beam is fast, as in this instrument, f/3.5, as it reduces to a minimum the diameter, and consequently the volume, of the sample needed to avoid vignetting of the beam by the sample cell. Secondly, it permits greater flexibility in the sample-reference space. In the design evolved, shown in Figure 2:9, the optics are arranged to accommodate a 10 cm cell in the sample cell. However, by replacing mirrors 18 and 19, 20 and 21 with a second set having a longer focal length it is possible to accommodate cells up to 25 cm long, e.g. liquid helium cryostats, etc.

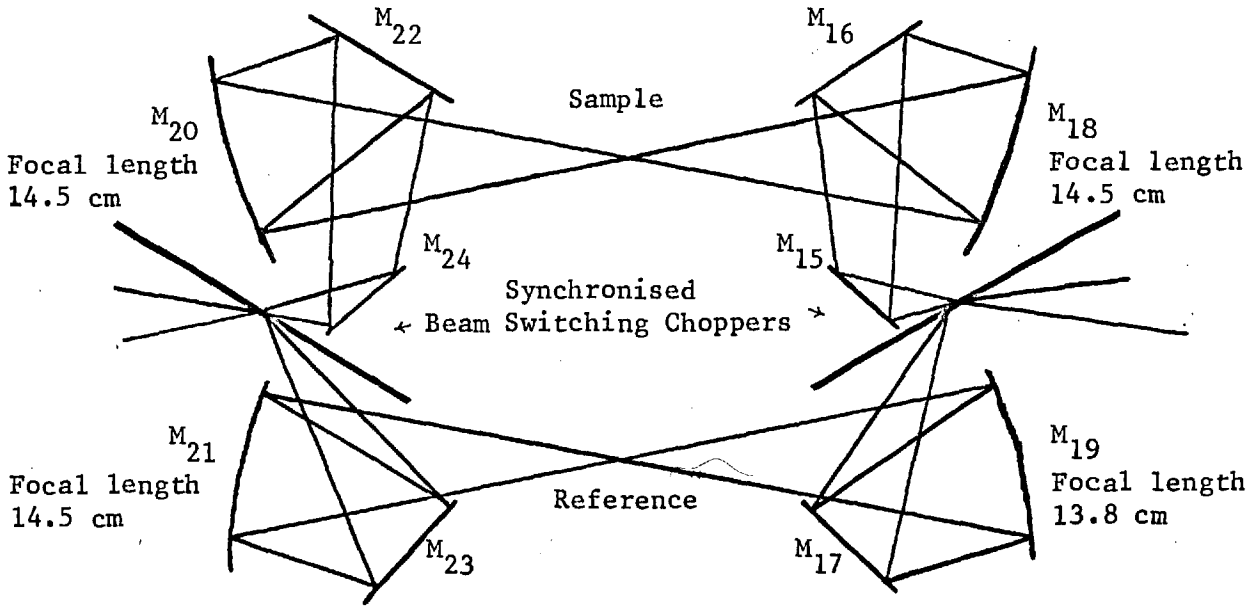

Figure 2:9 Design of the Beam Switching Optics

The plane mirrors, 16,17,22 and 23, are introduced in order to avoid having to use the spherical mirrors in a highly off-axis configuration. The minimisation of aberrations by using the mirrors as little off-axis as possible was one of the main difficulties in the design of the optics.

Unfortunately, in the above design, the aberrations caused by mirrors 18 and 20 and by mirrors 19 and 21 are cumulative and this resulted in some difficulty being experienced in focussing the beam in later stages of the optics.

The actual beam switching is accomplished by a 180^{o} rotating mirror sector. The sector is of the largest possible dimensions, diameter 27 cms, in order to preserve the optical waveform: this ensures complete beam switching for 156^{o} and an interphase period of 48^{o}. This is almost

identical to the interphase period of the potassium bromide chopper, so, in this case, the distortion of the wave form is caused equally by the crystal chopper and by the beam switching chopper. With the caesium iodide chopper, however, the majority of the distortion arises from the crystal chopper where the interphase period is increased to 120^{o} due to it being mounted concentrically with the source, Section 2:2:2:3.

In order to reduce the weight of the beam switching choppers they are fabricated from 4mm sheet aluminium rather than glass: after milling, the aluminium was lapped by hand using chromic oxide until a satisfactory surface was obtained. Despite the possibility of preferential high frequency scattering from these choppers no difficulties have been experienced with them.

It will be shown in Section 2:3:2:2 when considering the electronics that not only must the two beam switching choppers be run in synchonisation but that they must be run 90^{o} out of phase with the source chopper. Since the starting torque of a synchronous motor is small a ratchet is incorporated into the output shaft to allow the load to gradually reach synchronous speed. The presence of the ratchet necessitates the provision of some means whereby the motors can be brought into synchronisation after being started at random. This is achieved by mounting the motors within a 180 tooth gear wheel which is rotated by a worm shaft through an 'O' ring seal from outside the drum. One revolution of the worm shaft, therefore, corresponds to a two degree re-phasing of the motor. In order to know when the motors are synchronised, each rotating component carries a small rotating magnet which passes over a small coil, about 2,000 turns of 38 guage copper wire. The induced current in the coils is displayed on an oscilloscope and the positions of each coil adjusted until superposition of the induced spikes from all three coils corresponds to the correct optical phasing between the chopper and the beam switching sectors.

2:2:6 Filtering

The main filtering is achieved by two 'crossed' reststrahlen filters and a transmission filter. Previous experience on a single beam instrument constructed in this laboratory (86) had shown that at least six pairs of reststrahlen filters were required to cover the region 400 to 60 cm^{-1} and consequently provision was made for the insertion of eight pairs. In the previous instrument, the reststrahlen had been mounted in quartets on four of the faces of a cube and the desired crystal brought into the light beam by rotation about an axis through the centre of the remaining two faces of the cube (87). This resulted in the light intensity being extremely sensitive to the exact position of the reststrahlen mount. To prevent this the present design allows all eight crystals to be in a single plane; the light intensity is not, therefore, critically dependent on the exact position of the reststrahlen mount and great reproducibility in intensity from run to run is possible.

At the optical conjugate of the slit the beam is approximately one inch square and since the angle of incidence is 45^{o}, to approximate to the Brewster angle, the minimum dimensions of the reststrahlen crystal are 1 by 1.4 inches. To allow for less accurate positioning of the crystal each was made one and a half by two inches and eight, therefore, require a circular holder 9 inches in diameter. The arrangement shown in Figure 2:10 appeared to be the simplest within the given drum diameter

In order to reduce the diameter of the holder required, the transmission filters should also be placed near a focus. A convenient place is immediately in front of the Golay window. A filter holder containing six one inch apertures was designed to hold the filters.

The changing of the reststrahlen and transmission filters is facilitated by arranging, by a system of bevel gears and 'O' ring seals, to rotate their mounts from outside the drum. To assist in the correct positioning of the filters in the optical beam a pressure stop is provided when each component is correctly located.

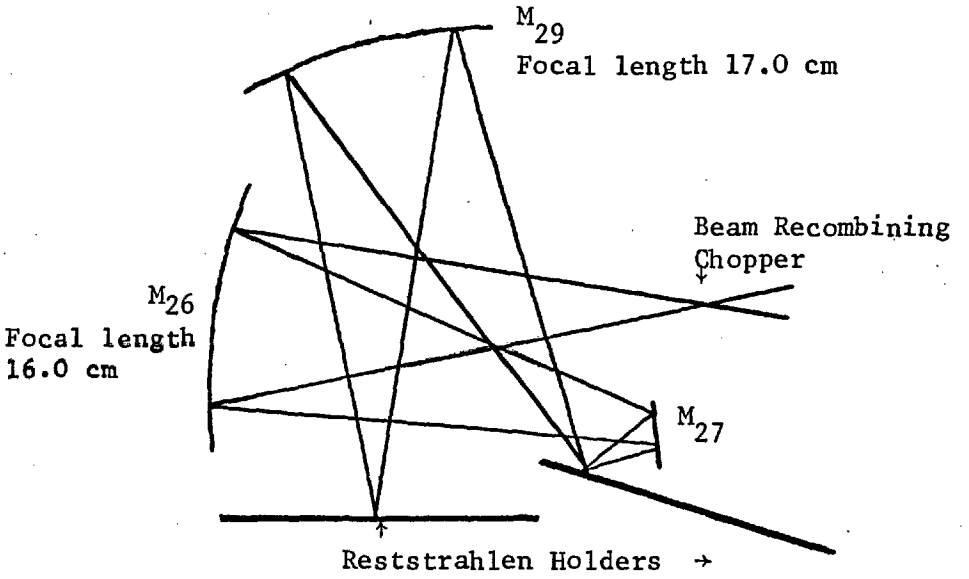

Figure 2:10 Optical Design of the Reststrahlen filters

2:2:7 Detector

The detector used is a Unicam Golay pneumatic detector with a 5mm diamond window and an acceptance aperture of f/1. Since the aperture of the remainder of the spectrometer is f/3.5 and the focussed image has an area of 25mm by 25mm it is necessary to effect a 4:1 demagnification onto the detector window. This may be effected either with a conical light pipe (88), a Greenler image reducer (89) or an ellipsoidal mirror (51). The light pipe was rejected due to difficulties in construction when required for use at high frequencies and the Greenler reducer was also unsuitable due to the fact that the convex mirror would have a thickness of at least 0.5 cm and the Golay window is recessed by at least an equal distance. Thus the Golay window is over 1 cm from the surface of the convex mirror and Taimsalu (90) found that insertion of an

aluminium foil cone into this recess gave a 50% increase in signal.

In order to effect the condensation with a single element, it was decided to use an ellipsoidal mirror and due to the bulky nature of the detector it is necessary to use it in a 90° off-axis configuration, as shown in Figure 2:11

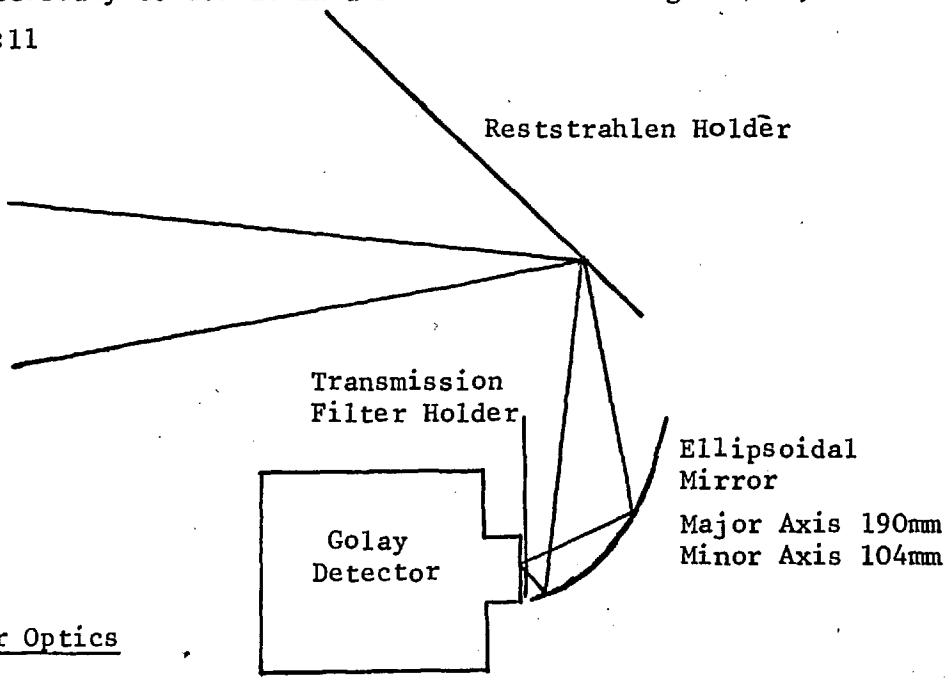

Figure 2:11 Detector Optics

The ellipsoid has a major axis of 190 mm and a minor axis of 104 mm, thus effecting a 4:1 condensation. It was turned from a solid duralumin cylinder, by means of a hardened steel template with a preformed ellipsoidal profile, and polished on a lathe. Although on the basis of the optical design a 120° section of the ellipsoid should have been adequate a 180° section was used to ensure that all possible radiation was directed onto the Golay window.

To eliminate low frequency noise the Golay cell must be electrically and mechanically isolated from the mounting bracket. This was achieved by mounting the Golay cell between two quarter inch sheets of expanded foam rubber as shown in Figure 2:12.

A disadvantage of this type of mounting is that the heat generated by

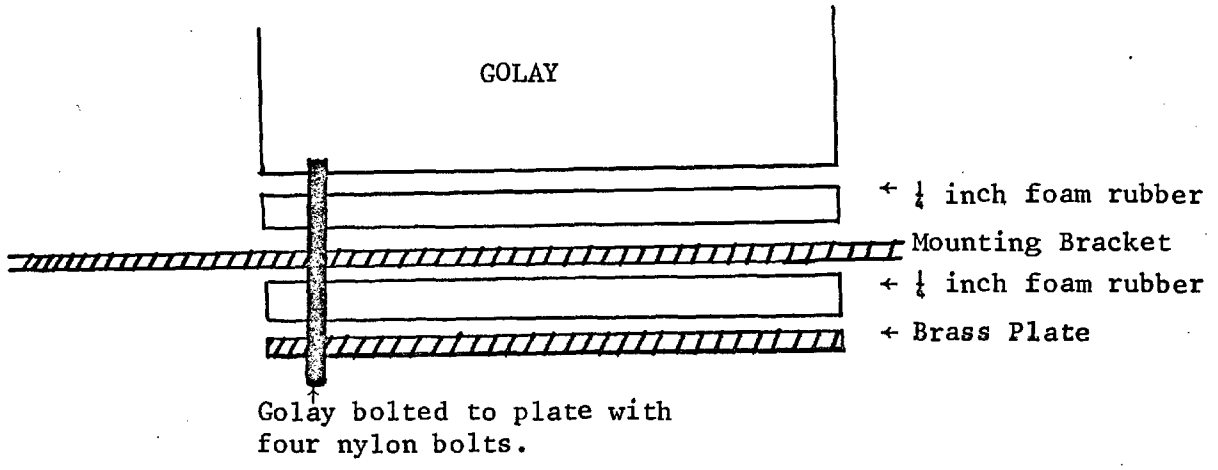

Figure 2:12 Electrical and Mechanical Insulation of the Golay Cell

the exciting lamp of the Golay cannot be dissipated by conduction and a slow decrease in the sensitivity of the detector is noticed after the lamp is switched on. When thermal equilibrium has been established after about two hours the total decrease in the signal was about 20%. Adams (91) observed a fall in the signal to noise ratio but it was not possible on this instrument to observe whether the noise level actually remained constant. In order to counteract this diminution of signal as the Golay temperature increases, Collins (92) designed a vibration insulated mounting with a large thermal capacity: in this instrument it was felt that the small decrease in signal was compensated for by the simpler mounting and complete absence of mechanically induced noise.

2:3 ELECTRONICS

2:3:1 Introduction

Two systems have been commonly used in the near infra-red to obtain a ratio recording double beam spectrometer: these are the optical null and the direct ratio systems.

2:3:1:1 Optical Null System

This represents by far the commonest near infra-red system. Radiation

from the sample and reference beams is alternately presented to the detector, usually at about 10 Hz, either by the double or twin beam optical systems described in Section 1:4. The A.C. component of the detected signal is amplified and used to operate a servomechanism which attenuates the reference beam until the detector receives zero A.C. signal. The position of the attenuator, usually a comb or aperture diaphragm, then indicates the ratio of the sample to reference beam intensities. Such a system has a noise factor of unity: i.e. an identical noise factor to a single chopped beam system (93). The low noise factor and basically simple electronics account for its prevalent use in near infra-red spectrometers. In the far infra-red it suffers from a number of major disadvantages:

1) The optical system does not incorporate a chopper whose function is to establish a zero radiation level. In single beam instruments the necessity to provide a chopper has been made use of as an additional aid to filtering, Section 1:5:4. Experience on single beam instruments has shown that the crystal chopper is an important element in the filtering chain and evidence will be presented to show that this is also true for a double beam instrument, Section 3:4:1. Despite this drawback a double beam far infra-red instrument has been constructed on the optical null principle (7), the high energy radiation being attenuated by two scatter plates rather than by a crystal chopper.

2) The optical null system is in balance when the total radiation transmitted through and emitted by the sample is equal to the total radiation transmitted through and emitted by the reference, with the attenuator comb at room temperature. If the amount of radiation emitted by the reference attenuator at the balance position is not equal to that emitted by the sample, then the balance position is in error since the transmissions of the two beams cannot be equal either. Since the attenuator comb is always at room temperature this makes the instrument sensitive to the sample temperature, especially at frequencies below 500 cm^{-1}. For

example, an opaque non-reflecting sample at either -196° or 250°C when compared to a room temperature attenuator will show a zero error of about 25% in the range 100 to 20 cm^{-1} (94) (a black body source at 1200°K was assumed in the calculation).

This effect was sufficiently severe to oblige Yoshinaga et al. to modify their optical null instrument (7). The modification involved the introduction of a 0.9 Hz chopper before the separation of the sample and reference beams which still occurred at 10 Hz. 0.9 was chosen so that its harmonics in the vicinity of the 10 Hz chopper would be small and yet it would be appreciably separated from the highest frequency components of the scanned absorption bands. The chopper may either be opaque or of filter-crystal. Synchronous rectification at 0.9 Hz is then used to eliminate the signal due to emission from the sample or reference and the resultant $I_{ref} - I_{sample}$ signal used to activate the attenuator. Since the energy is reduced by one half from the optical null system, which has a noise factor of unity, the noise factor of the Yoshinaga modified optical null system will be 1.4 which is fractionally better than the direct ratio types to be described. Apart from this, the system appears to have no virtues; if sample chopping and synchronous rectification are to be introduced it is, in effect, a direct ratio system and the ratio may be conveniently established on a potentiometric recorder rather than introducing the complication of a beam attenuator.

2:3:1:2 Direct Ratio Systems

In these the two D.C. levels which correspond to the sample and reference beam intensities are established separately and then ratioed. Such direct ratio systems may be divided into phase and amplitude systems.
1) Phase systems: This system was first proposed by Savitsky and Halford (37) in association with a split aperture optical system. There is no beam switching chopper and the detector is receiving radiation continuously from both the sample and reference beams; two optical choppers are, however, used to chop each beam at 90° out of phase with

the other. If the component of the signal representing the radiation through the reference beam is presented, together with its phase inverted replica at the two poles of a switch operating in synchronisation with the optical chopper then the resultant signal will be a D.C. level representing the radiation intensity in the reference beam. If, however, the switch is 90^{o} out of phase with the optical chopper, no D.C. component appears at the output of the switch. Thus, the signal falling onto the detector may be resolved into its two components, that due to the reference beam radiation and that due to the sample beam, by a pair of switches differing in phase by 90^{o}. Golay (93) has shown that when the sample transmission is zero the noise factor is 2, and 100% transmission the noise factor is 2.82, the R.M.S. noise factor over all transmissions is 2.32. Because of this high noise factor the phase system was rejected in favour of the amplitude system.

2) Amplitude system: This system uses both a beam switching and a crystal filter chopper; the signal entering the detector, therefore, consists of four distinct phases: sample beam chopped, sample beam unchopped, reference beam chopped and reference beam unchopped (afterwards referred to as SC, SU, RC and RU). Golay (93) has shown that the R.M.S. noise factor over all transmission values for such a system is 1.63, which is appreciably superior to the phase system discussed above and only slightly inferior to the Yoshinaga modified optical null system (94).

In principle it is immaterial in which order the phases arrive, and the choice is made mainly on the basis of mechanical convenience. One criterion for a good multiple chopping system is that the amount of time for which the signal comprises a mixture of phases should be a minimum, since instantaneous optical chopping is not possible. It is also desirable that only two phases should be mixed at any one optical switching for then, in theory, a point in time can be selected for the electronic switching of the detector output which will divide the mixed

signal with correct weightings between the preceding and succeeding portions. This is an important consideration when the detector in use, a Golay cell, has a time constant of around 50 to 100 milliseconds (77) which is comparable with feasible chopping and beam switching rates. These must themselves be fast compared with the scanning of the spectrometer grating and sufficiently rapid to permit A.C. amplification of the detector output. The chopping cycle chosen for this instrument was accordingly SU, SC, RC, RU, needing only a single optical switching of both the beam switching and the optical choppers but with a 90^{o} phase lag between them. This system mixes only two optical phases at a time and is easily achieved using identical synchronous motors; the use of reciprocating units was rejected because of the known microphony of the Golay cell, Section 2:2:7. This system has an advantage over other possibilities, such as RC, RU, SC, SU, in that the crystal chopper, which has a more extended period of intermediacy between its two optical states than do the beam switching choppers, has to make only one chop per cycle.

The assymmetry of the chopping cycle, however, precludes the subsequent electronic resolution of the signal into its components by two phase sensitive detectors in quadrature as recommended by Hornig et al. (95). At the design stage the likely response of the Golay to transients and the actual effect on the overall spectrometric precision of the periods during which the signal magnitude was undergoing large changes was not known. A fairly slow cycle repetition frequency of 25/6 Hz was, therefore, chosen giving some 17 phases of signal entering the detector every second and a very flexible resolving circuit designed in which any fraction of any phase or interphase state could be excluded; the selected fractions of each phase being isolated by discrete switching. This approach also lends itself to possible phase by phase digital outputting of the signal onto punched tapes for computer processing should this be desired.

2:3:2 Electronic Design

2:3:2:1 Amplifiers and power supplies

The Golay pneumatic cell (Section 1:6:3)embodies a lamp and photocell monitoring the incident radiation onto the detector window. The photocell and a 10 megohm resistance form a potential divider whose mid-point controls the signal grid of a 6BR7 electrometer pentode acting as a cathode follower. The power for the lamp and the heater of the 6BR7, about 1 amp at 4 volts, is supplied by lead acid accumulators as these are the simplest and most convenient high current stable power supplies. The cathode resistance of the valve is 100 kilohms and a quiescent voltage of about 15 volts is developed across it, the signal output expected on this cathode was, from previous experience, of the order of a few millivolts. The possibility of backing-off the 10 volt cathode potential by a potential divider and following the few millivolts of actual signal with a D.C. amplifier was eliminated due to the problems associated with drift which had been marked in the single beam instrument (96) whose output was at one time backed-off in this way. The possibility of using a high frequency chopper, say 400 Hz, immediately following the Golay and amplifying only this frequency in a tuned amplifier to reject the drift appeared to embody unattractive complications and it was decided to amplify the Golay output by a straight A.C. coupled amplifier.

It is not possible, however, to amplify a signal of the type delivered by the Golay cell by amplifiers of finite time constant without introducing interaction between the beams. This is illustrated in Figure 2:13 which shows that, with a D.C. amplifier, the correct integrated signal differences are obtained irrespective of the relative magnitude of the signals in the two beams, Figure 13 A and B. With an A.C. coupled amplifier, however, although the correct signal differences are obtained if the sample and reference signals are equal, Figure 13 C, if one of the signals falls to zero while the other remains at unity, as illustrated

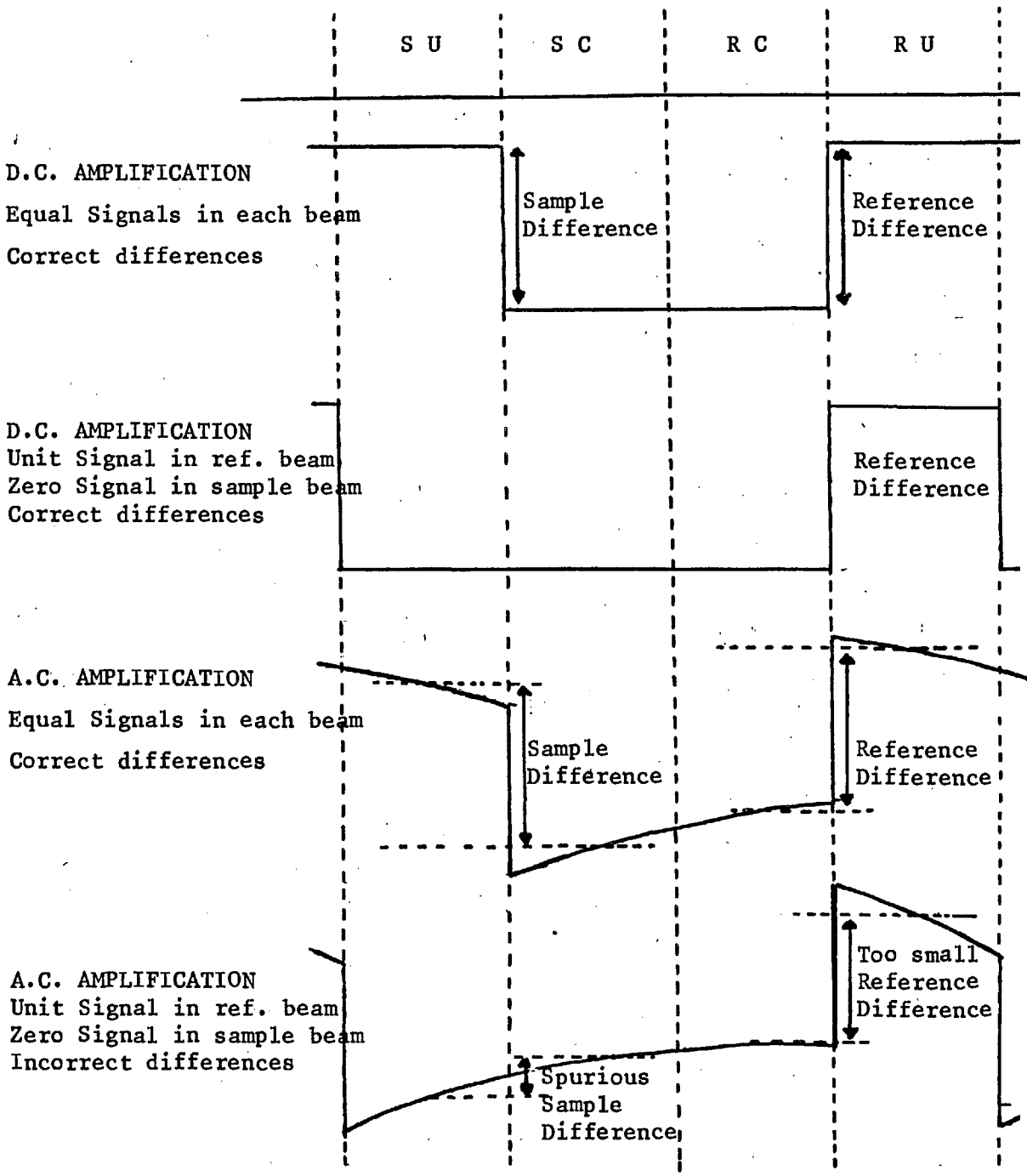

Figure 2:13 Beam Interaction as a result of the Limited Low Frequency Response of the Amplifier

in Figure 13 D, then a spurious integrated signal difference is still obtained for the zero signal while the other signal difference is reduced to some value below unity by the finite time constant of the amplifier. The magnitude of this beam interaction decreases as the low frequency response of the A.C. coupled amplifier increases. The amplifier chain must, therefore, have a long overall time constant, greater than 1 second, so that the interaction is reduced to negligible proportions, about 2% (i.e. if the transmission of one beam drops from 100% to 0% the value recorded by the other beam falls by 2%).

The output from the Golay cell is first amplified by a low noise, battery powered Phillips measuring amplifier (type GM 4574) mounted close to the cell itself so as to reduce mains pickup from the leads and power supplies. The output from this amplifier, which is around 0.1 volts, r.m.s., goes via a sensitivity control (a potential divider of wide attenuation range) to the main amplifier, whose circuit is shown in Figure 2:14. This consists of two ECC 83's in cascade with generous feedback around the output pair and a high frequency attenuation RC network with a turnover point variable from between 40 and 1,000 Hz. This removes only very high frequency noise and, in practice, no circumstances have been found when any benefit is derived from its use. It had been intended to use it to remove high frequency noise that would otherwise overload the amplifier at high gain settings. In practice it has been found that if the noise is sufficiently high to overload the amplifier then it is also too high for the recording of spectra.

The power supply for this amplifier and the subsequent resolution circuit is supplied by a Phillips stabilised power supply (type PE 4882). The H.T. for the Golay cell is also derived via extensive RC smoothing networks from this supply. The low frequency response of the whole amplifier chain extends to at least 0.2 Hz (-3 db) to minimise beam interaction.

The long time constants of the capacitor-couplings in the circuit have the disadvantage that sudden overloading of the amplifier by transients

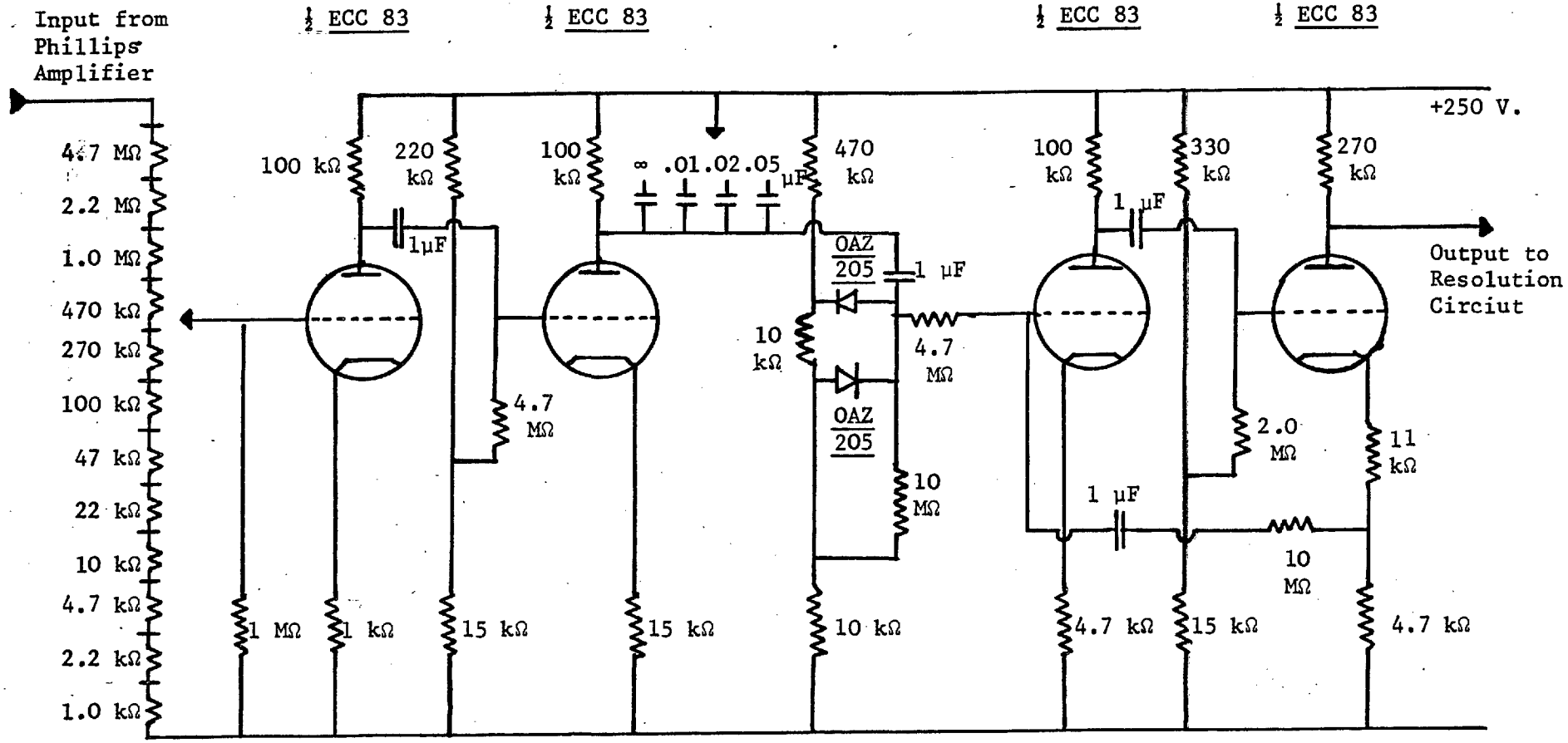

Figure 2:14 Circuit Diagram of Main Amplifier

take a long time to clear. For this reason a peak clipping network of two Zener diodes was inserted between the second and third stages to prevent any signal capable of overloading the output stages from reaching them. In actual operation this is extremely rare and arises only under fault conditions.

This peak clipping system and the very large amplifier gain, about 30 db greater than required, arose from the fact that much of the development work was performed on a Golay cell which subsequently proved to be defective both in the magnitude of its output signal and in its propensity to overload, as a result of air leaking into the argon filled cell. The output of the main amplifier is typically about 10 volts superimposed on an anode voltage of 100 volts and is direct coupled to an ECC 82 in the cathode follower configuration; its low anode resistance enables this valve to follow voltages rising well above 100 volts in this configuration. This acts as a low impedance signal source for the resolution circuits.

2:3:2:2 Resolution Circuits

The operations which this circuit must perform are:

1) It must separate each phase of the signal, allowing for any dead time in between phases.

2) It must record for subsequent comparison the smoothed voltage of each.

3) It must subtract chopped from unchopped signals for both sample and reference beams and output both results.

4) It must divide the sample signal by the reference signal and record that.

2:3:2:2:1 Separation of each phase of signal

It was decided to perform this in as flexible a manner as possible so as to be able to find out empirically what percentage of each signal could be retained and whether the optical and electronic phasings could, with advantage, be shifted relative to each other. It was decided to

select, by direct switching, the desired section of each phase and to integrate it separately. In this way all the noise frequencies higher than the chopping frequency are totally removed without the circuit losing any of the time resolution of the interphase periods which would have been incurred by prior high frequency attenuation.

The obvious method for integrating a voltage is by an RC network and this also provides a capacitor on which the integrated voltage can be stored for subsequent comparison with the succeeding one, so that the subtraction function can be carried out. The use of capacitor storage methods, however, requires switching with a very high open circuit resistance to prevent leakage and a very low closed circuit resistance so that the capacitor can be quickly discharged ready for the next phase. It was felt that mechanical switching rather than valve or transistor switching more nearly met this requirement and, with the introduction of reed-relays with switching times of around 1 millisecond and low load endurances of 10^9 operations, the design of the circuit was straightforward.

Total flexibility of all switching functions was achieved by driving the reed-relays from a series of sectors driven by a synchronous motor at the same speed as the optical choppers. These sectors interrupt the illumination of a number of phototransistors (Mullard type OCP 71) whose amplified output actuates the relays. The reed-relays employed (E.R.G., Luton, Bedfordshire type 1600) require only 160 mW to operate them so a very simple transistor amplifier culminating in an OC 72 transistor operating in the emitter-follower mode suffices to drive them. The power supply for this section of the circuit is an 18 volt 0.5 amp transistorised power supply (A.P.T., Byfleet, Surrey type TSU-0500). The circuit is shown in Figure 2:15.

The optimum timings, rejection periods of interphase signals, etc. can therefore be altered at will by altering the geometry of the sectors, their relative positions on the motor shaft and the phasing between this

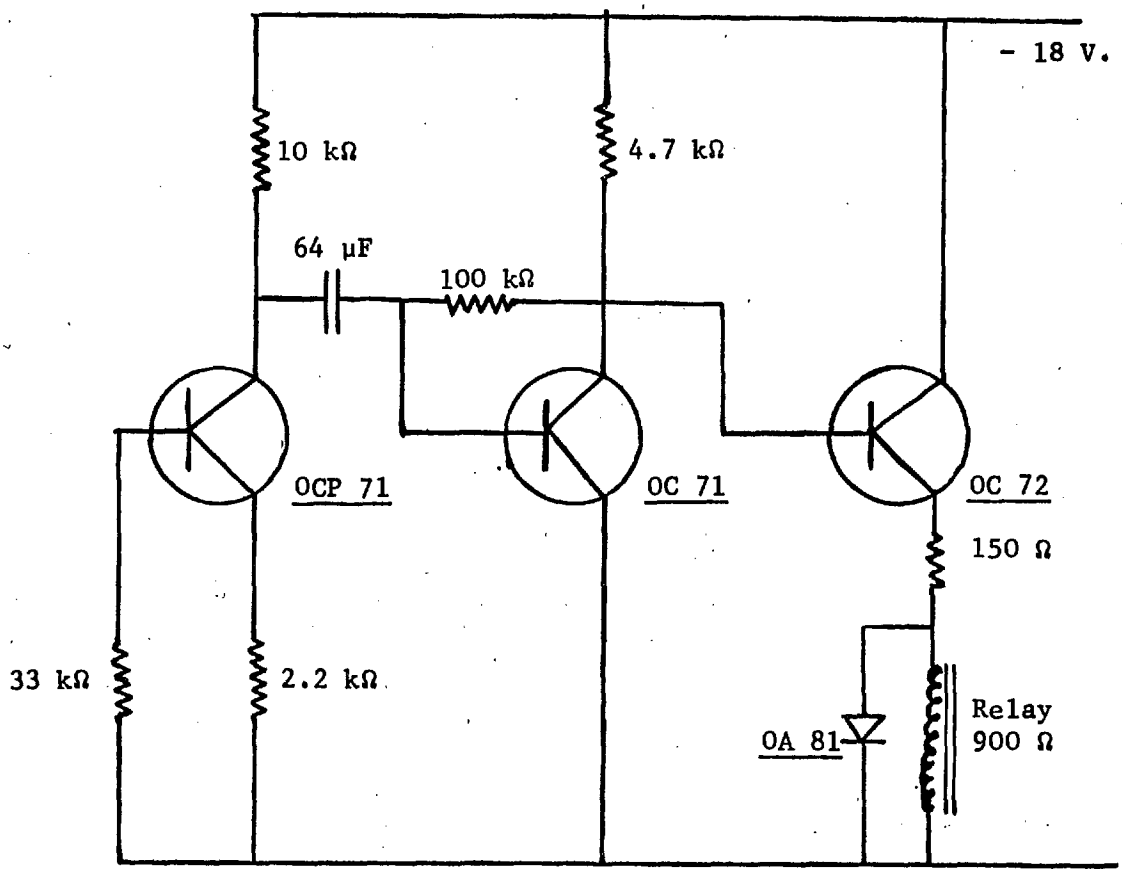

Figure 2:15 Driving Circuit for the Reed Relays

synchronous motor and those driving the optical choppers. While the purely static electronic equipment is left on permanently, the relay section is only energised during actual running of spectra to prolong the lifetimes of the relays. The contacts marked SB in Figures 2:16 and 2:18 are closed when the relays are not in operation, to anchor the respective valve-grids at levels that will not cause excessive anode-currents

2:3:2:2:2 Signal Separation, Integration and Subtraction

These operations will be considered together. The electronic circuit is shown in Figure 2:16 and the operation of the circuit may be followed by reference to Figure 2:17 which illustrates the relative phasings of the switching components.

The input to the circuit is from the cathode of an ECC 82 at a quiescent voltage of about 100 volts, upon which about 10 volts of A.C. signal are superimposed. At the commencement of SU, SW-1 transfers the signal voltage from the cathode-follower of the ECC 82, V_{1a}, to the integrating network R_1C_1; the shorting switch SW-4 opens and integration of SU commences. V_{2a} in the cathode-follower mode reproduces this voltage (plus the constant cathode-grid spacing of about 3 volts) at its cathode. At the change-over to SC, SW-1 transfers the signal to integrating network R_2C_2; SW-5 opens and this phase is integrated and represented, again plus a constant cathode-grid potential, at the cathode of V_{2b}. There is no leakage from C_1 in the absence of grid current of V_{2a}; hence this voltage is constantly stored on C_1 and reproduced by the cathode of V_{2a}. Consequently at the termination of SU,SC, both cathodes now carry the voltages corresponding to these phases, and the voltage-difference between them is (SU - SC).

It may be noted that the elimination of the D.C. component of the input, which may be an order of magnitude greater than the signal, is achieved by the use of the other half of V_{1a}, i.e. V_{1b}, as a cathode-follower

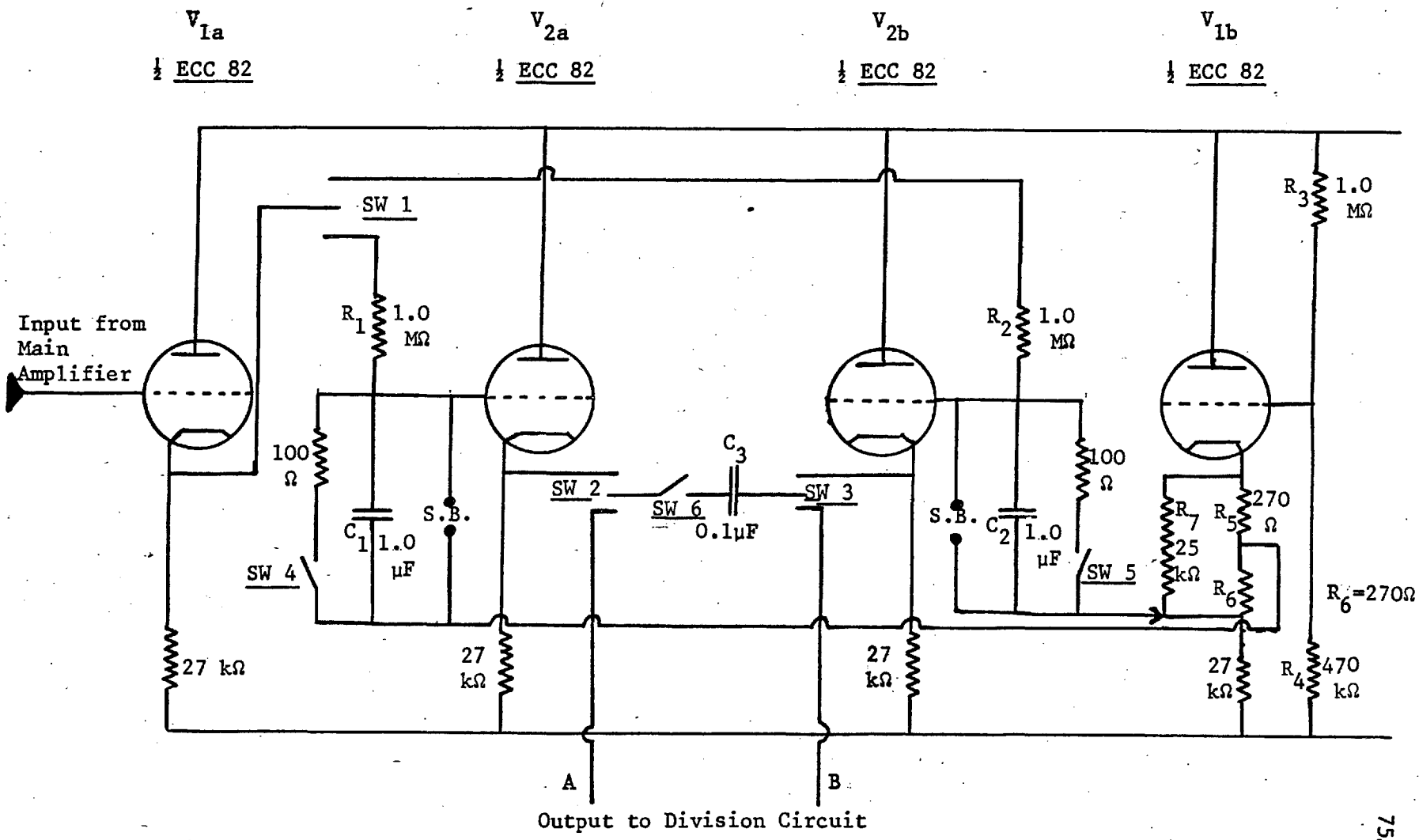

Figure 2:16 Circuit Diagram for the Resolution Circuit

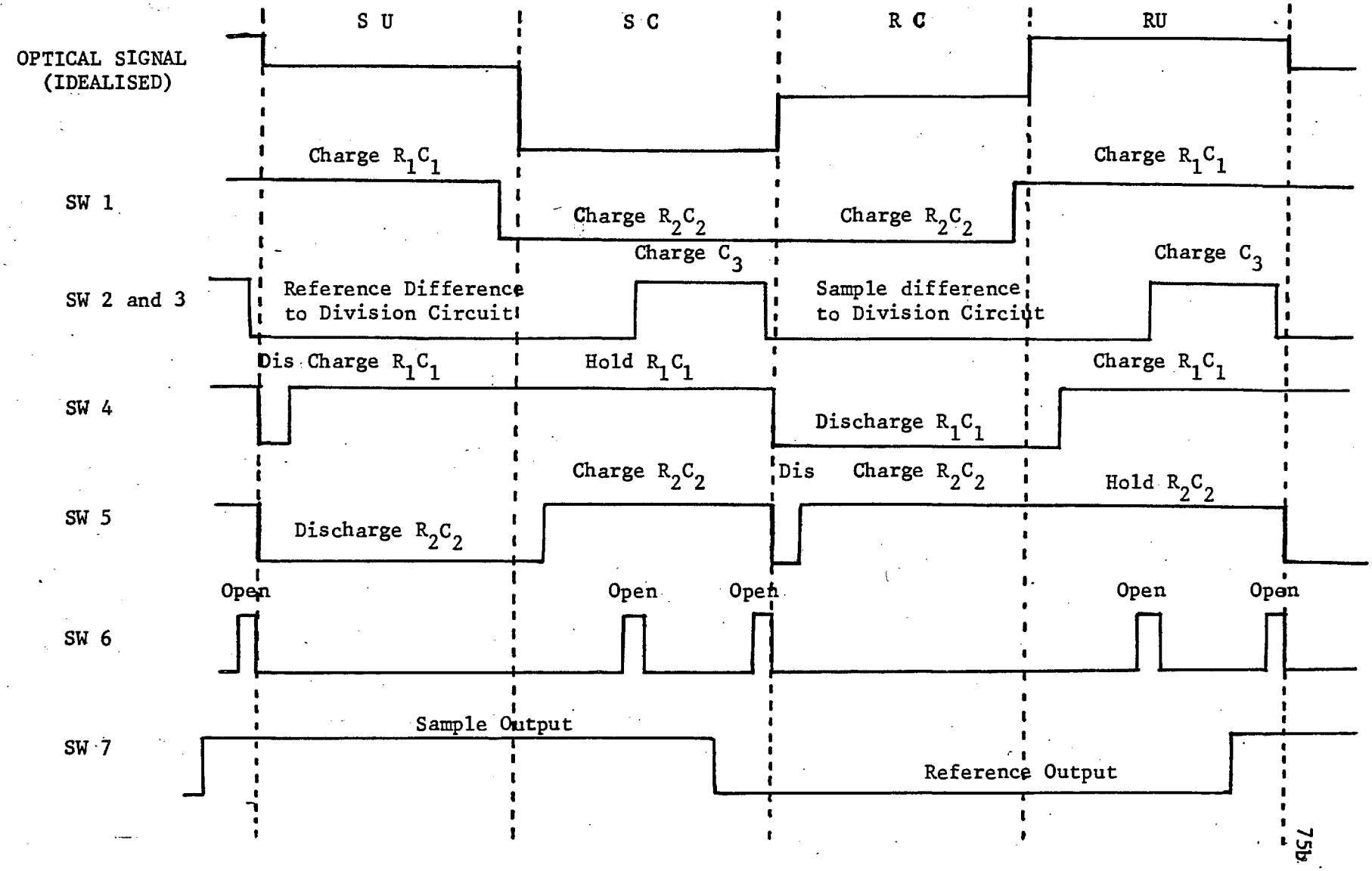

Figure 2:17 Relative Phasings of the Switching Components in Resolution Circuits

held at a potential as near as possible that of the quiescent signal input by the potential-divider R_3R_4. This system has the advantage, firstly, that since input voltage and reference are handled by the two halves of one valve, any drift due to variation of HT supply, etc. is likely to be mutual and to cancel, and secondly, the cathode of V_{1b} from which the base-voltage against which the signals are integrated supplies this voltage at the very low impedance characteristic of this mode of operation, and so is much less affected by charging currents than a straight potential-divider would be.

The time-constants of R_1C_1 and R_2C_2 are each one second, made equal by careful selection of high-stability resistors, R_1,R_2, until the voltages developed on C_1 and C_2 by their successive integration of a constant voltage were exactly equal. In this way any possible imbalance in their respective integration-times due to uneven-ness of the switching sectors was cancelled. This time-constant is perhaps needlessly long: for while perfect integration of a signal is only achieved by an RC network for a time which is short compared to its time-constant, the use of a 1-second time-constant to integrate signals of about 60 msec implies that the voltages stored on C_1 and C_2 are only some 5% of the values of the average signal excursions at the input. A time-constant of 0.1 seconds, giving about 40% of the signal value transferred to the capacitors, would probably have given adequate integration without undue weighting of the integral in favour of the initial periods of each phase. However, as explained previously (Section 2:3:2:1) there was a great reserve of gain in hand and, having provided this excess gain, nothing was lost by the more perfect integration. In fact the voltage-difference developed across the cathodes of V_{2a} and V_{2b} at the end of SU;SC does not quite represent the difference between these phases, for although the signals are handled by the two halves of the same valve, the cathode-to-grid voltages of the two halves are not quite identical. This small deviation would appear as a constant error in the ultimate outputs of sample and reference signals, almost certainly small compared to the constant voltages

later to be added or subtracted from them for the zeroing purposes of pen-recording display. Nonetheless it was considered worthwhile to remove this small source of error by the network $R_5R_6R_7$, which allows the base-voltages of the integrators R_1C_1 and R_2C_2 to be altered slightly so that, after successive integrations of a constant input voltage, the intercathode voltage between V_{2a} and V_{2b} could be made exactly zero. In this way completely accurate signals were available from this part of the circuit if, for example, digital presentation of them was contemplated.

Returning to the signal integrating cycle represented by Figure 2:17, it is observed initially that the next two phases, RC and RU, are in reverse order to those of the sample. Both RC networks are reset to zero by the closing of SW-4 and SW-5 for a suitable interphase period (about 6 millisec) before SW-5 opens to commence the integration of R_2C_2. SW-4 remains closed for the duration of this phase and its following interphase period, while SW-1 is charging R_2C_2, but following the switching of SW-1 back to R_1C_1, SW-4 opens and the integration of RU can commence.

Following the discussion given for the sample cycle;at the end of the cycle the voltage difference between the cathodes of V_{2a} and V_{2b} accurately represents (RU - RC).

Thus despite the asymmetry of the chopping-cycle, the unchopped phases always charge R_1C_1 and the chopped ones R_2C_2 , and the difference-voltage carried over by C_3 to the next part of the circuit is always in the correct sense.

The duration and phasing of the interphase 'dead times' is controlled by the shorting-switches SW-4 and SW-5, which by remaining closed for a controllable period after the initiation of any phase can remove as much of its leading-edge as experience indicates necessary. The electrical and optical chopping cycles can also of course be slightly displaced with respect to each other so that these dead periods can cover any part of

the actual optical transitions. At present about 6 msec are eliminated between 60 msec phases, approximately covering the central half of the 'slope' between signal levels observed on an oscilloscope.

It has been observed that the optimum phasing between the electronic and optical choppers, for the minimisation of beam interaction, discussed in Section 2:3:2:1, and the elimination of zero drift due to differences in temperature between the two cells, do not coincide. This suggests that the interphase rejection period is too short at present and should be increased to the region of 10 msec.

Returning to the electronic circuit of Figure 2:16, the intercathode voltage on V_{2a} and V_{2b}, representing (SU - SC) is impressed across the 0.1 Microfarad capacitor C_3 by SW-2 and SW-3, with SW-6 closed. The time-constant represented by this capacitor and the effective output impedances of the two cathodes is so low (around a few hundred microseconds) that the time of introduction of C_3 across the cathodes during SU, SC is not at all critical. In fact it is introduced about half-way through SC, so having some 30 msec to acquire the inter-cathode potential. The actual termination of SC is caused by the opening of SW-6, which isolates C_3. At first it had been hoped that this termination could be achieved by the simultaneous change-overs of SW-2 and SW-3, which transfer the recorded difference to the next stage of the circuit: but even a few tens of microseconds of contact bounce in either of these relays, momentarily connecting say the cathode of V_{2a} with point B, resulted in a flow of charge rendering meaningless the voltage transferred by C_3. SW-6 was therefore needed to isolate C_3 during its transferrals by SW-2 and SW-3.

After SW-6 is opened, SW-2 and SW-3 are opened to the ratio portion of the circuit (Section 2:3:2:2:3) to present the sample difference (SU - SC) to this portion of the electronics for further processing. Half-way through RC, SW-2, SW-3 and SW-6 are closed to impress the reference difference (RU - RC) on C_3 and this is similarly presented to the ratioing circuit during the first portion of the sample cycle.

2:3:2:2:3 Division of Sample Signal by Reference

This is achieved by means of a re-transmitting slidewire on one of the pens of a two-pen potentiometric recorder. Before this can be achieved, however, the sample and reference differences being received from C_3 must be processed into a suitable form. The circuit for effecting this is shown in Figure 2:18.

The circuit receives successive voltages from C_3 across points A and B representing the values (SU - SC) and (RU - RC), and has the relatively simple task of switching them alternately between the 'sample out' and 'reference out' terminals, smoothing them free of chopping frequencies and providing zeroing controls so that they can be conveniently displaced to any region of a two-channel pen-recorder's travel.

The voltages on C_3 are transferred successively to the grids of ECC 83's V_{3a} and V_{4a} by SW-7; the base voltage on which these signals are superimposed is provided by the potential divider R_8R_9,$R_{10}R_{11}$ and is about 5 volts positive with respect to earth, which provides flexibility in zeroing ability.

In order to reduce switching frequency components in the two outputs, thecapacitors C_4 and C_5 are incorporated to store the charge on the valve grids, without appreciable drift, while C_3 is either transferred to the previous circuit or charging the other output section. C_4 and C_5 must, at the same time, be small enough to be completely swamped by the charge on C_3 when it is paralleled with them: 0.001 Microfarad was found a satisfactory value. This implies that each cycle, as represented by the voltage on the cathodes of V_{3a} and V_{4a}, will "remember" the previous one to only about 1%. As the possible use of digital, cycle-by-cycle punched-tape recording of spectra on this machine for computer reduction was envisaged, such a provision is important.

The zeroing controls are provided by backing-off cathode-followers V_{3b} and V_{4b}, with the other halves of their respective signal valves to

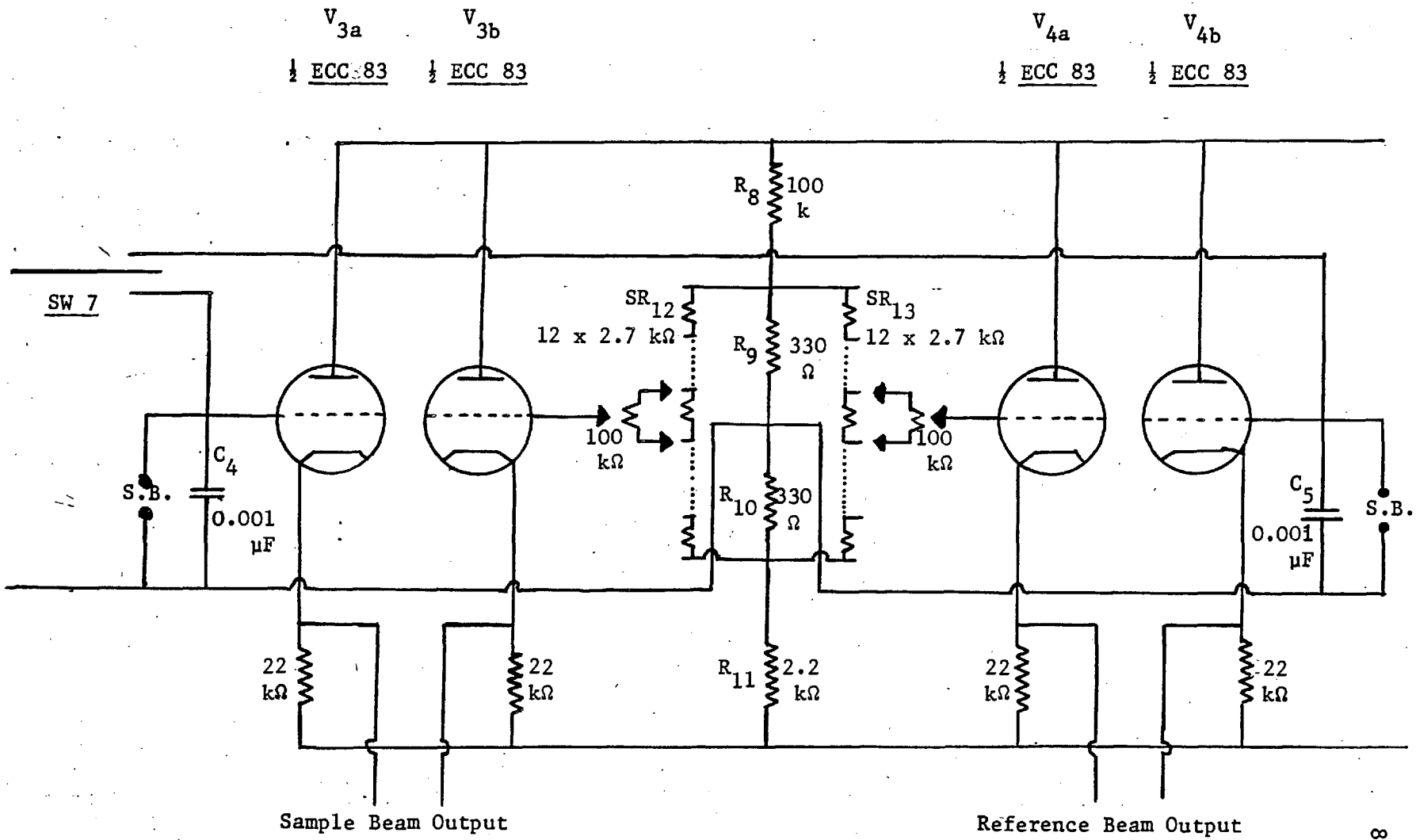

Figure 2:18 Circuit Diagram for the Division and Zeroing Circuits

minimise possible drift. The elaborate potential divider-chains SR_{12} and SR_{13} provide coarse and fine zero adjustments so that the two outputs (the differences in cathode-potentials within the two halves of V_3 and V_4) may be presented on any section of the two-channel recorder currently employed.

The presentation of the ratio of the energies in the two beams is a valuable ability, and is indeed one of the main raisons d'etre of a two-beam instrument. Several possible methods of achieving this presented themselves, including digital computation, the use of logarithmic diodes, operational amplifiers or a re-transmitting slidewire on the two-channel pen-recorder.

It is difficult to obtain manufactured diodes guaranteed to be accurately logarithmic over a wide range. The other disadvantage of these is that the voltage across them is logarithmically proportional to the current they carry: hence they ideally require a signal current derived from a source with a very high output impedance. This is quite the opposite situation from that of the output of this equipment, which explicitly employs cathode-follower outputs to present signal voltages from a low impedance.

A suitable operational amplifier could not be found and it was decided to use a two-channel potentiometric pen-recorder with a 10 kilohm re-transmitting slidewire. The recorder chosen was a Texas Instruments FS02 W5A Two-channel Recorder.

The principles of the ratioing circuit are shown in Figure 2:19.

The functioning of the green recorder has been altered so that it no longer seeks zero potential difference between its input and the signal derived from its slidewire but now is driven directly by the input signal. At a given instant let the voltage derived from the green slidewire be V volts and let this be applied across the re-transmitting slidewire of the red pen. The position of the red pen is governed by the

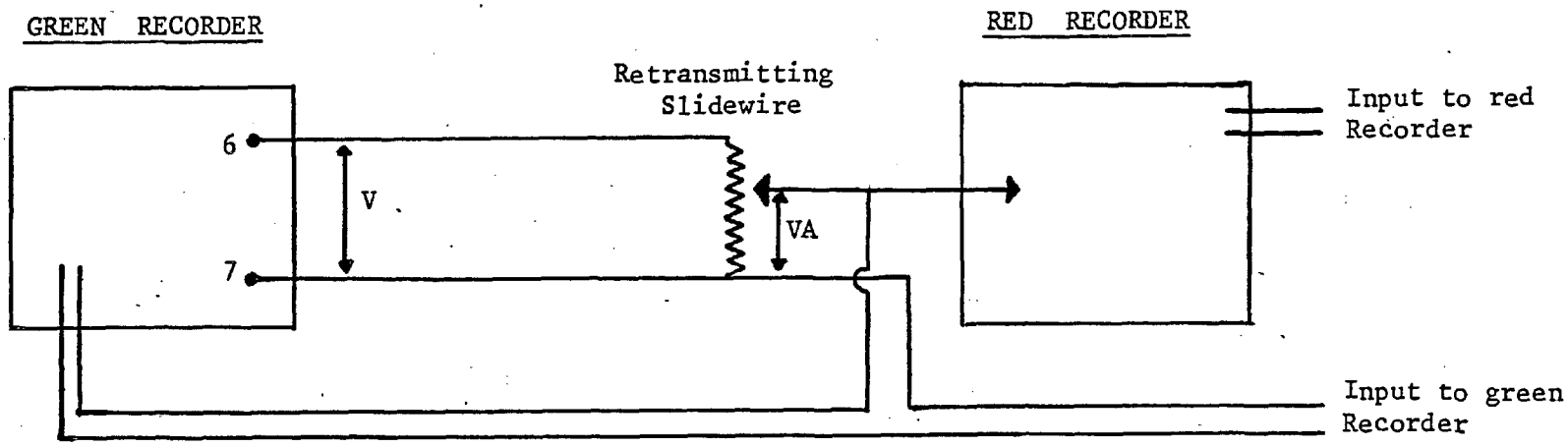

Figure 2:19 Schematic diagram Illustrating Principles of the Ratioing Circuit

input signal,A, the voltage between the wiper and the end of the re-transmitting slidewire is therefore VA volts, and this is applied together with the second signal,B, to the input of the green recorder. Since the green recorder is being driven by this input, in the stationary state:

$VA = B$ or V = Displacement of Green Pen = $B/A = \frac{\text{SAMPLE SIGNAL}}{\text{REFERENCE SIGNAL}}$

The practical ratioing circuit is shown in Figure 2:20.
The so-called double 'single' beam operation will be described first. In this the red pen shows directly the radiation intensity in the reference beam and the green pen the intensity in the sample beam. In this mode of operation the cathode outputs of V_{3a}, V_{3b} and V_{4a},V_{4b} are connected across the input terminals of each recorder channel by an RC network as shown for the red channel in figure 2:20. Four time constants are available as shown in Table 2:3.

TABLE 2:3

Time Constant	1	2	3	4
Value of C_1 and C_3 in μF	0.5	0.5	2.5	2.5
Value of C_2 in μF	0.5	2.5	2.5	8.5

The full scale deflection of either pen may be independently altered by the input attenuator provided on the face of the recorder: this facility is provided by replacing the fixed resistance on the span card of the recorder between terminals H and K by the values given in Table 2:4.

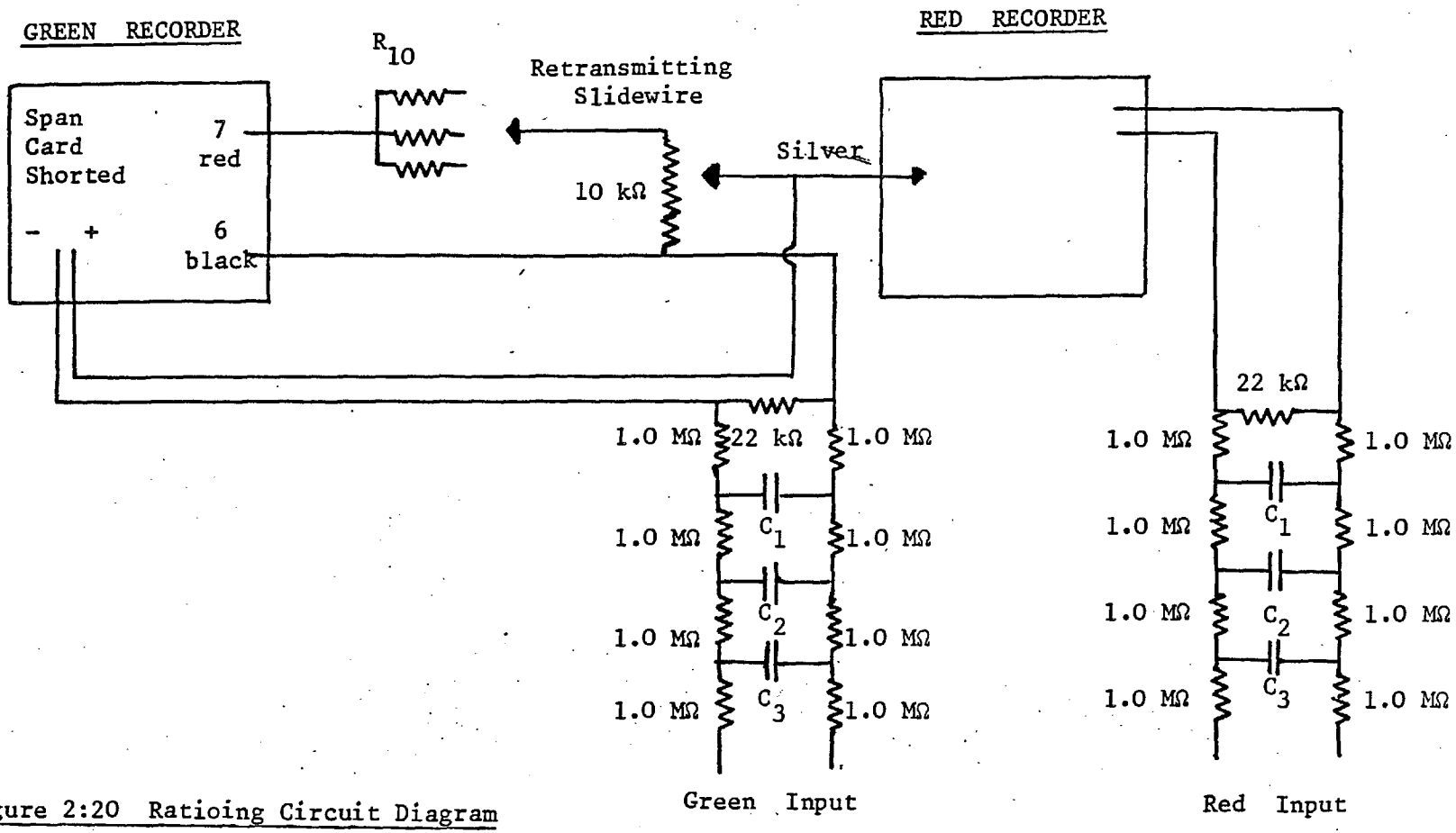

Figure 2:20 Ratioing Circuit Diagram

TABLE 2:4

Value of Resistance in ohms	100	150	220	500	1000	2200
Approximate full scale deflection in mV	1	1.5	2.2	5	10	22

Double beam operation in which the red pen records the radiation intensity in the reference beam and the green pen the ratio of the intensities in the sample and reference beams is effected by operation of a switch on the face of the recorder. This switch does not alter the operation of the red pen in any way but alters the green pen in the manner described above. The operation of the switch is summarised in Table 2:5.

TABLE 2:5

		Single Beam	Double Beam
Range Card	H - Black	Shorted to J	Shorted to K
	J - Red	H and attenuator	Transformer White
	K - Green	S.B. attenuator	Shorted to H
Transformer White		Pin W (grey Co-ax)	Red from J
Pin 6	P.T.F.E.	-	Attenuator slidewire
7	Red P.T.F.E.	-	Double beam scale
Retrans Slidewire	red	-	Double beam scale
	black	-	Pin 6 - attenuator
	silver	-	22K - E.A. black
Error Amplifier	Black	22K and attenuator	22K - slidewire
	Red	Red of attenuator	Red of attenuator

It will be observed that the RC filtering network on the green pen functions identically in both single beam and double beam operation.

In the latter case the single beam input attenuator no longer functions and is replaced by a double beam scale control. The function of this is to alter the potential difference across the re-transmitting slide-wire for a constant position of the green pen by altering the value of R_{10} (Figure 2:20). The values of R_{10} and its effect on the 100% transmission line as observed on the recorder are shown in Table 2:6. It should be noted that the position of the 0% transmission line remains on the recorder zero irrespective of the value of R_{10}.

TABLE 2:6

Value of R_{10} in Kohms	20	33	47	75	150	315
V. across retrans. in mV	513	358	270	181	96	47
V/V_{358}	1.43	1.00	0.75	0.51	0.27	0.13
Position of 100% trans line on recorder	67.5	100	130	200	400	750

Potential difference across pins 6 and 7 = 1.54 volts

The effect of altering R_{10} is, therefore, to expand the ratio scale. It should be noted that due to the end effects in the re-transmitting slide-wire the green zero should be offset by 5 divisions of the recorder with respect to the red pen in order to obtain a perfectly flat 100% trans-mission line as shown in Figure 3:18

With a conventional single pen, double beam ratio recorder there is no indication when the energy in both beams has fallen so low, due to solvent absorption, end of reststrahlen reflection, etc., that their ratio no longer has any meaning: this may result in the acceptance of spurious bands in such regions. In this system , the simultaneous presentation of both the ratio and the reference beam intensity enables

the significance of any alteration in the ratio to be immediately assessed.

2:3:3 Conclusions

The effectiveness of the whole electronic system depends on the reliability of the reed-relays and the optical driving circuits which define their switching times. Oscilloscope studies show that while 1.5 msec is typically required for a change-over reed to operate, with one or more bounces occurring, jitter in the system (random variation about the mean switching-initiation time) was not detectable on the oscilloscope used (Telequipment D52) even at maximum practicable time-base expansion, and must therefore be less than 10 microseconds. No noise in the output due to jitter could be detected and, as should be the case, the noise-limit is set by optical noise in the detector.

The phasing of the switching circuits is perfectly held. This is true both in the short term, in that slippage between the four synchronous motors of the system has never occurred, and in the long term in the sense that gradual alteration in the relative phasing of the relays, possibly due to ageing of them or their driving circuits, has not been observed over a period of ten months. It is estimated that the relay's lifetime of 10^9 operations suffices for a year's actual running time (about 6 miles of chart-paper) before the replacement of the reeds, a simple operation, becomes necessary.

Altogether the operation of the electronics of the spectrometer has been perfectly satisfactory over the first eighteen months of their use, justifying the basically simple concept of their design.

3) OPERATION AND PERFORMANCE OF FAR INFRA-RED SPECTROMETER

3:1 CALIBRATION

The problems associated with the calibration of far infra-red spectrometers has been discussed by Plyler (97). In general two methods may be used.

3:1:1 Calculation

The diffraction formula for a grating is

$$n\lambda = d(\sin\gamma \pm \sin\psi) \qquad \text{EQUATION 3:1}$$

where d = groove separation

γ = angle of incidence

ψ = angle of diffraction

n = order of the spectrum

If the spectra are brought into view by rotation of the grating with fixed angles of incidence and diffraction, as in this instrument, then, for the first order spectrum

$$\lambda = 2d \cos \alpha/2 \sin\theta \qquad \text{EQUATION 3:2}$$

where θ = angle of rotation of the grating from from specular position

α = angle between the incident and diffracted beams

The frequency at any given rotation of the grating is therefore given by

$$\nu = (1/2d) \operatorname{cosec}\theta \sec \alpha/2 \qquad \text{EQUATION 3:3}$$

This frequency may therefore be calculated with an accuracy dependent on the uncertainties in d, θ and α.

α is a constant dependent on the geometry of the monochromator and in this instrument is approximately 28°.

θ may be estimated from the fiducial marks placed on the chart by the rotation of the grating shaft, providing the reading corresponding to the specular position is known.

By an iterative procedure the uncertainties in d and α may be made negligible and the accuracy is then limited by the sharpness of the band which governs the uncertainty in the value of θ

3:1:2 Calibration Against a Known Spectrum

Since it may be readily introduced into the optical path, water vapour provides a very convenient method of calibration. The low frequency spectrum, 18 to 111 cm^{-1}, has been tabulated by Hall et al. (98) and the best high frequency values, 53 to 300 cm^{-1}, by Plyler (97).
Since the bands are irregularly spaced and of unequal intensity only a very approximate, $\pm$ 50 cm^{-1}, idea of the frequency is required to ensure correct correspondence between the observed bands and those illustrated in the literature. In practice, to ensure the correct assignment of each band, a calibration curve of 'pip mark' against frequency is drawn from the observed bands and their frequencies as given in the literature: clearly this curve should be a smooth cosecant curve. As a further check the frequencies may also be calculated from the angle of rotation of the grating.

The number of water bands below 50 cm^{-1} is limited and insufficient to provide an adequate calibration, in this region it is necessary to observe the pure rotation spectra of linear molecules such as N_2O, which has a series of bands separated by approximately 0.8 cm^{-1}, or HCN where the band separation is about 3 cm^{-1}. The exact rotation frequencies as deduced from the rotational constants measured by microwave spectroscopy

have been tabulated by Plyler. Since the bands are approximately equally spaced and show only a slight decrease in intensity towards low frequencies it is necessary to know the approximate frequency at which the spectra are being observed to a much greater degree of accuracy than was the case with the water vapour spectrum, before a correct correspondence between the observed and literature spectrum can be achieved. In the case of the HCN spectrum it is necessary to know the frequency to within $\pm$ 1 cm^{-1} and this can only be achieved by a reasonably accurate calculation from the angle of rotation of the grating. The comparison method, therefore, has its greatest use in association with the water vapour spectrum.

3:1:3 Calibration of this Instrument

In the region 35 cm^{-1} to 350 cm^{-1} a 10 cm path length of atmospheric water vapour was used. Some pressure broadening of the lines was apparent at low frequencies which could be avoided by using a longer path length at a lower pressure, this, however, presents some problems in double beam use. Figure 3:1 shows a typical calibration run in the 2KCl reststrahlen region. From their relative positions and intensities these bands were associated with those in the published spectrum of Plyler and their frequencies inserted as shown. A graph of frequency against 'pip mark' produced a smooth curve with all the points lying on the curve. As a further check the frequencies were calculated, both for this region and for the 2KBr and the 2CsBr reststrahlen using Equation 3:1:1 and the values tabulated in Table 3:1.

The correspondence between the calculated values and those of Plyler are, in general, better than $\pm$ 0.1 cm^{-1}. The largest errors occur in those frequencies appearing in brackets which represent unresolved multiplets.

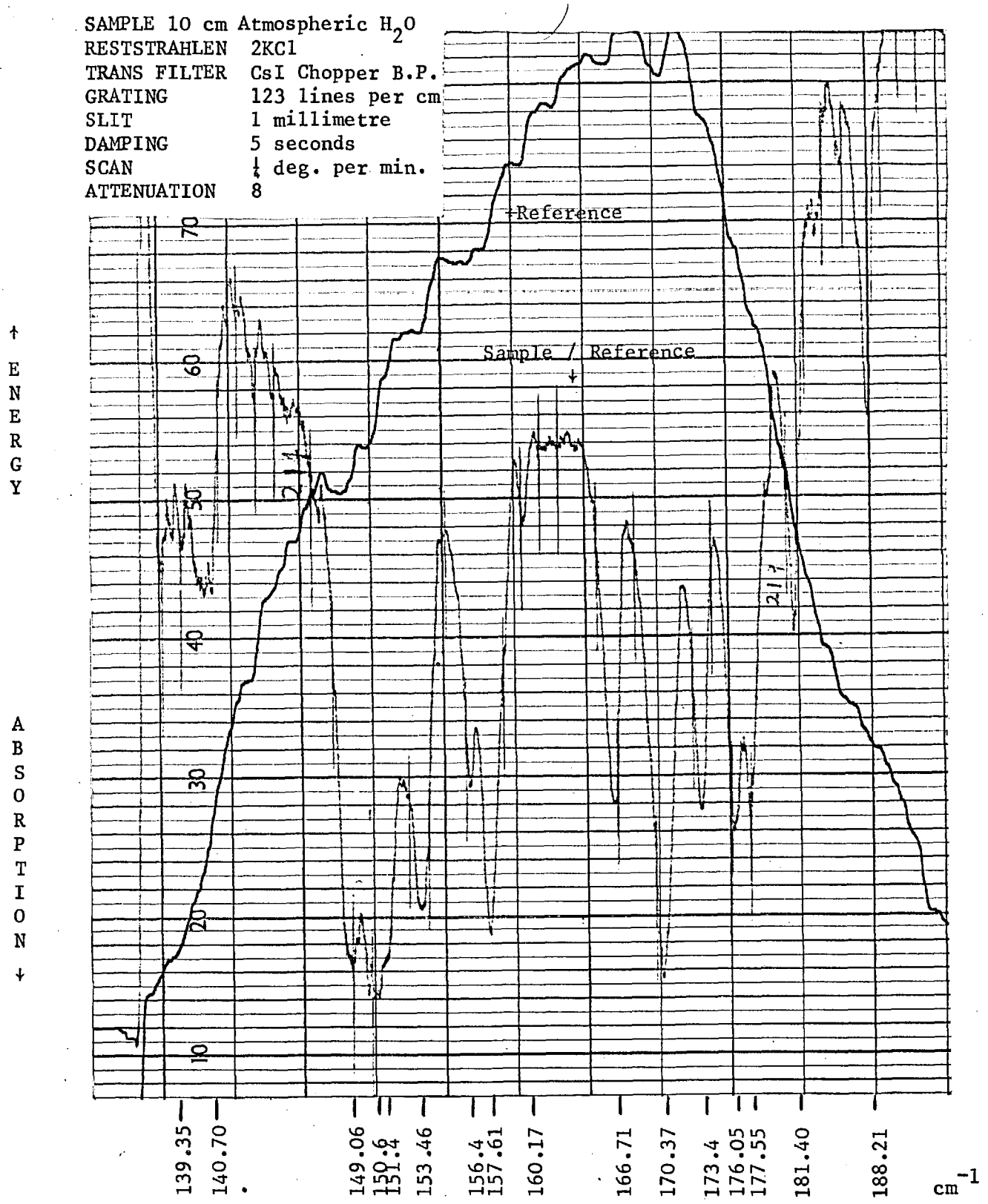

Figure 3.1 Calibration Run in the 2KC1 Reststrahlen Region

TABLE 3:1 CALCULATED WATER VAPOUR ABSORPTION FREQUENCIES

$\nu = 63.47 \operatorname{cosec} \theta$

Plyler	'pip No"	θ	ν calculated	ν calculated $- \nu$ (Plyler)
193.45	220.65	19.15	193.50	+0.05
188.21	220.00	19.80	187.41	+0.20
183.46	219.55	20.25	183.36	-0.10
181.40	219.30	20.50	181.24	-0.16
177.55	218.85	20.95	177.53	-0.02
176.05	218.65	21.15	175.94	-0.11
(173.4)	218.30	21.50	173.18	(-0.22)
(170.37) (169.93)	217.90	21.90	170.17	0.00
166.71	217.40	22.40	166.56	-0.15
161.79	217.70	23.10	161.77	-0.02
160.17	216.45	23.35	160.13	-0.02
157.61	216.05	23.75	157.60	-0.01
(156.4)	215.90	23.90	156.66	(+0.26)
153.46	215.40	24.40	153.64	+0.18
149.06	214.60	25.20	149.07	+0.01
140.70	213.00	26.80	140.77	+0.07
139.77	212.80	27.00	139.81	+0.04
139.02	212.65	27.15	139.10	+0.08
132.67	211.20	28.60	132.59	-0.08
127.02	209.80	30.00	126.94	-0.08
121.88	208.45	31.35	121.99	+0.11
120.12	207.90	31.90	120.11	-0.01
117.92	207.25	32.55	117.96	+0.04
111.11	204.90	34.90	110.93	-0.18
105.67	202.85	36.95	105.58	-0.07
104.55	202.40	37.40	104.50	-0.05
101.55	201.2	38.60	101.74	+0.19
100.53	200.65	39.15	100.52	-0.01
99.07	199.90	39.90	98.95	-0.12

TABLE 3:1 (Continued)

Plyler	'pip No'	θ	ν calculated	ν calculated −ν (Plyler)
96.11	198.50	41.30	96.16	+0.05
92.54	196.50	44.30	92.55	+0.01
89.53	194.70	45.10	89.61	+0.08
88.87	194.30	45.50	88.98	+0.11
88.06	193.70	46.10	88.08	+0.02
82.11	189.30	50.50	82.26	+0.15
80.98	188.20	51.60	80.99	+0.01
79.77	187.15	52.65	79.85	+0.08
78.97	186.35	53.45	79.01	+0.04
78.21	185.70	54.10	78.35	+0.14
77.54	184.70	55.10	77.39	−0.15
75.55	182.70	57.10	75.59	+0.04
74.09	181.00	58.80	74.20	+0.11
73.24	180.10	59.70	73.36	+0.12

For calibration below 50 cm^{-1} the spectrum of 20 cm pressure of HCN in a 10 cm path length cell was observed. The frequencies were calculated from Equation 3:3 using the empirical values of, d and α. A comparison between the calculated frequencies and those of Plyler are shown in Table 3:2.

There appears to be a slight systematic error, probably arising from an error in d or α which could be eliminated by an iterative procedure if desired: in this instance the observed accuracy of $\pm$ 0.05 cm^{-1} was, however, adequate.

The procedures described can readily give an accuracy of $\pm$ 0.1 cm^{-1} in the calibration, which is adequate for most applications in far infra-red spectroscopy where the band widths are relatively broad, for instance in the low frequency interionic vibrations to be described the average line width at half height is in the region of 50 cm^{-1} so little purpose is served by attempting to increase the accuracy of the calibration.

TABLE 3:2 OBSERVED AND CALCULATED HYDROGEN CYANIDE ABSORPTION FREQUENCIES

ν = 10.15 cosec

θ_o = 599.60

J	ν Plyler in cm^{-1}	'pip No'		ν calc	ν calc $-\nu$Plyler
0	2.96				
1	5.91				
2	8.87				
3	11.83				
4	14.78	556.0	43.8	14.66	-0.02
5	17.74	564.6	35.00	17.69	-0.05
6	20.69	570.2	29.4	20.66	-0.03
7	23.65	574.2	25.4	23.66	-0.01
8	26.60	577.1	22.5	26.53	-0.07
9	29.55	579.5	20.1	29.54	-0.01
10	32.51	581.4	18.2	32.50	-0.01
11	35.46	583.0	16.6	35.52	+0.06
12	38.41	584.3	15.3	38.46	+0.05
13	41.36	585.4	14.2	41.37	+0.01
14	44.31	586.4	13.2	44.44	+0.13
15	47.26	587.2	12.4	47.27	+0.01
16	50.20	587.95	11.65	50.24	+0.04
17	53.14	588.60	11.00	53.19	+0.05

3:2 Spectral Slit Width

The wavelength of the radiation diffracted by the grating, in the first order, is given by Equation 3:3 as

$$\lambda = d \ (\sin \gamma \pm \sin \psi)$$

The experimental case most frequently encountered is shown in Figure 3:2

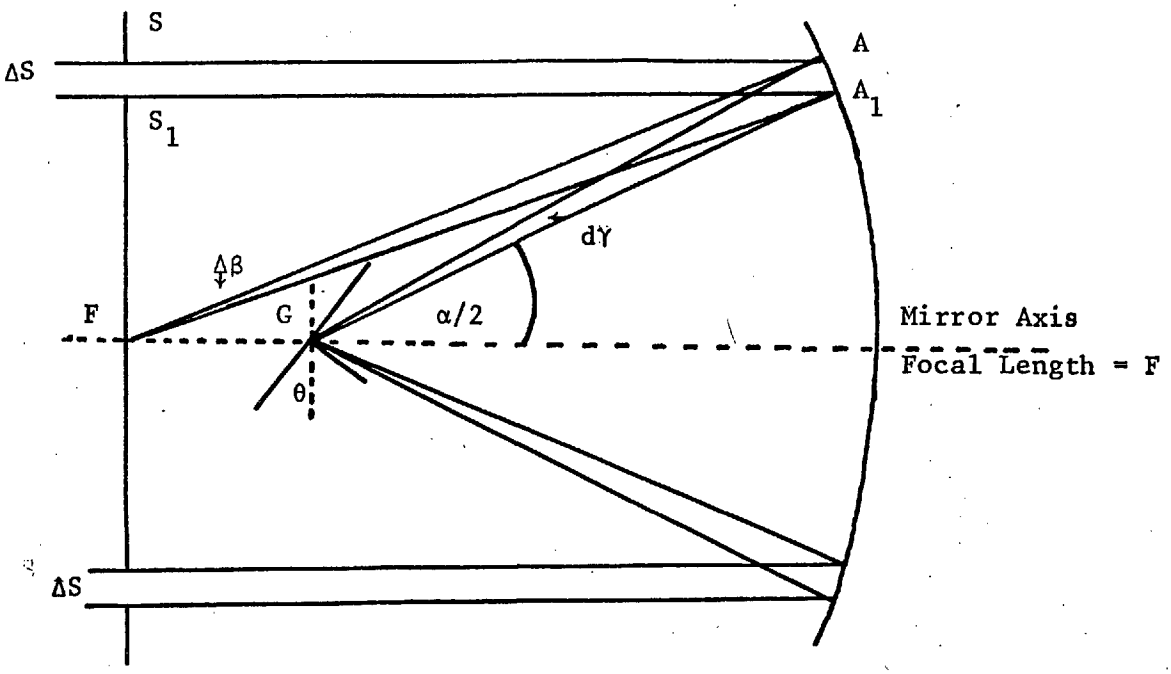

Figure 3:2 Diagram of Monochromator to show Spectral Slit Width

In this case the incident and diffracted rays are both on the same side of the grating normal and the diffracted wavelength is given by

$$\lambda = d \ (\sin\gamma + \sin\psi \ )$$ EQUATION 3:4

The spectra are brought into view by the rotation of the grating, therefore the angles of incidence and diffraction are related to the

angle of rotation of the grating, θ, and the angle between the incident and diffracted rays, α (which in this monochromator is 28^{o}) by

$$\gamma + \psi = 2\theta$$

$$\gamma - \psi = 2\alpha$$

Equation 3:4 may be differentiated to give $d\lambda$

$$d\lambda = d\cos\gamma\ (d\gamma)_{\psi} + d\cos\psi\ (d\psi)_{\gamma}$$

$d\gamma$ must by symmetry be equal to $d\psi$ and may be related to the mechanical slit width, s, by the construction shown in Figure 3:2

Any ray such as SA or SA' parallel to the mirror axis will be reflected towards the focal point, therefore

$$s = F\,\Delta\beta$$

The required angle $d\gamma$ equal to AGA' is, to a first approximation, equal to $\Delta\beta$ since the grating is not significantly in front of the focal plane of the mirror. Therefore

$$d\lambda = (ds/F)\ (\cos\gamma + \cos\psi)$$

and

$$\lambda/d\lambda = \nu/d\nu = (F/s)\ (\{\sin\gamma + \sin\psi\}/\{\cos\gamma + \cos\psi)$$

$$= (F/s)\ \left(\sin\frac{\gamma+\psi}{2} \Big/ \cos\frac{\gamma+\psi}{2}\right)$$

$$= (F/s)\ \tan\theta \qquad \text{EQUATION 3:5}$$

For the alternative case where the incident and diffracted rays are on opposite sides of the grating normal the above analysis may be repeated with suitable changes in the relationships derived to give the identical relation for $\nu/d\nu$.

We have seen in Equation 3:3 that θ may be expressed in terms of the frequency and the grating constant, d, if we approximate the formula by

taking sec $\alpha/2$ equal to unity then we may substitute the value of $(4d^2\nu^2 - 1)^{-\frac{1}{2}}$ for $\tan\theta$ in equation 3:5 to give:

$$d\nu = (\nu s/F) (4d^2\nu^2 - 1)^{\frac{1}{2}} \qquad \text{EQUATION 3:6}$$

This is the equation relating the spectral slit width in wavenumbers to the mechanical slit width in centimetres.

For the specific case of light incident normally on the grating the same relation may be derived from the equation given by Strong (23) relating the slit width in wavenumbers and centimetres, i.e.

$$\nu = s/ F \lambda^2 d\gamma/d\lambda$$

Previous workers in this laboratory have calculated spectral slit widths from the relation:

$$d\nu = (\nu s/ 2D) (4d^2\nu^2 - 1)^{\frac{1}{2}}$$

where D = distance from the slit to grating

The values of the spectral slit widths used by these workers must, therefore, be mulitplied by a correction factor of approximately 3.6 to take into account the difference between twice the slit to grating distance, 106 cms, and the focal length of the monochromator mirror, 30 cms. The values obtained with this correction factor appear to accord with the resolution actually obtained in sample spectra on that instrument.

Typical spectral slit widths for routine gaseous samples taken on this instrument are shown in Table 3:3.

TABLE 3:3

Restrahlen	Frequency in cm^{-1}	Grating (lines $inch^{-1}$)	Slit in mm.	Spectral Slit Width
2 NaF	370-240	625	1.2	1.51cm^{-1} at 300cm^{-1}
2 NaCl	270-170	625	1.6	0.78 at 200
2 KCl	195-145	312	1.6	1.24 at 160
2 KBr	150-115	312	2.8	1.02 at 130
2 CsBr	120- 70	166	3.2	1.32 at 85
2 CsI	82- 57	166	4.0	1.12 at 70
Mesh+W+W/z	60-30	50	8.0	2.33 at 40
Mesh+W+W/z	30-14	20	8.0	1.48 at 20

3:3 Interference Effects

Interference effects from the polythene windows of the cells had been previously noted during single beam operation (98). Figure 3:3a shows a typical single beam run with a normal grade of polythene 0.25 mm thick. The use of very poor quality polythene for the windows while decreasing the radiation intensity by scattering effectively eliminates the interference effects as shown in Figure 3:3b.

Interference effects become more pronounced at low frequencies with the result that even this low quality polythene shows interference bands below 100 cm^{-1}. Normally this is scarcely noticeable on single beam runs since the bands are very broad and blend into the general undulatory form of the background. On double beam working the ratio of the intensities

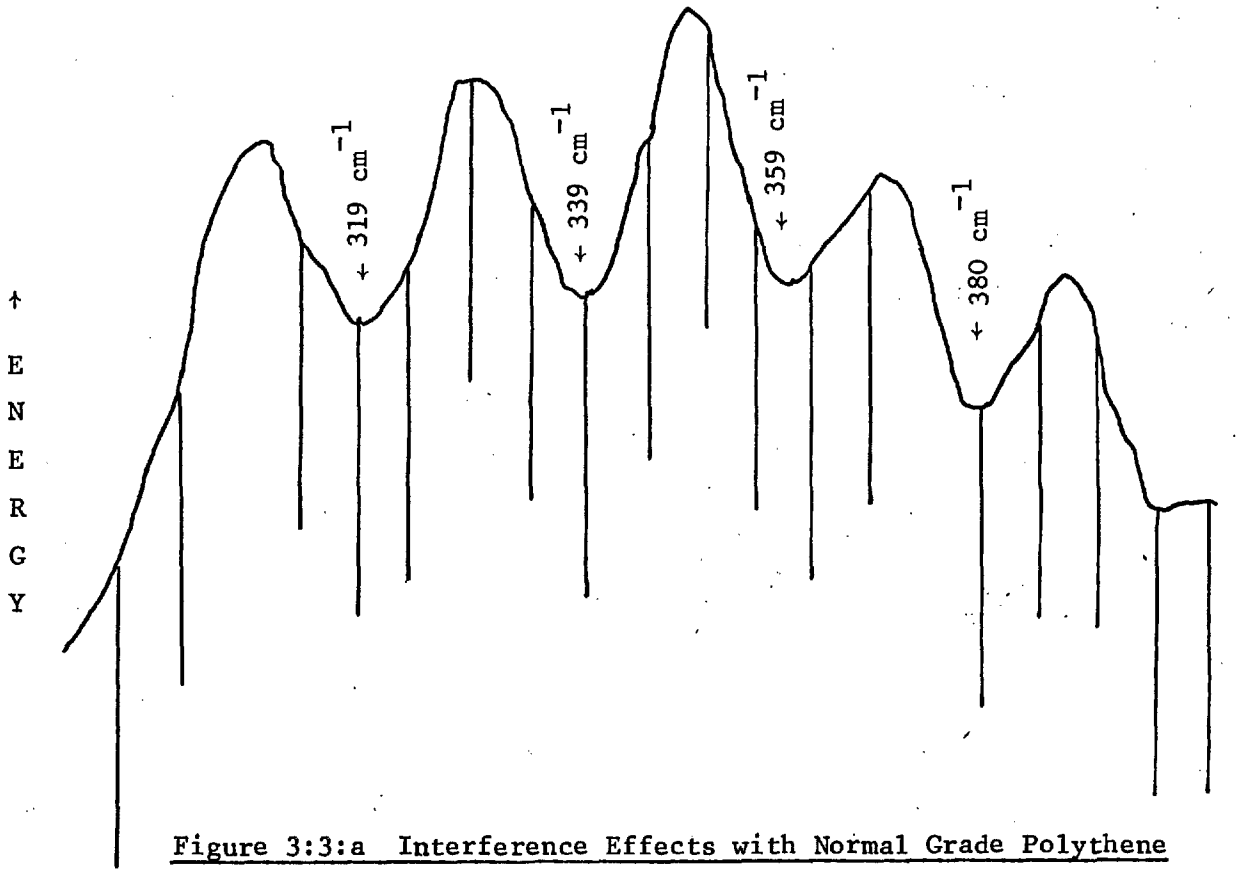

Figure 3:3:a Interference Effects with Normal Grade Polythene

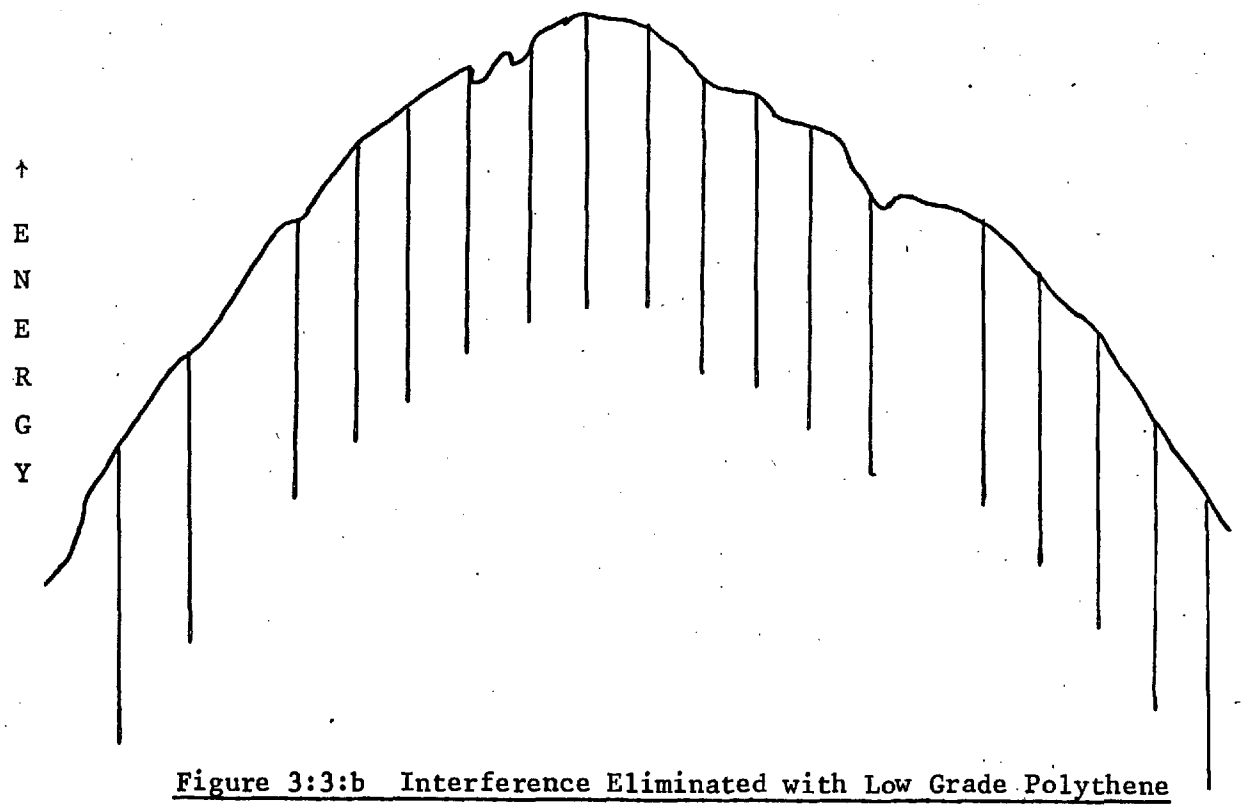

Figure 3:3:b Interference Eliminated with Low Grade Polythene

in the two beams should be constant and consequently any interference effects that are not identical in both beams are more readily obvious on the ratio plot. Figure 3:4 shows a particularly bad example caused by severe interference in the sample beam and relatively little interference in the reference beam. In all, five bands were observed, at 44, 59, 74, 88 and 102 cm^{-1} corresponding to an interference film thickness of 9 thousandths of an inch (for a refractive index of 1.51) the calculated thickness being very close to that expected for 1,000 gauge polythene.

Trouble had been previously experienced in the form of an undulatory pattern, with a peak to trough absorption of about 5%, occurring on the 100% transmission double beam ratio. After noticing the example shown in Figure 3:4 the previous runs were re-examined and, although the pattern was very much less pronounced, analysis confirmed that this was an interference effect.

It was found impossible to purchase any polythene with appreciably less parallel sides than that already employed and attempts to deform the 0.25 mm polythene were not satisfactory. The most effective method of eliminating the interference patterns appears to be the use of 0.75 mm polythene sheet which may either be deformed by hot pressing to give an angle of about 2^{o} between the faces, or more simply, may be imprinted with a mesh pattern in the centre of the window by pressing four strips of polythene, 2.0 by 0.25 by 0.075 cm, into the window while hot. In this way it was possible to obtain an almost straight plot for the 100% transmission line, as shown in Figure 3:5. The residual lack of complete straightness might be attributed to interference in the polythene transmission filter as the two beams may not pass identical portions of the filter.

Careful insertion of 0.25 mm windows cut from adjacent portions of the same sheet of polythene also proved satisfactory for most applications.

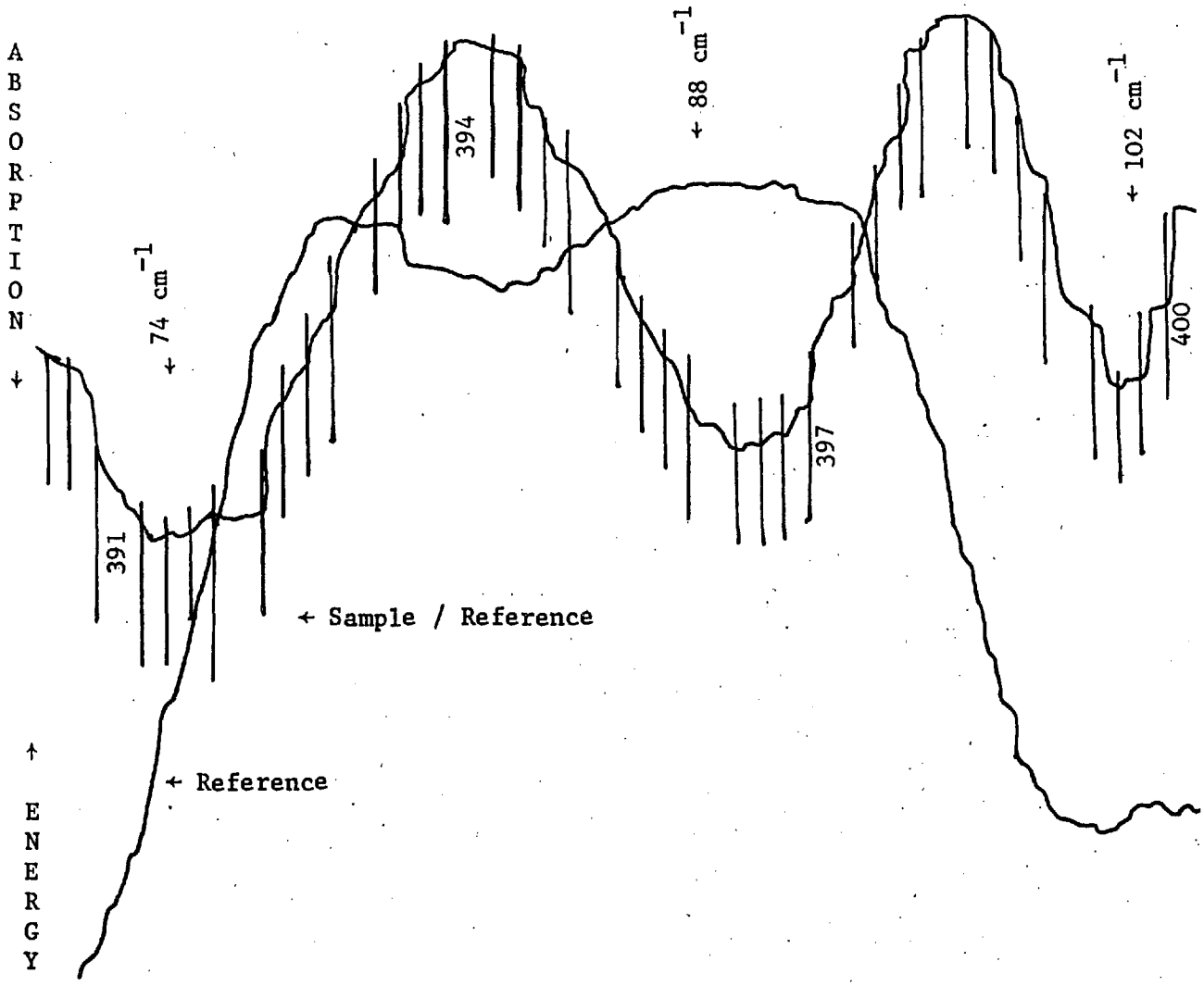

Figure 3:4 Interference Effects on Double Beam Ratio

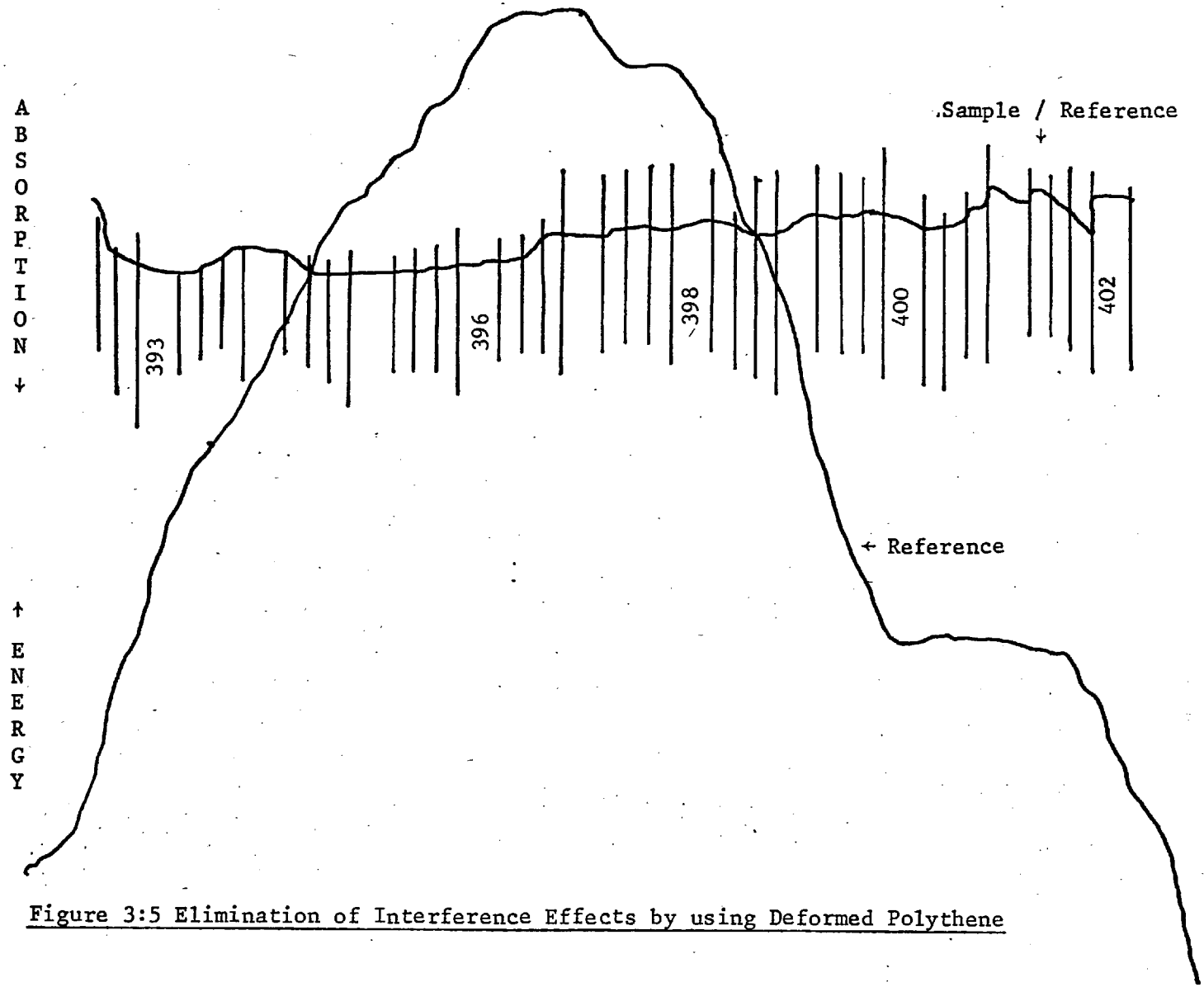

Figure 3:5 Elimination of Interference Effects by using Deformed Polythene

3:4 Filtering

A number of significant improvements to the filtering have been made compared with that employed on the single beam instrument and these will be described:

3:4:1 Chopper Compensation

Previous workers in this laboratory (100) have commented unfavourably on the efficiency of caesium iodide as a reststrahlen filter. In the present instrument the blaze of the 65.5 line grating is at 76 cm^{-1}, almost in the centre of the caesium iodide reststrahlen region. It has been previously shown (Section 1:5:3) that the filtering efficiency must be extremely good if it is desired to work across the blaze frequency of the gratings. The combination of grating blaze and poor reststrahlen discrimination against high frequency is shown in Figure 3:6. This clearly shows the concentration of higher orders into the blaze position.

The optical chopper is not completely efficient since its function is to modulate the low frequency radiation and to leave the high frequency radiation completely unmodulated. The crystal blades are, however, not absolutely transparent to the near infra-red and visible radiation due to specular reflection at the surfaces of the crystal. This results in slight modulation of the high frequency radiation, which can be eliminated by reducing the radiation intensity on the open side of the chopper by a fraction equal to the specular reflection of the crystals. The radiation intensity on the open side may be reduced by inserting an opaque substance such as a brass mesh into the open side. Near infra-red measurements on a highly polished crystal blade using a Grubb Parsons Spectromaster in the 5 to 25 micron range showed that it was difficult to raise the transmission of a caesium iodide or potassium bromide blade above 85%. The compensation required on the open side of the chopper was, therefore, about 15% and this was achieved by screwing a suitable number of 2 mm brass rods into the open side.

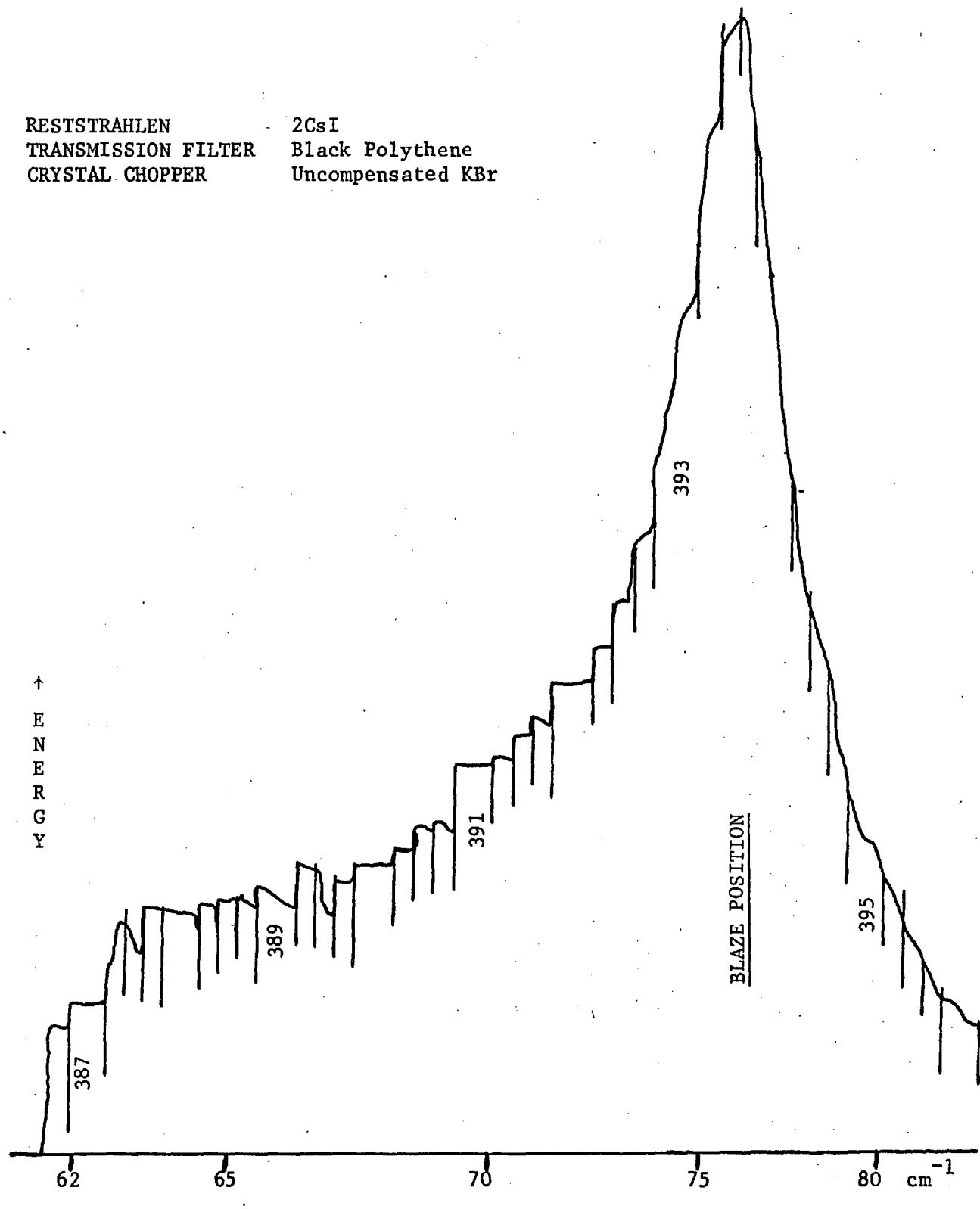

Figure 3:6 Higher Order Radiation at Grating Blaze - Chopper Uncompensated

Exact compensation was achieved empirically by placing a 3 mm thick caesium iodide crystal in the optical path. This should eliminate all radiation below 200 cm^{-1} and the compensation was adjusted until the chopper eliminated all the remaining signal due to radiation above 200 cm^{-1}.

The effect of this compensation on the two caesium iodide reststrahlen peak is shown in Figure 3:7. It should be noted that this run was taken under identical experimental conditions to those for Figure 3:6.

Comparison of Figures 6 and 7 shows that the ratio of true to false radiation at the blaze position with an uncompensated chopper is about 1:2. Since the compensation required is about 15% we might expect the ratio of true to false radiation to rise to about 1:12 with a chopper with completely opaque blades which had no filtering action at all, such as aluminium. Provision for the use of a crystal chopper and especially a chopper compensated against reflection losses, would appear to be an important element in any projected filtering system. A disadvantage of compensating the chopper is that in regions where the filtering is virtually 100% efficient already, such as the 2 KCl reststrahlen peak, the only effect of compensating the chopper is to reduce the first order radiation intensity be about 15%. This is shown in Figure 3:8 where it is necessary to open the slit from 2.0 mm with an uncompensated chopper to 2.4 mm with a compensated chopper to achieve the same signal level. The slight decrease in energy on the high frequency side of the peak is due to the lower cut-off of the compensated caesium iodide chopper compared with the uncompensated potassium bromide chopper.

3:4:2 Reststrahlen

The secondary filtering system chosen in the 60 to 400 cm^{-1} region was two 'crossed' reststrahlen filters. It will be shown that two crossed reststrahlen filters are sufficient to isolate pure first order radiation when used in conjunction with a compensated chopper and black polythene transmission filter. Since the peak reflectivities of a single crystal

RESTSTRAHLEN	2CsI
TRANSMISSION FILTER	Black Polythene
CRYSTAL CHOPPER	Compensated CsI

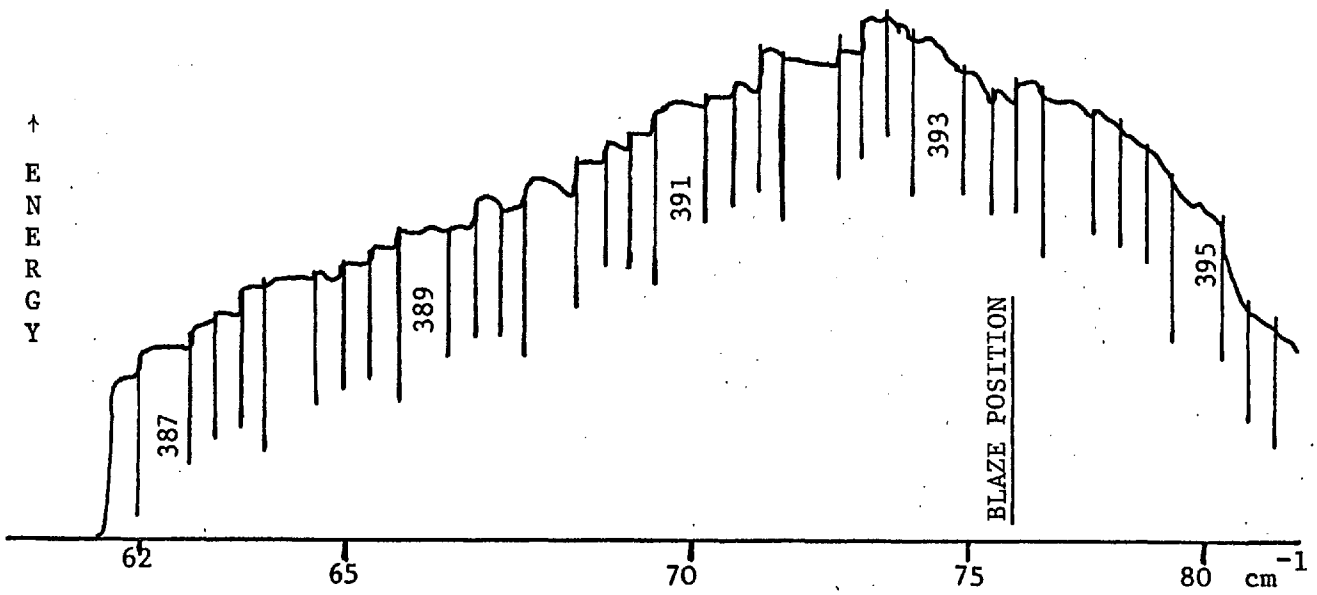

Figure 3:7 Higher Order Radiation Eliminated - Chopper Compensated

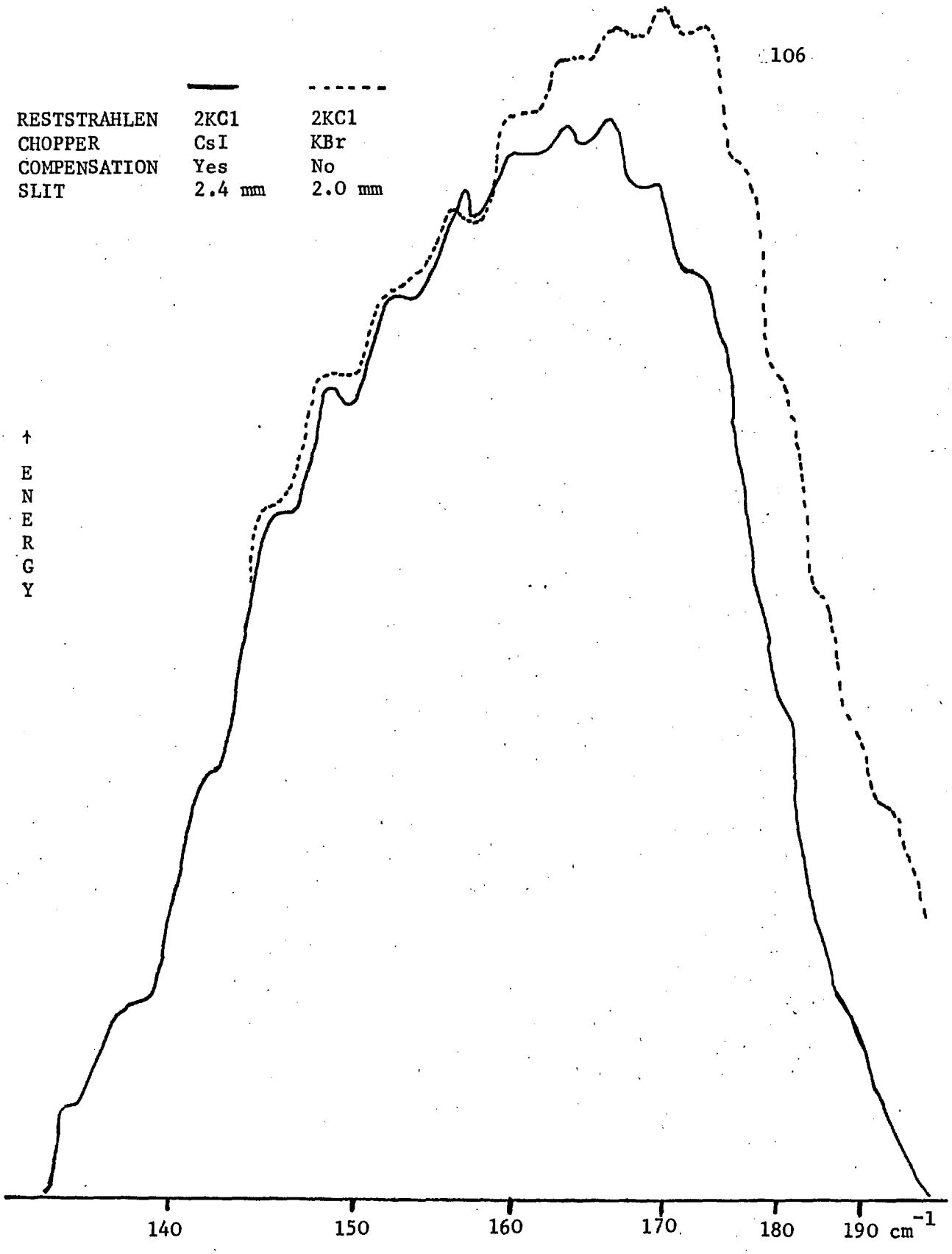

Figure 3:8 Compensation of the Chopper in the 2KCl Reststrahlen Region

are in the region of 0.9 it also represents a very efficient method of isolating first order radiation. The principal drawback is the relatively narrow bandwidth of each reststrahlen peak. If no reststrahlen peak is to be used when its reflectivity has fallen below, say, 40% of its peak value then six to eight sets of crystals are required to cover the 60 to 400 cm^{-1} range. This results in an apparently large number of filter changes being necessary. Since, however, the above range covers three octaves and it is difficult to see how a filter can function efficiently over more than half an octave, the number of reststrahlen crystals required is not abnormally high. The general shape and overlap of the reststrahlen filters used in this instrument is shown in Figure 3:9.

The primary filtering of a crystal chopper and 0.12 mm black polythene transmission filter is similar to that employed on the single beam instrument and the conclusions drawn about the reststrahlen from experience on that instrument will, in general, be relevant here. The compensation of the crystal chopper will ensure that the filtering is even more rigorous in this instrument. In six years of use of the single beam instrument the filtering employed has become ever more rigorous as the demanded spectral purity has risen from 95% to greater than 99.5%. High spectral purity is especially important when highly absorbing samples are being investigated at high gain settings since very small percentages of high frequency radiation can give rise to spurious bands.

The position above 120 cm^{-1} has been summarised by Radcliffe (100). A single reflection from NaCl, KCl or KBr has been shown to allow considerable quantities of higher order radiation to be reflected and this has been shown by Campagnaro (96) to be mainly second order radiation. This will not be attenuated by compensation of the chopper and we may infer that pure first order radiation can only be obtained in this instrument by using two crossed reststrahlen filters, as has been found necessary in the single beam instrument.

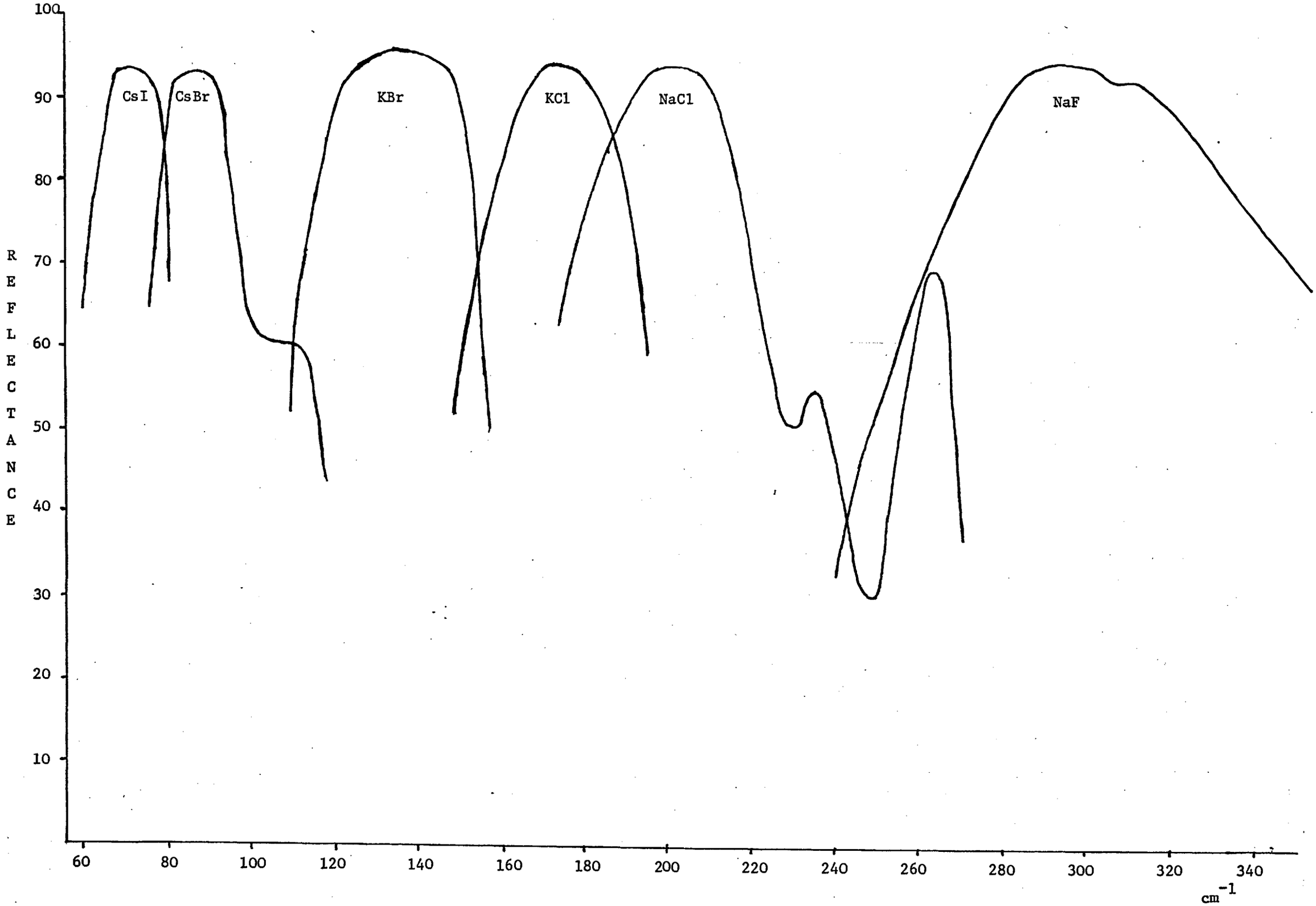

Figure 3:9 Reflactances of some Crossed Reststrahlen Crystals - All peaks have been normalised to 95% Reflectance

Below 110 cm^{-1} the position has been confused in the past due to attempts to use KRS-5 and CsI in the 80 to 100 cm^{-1} region where they do not have a reststrahlen peak: At 100 cm^{-1} using 2KRS-5 or 1 KRS-5 and a crystal quartz transmission filter the spectral purity has since been established as only about 10%. The region between 75 and 115 cm^{-1} may be conveniently covered by the use of caesium bromide as a reststrahlen filter and the region from 57 to 83 cm^{-1} with caesium iodide.

It was seen in Section 3:4:1 that the spectral purity in the blaze position with 2 CsI was only 33% with an uncompensated chopper; compensation of the chopper clearly improved this and the improvement was checked quantitatively by the method of Genzel (10). In this the grating with a spacing, d, used to observe the spectrum is replaced by a second grating with a spacing, d/2. Providing the second grating is blazed at the same angle and was manufactured by the same process so that the reflectivities are similar, then the only effect of exchanging the gratings will be to remove the radiation of odd orders from the spectrum. This appears to be the best method of testing for higher order radiation in general since other methods, such as the observation of absorption bands in the second order, or the insertion of a KBr plate to eliminate radiation below 400 cm^{-1}, test only for the presence of a selected portion of the higher orders which might be present.

Using this method the spectral purity at the blaze position was established as being greater than 98% for the 2CsI reststrahlen and greater than 99% for the 2 CsBr reststrahlen. As these measurements were made at the blaze position it would be expected that the spectral purity at other positions on the reststrahlen peaks would be very much greater. If it is necessary, the spectral purity at the blaze position may be raised to greater than 99.5% on the CsI and greater than 99.7% on the CsBr by the insertion of a transmission filter, e.g. 1 mm of crystal quartz or a Manley Filter 'G' with a concomitant loss of about 40% in the first

order signal.

It can be seen from Figure 3:9 that the overlap at certain points between adjacent reststrahlen is poor.. This is especially the case at 250 cm^{-1} on the overlap between NaF and NaCl and again at 120 cm^{-1} between KBr and CsBr. The first might be improved by the substitution of BaF_2 for NaCl, BaF_2 having a good overlap with NaF and an adequate overlap with KCl. The position at 120 cm^{-1} could, it appears, only be improved by the addition of a further pair of KI crystals to the set of reststrahlen in use: KI has an excellent overlap with both KBr and CsBr.

3:4:3 Polythene Embedded Transmission Filters

A number of polythene embedded metal halide and oxide transmission filters (49) were supplied by Dr. T. R. Manley. Their approximate compositions and cut-on points, as measured on a Grubb Parsons interferometer by Manley, are given in Table 3:4.

TABLE 3:4

Filter	Cut-on	Composition
W/X	200 cm^{-1}	
S3/D1	200 cm^{-1}	
G	140 cm^{-1}	Cu_2O (18%) WO_3 (18%)
RRE	140 cm^{-1}	Cu_2O (18%) WO_3 (18%)
I	105 cm^{-1}	Cr_2O_3 (12%) Al_2O_3 (18%) KCl (12%)
S1/H1	120 cm^{-1}	
W	105 cm^{-1}	
W/Z	110 cm^{-1}	

Since for the majority of these filters no published details of their transmission were available this was measured for all eight filters in the 10,000 to 60 cm^{-1} region. A Grubb Parsons Spectromaster was used for the 10,000 to 400 cm^{-1} region and a Grubb Parsons DM-4 caesium iodide prism instrument for the 500 to 200 cm^{-1} region. The results in this region of the spectrum are shown in Figure 3:10.

The results of Figure 3:10 may be summarised:

Filter	W/X	S3/D1	G	RRE	I	S1/H1	W	W/Z
Windows above 200 cm^{-1}	1250 2000	2000	500	500	1100	-	-	500

In addition the filters, I, W/X and S3/D1 are appreciably less efficient in attenuating high frequency even than black polythene. The claim by Manley that these filters have less than 1% transmission between 10,000 cm^{-1} and their cut-on points is not substantiated, and this will clearly restrict their use.

The transmission of the filters in the 60 to 260 cm^{-1} range was measured on the instrument described in the previous section using two crossed reststrahlen filters, a compensated optical chopper and 0.12 mm of black polythene to ensure a spectral purity of greater than 99.5% over the whole region investigated. The results are shown in Figure 3:11.

If the cut-on point is redefined as the frequency at which the transmission rises to 10% on the low frequency side of the reststrahlen absorption then the comparison of the measured cut-on points and those given by Manley is shown in Table 5.

TABLE 5

Filter	W/X	S3/D1	G	RRE	I	S1/H1	W	W/Z
Observed Cut-on	220	140	130	125	120	110	120	72
Cut-on: Manley	200	200	140	140	105	120	105	110

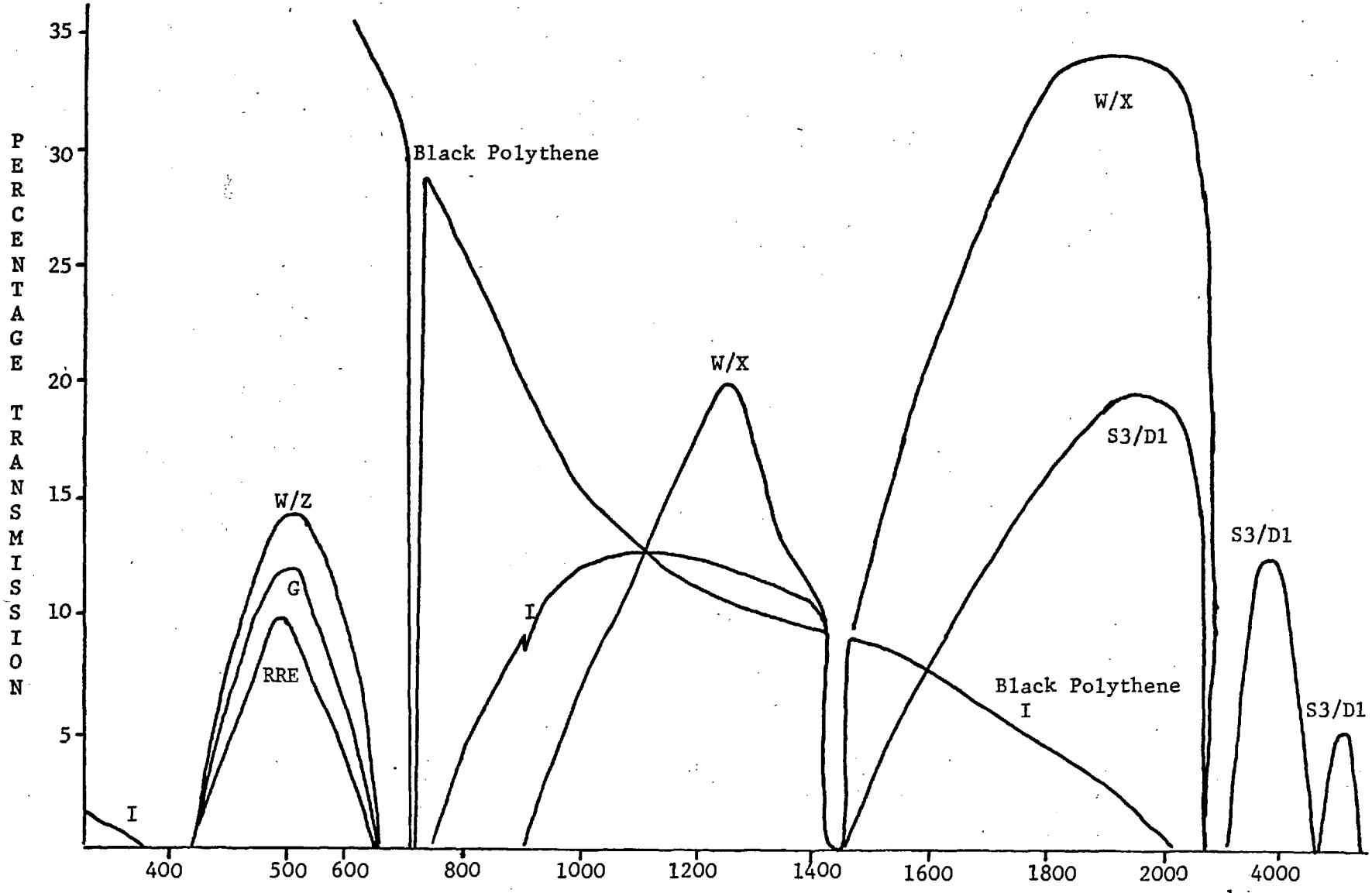

Figure 3:10 High Frequency Transmission of Manley Transmission Filters

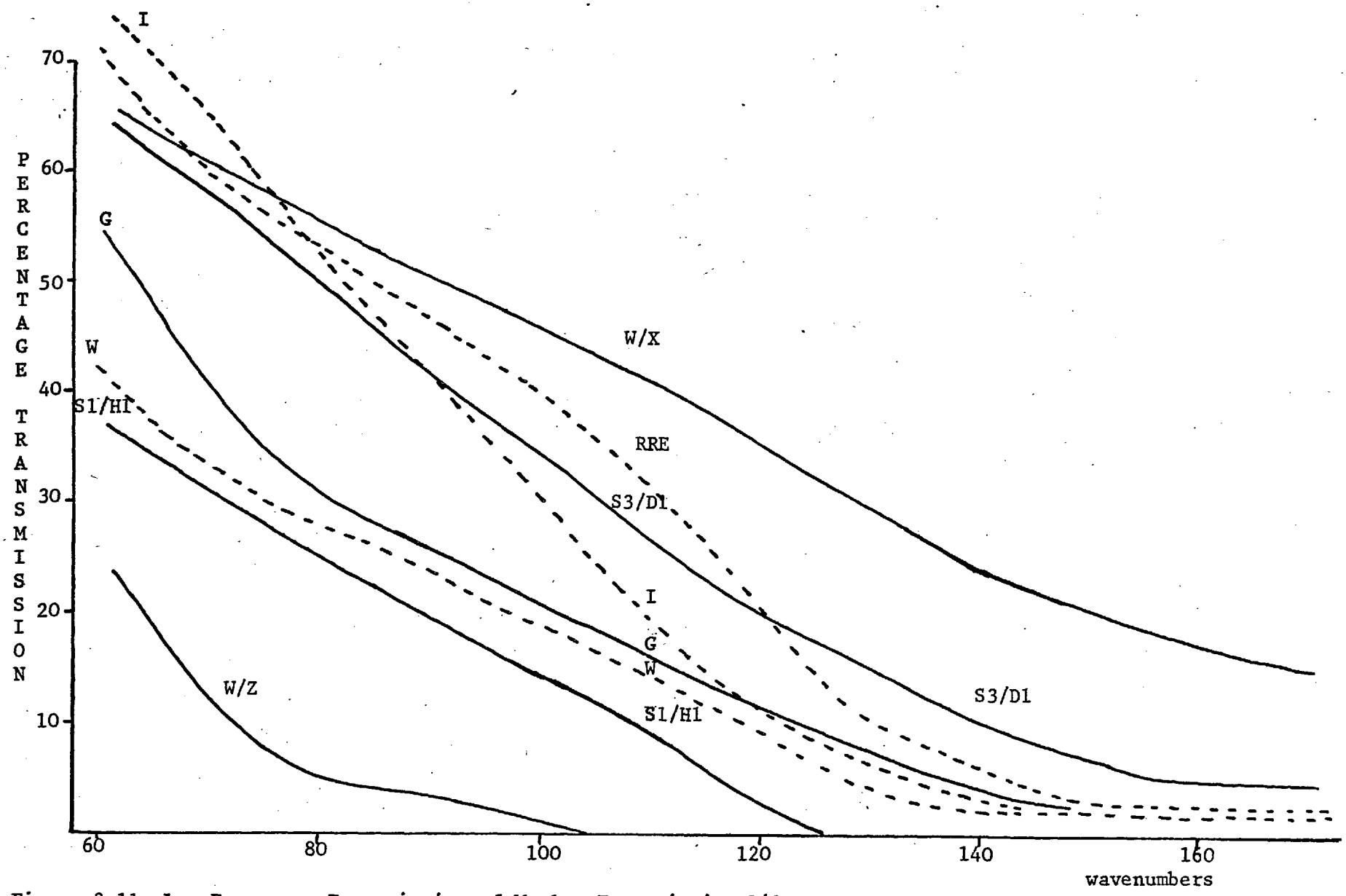

Figure 3:11 Low Frequency Transmission of Manley Transmission Filters

Clearly in the 60 to 260 cm^{-1} range none of these filters show comparable discrimination of low frequencies to that obtainable with reststrahlen filters. This is in accord with the general practice in far infra-red spectroscopy to use at least one reststrahlen reflection to isolate first order radiation in the 60 to 400 cm^{-1} region. Only one recent spectrometer working in this region (6) appears to dispense with the use of reststrahlen filters in favour of transmission filters and no details of the filters used in that instrument have been published. From the measurements on these metal oxide and halide filters it would appear that a several fold improvement in their characteristics would be necessary before they could be utilised in place of reststrahlen filters.

No common reststrahlen crystal has a reststrahlen peak below of that of CsI at 70 cm^{-1}, and as a result, below 60 cm^{-1} alternative methods of filtering have to be employed to that used above. It had been hoped to employ only transmission filters in the region below 60 cm^{-1}: Figure 3:11 clearly shows that this is impossible, for example, G and I in series would be expected to give a spectral purity of only 80% at 50 cm^{-1}. As a result first order radiation was isolated in the region below 60 cm^{-1} by a combination of transmission filters and metal mesh reflection filters. These will be discussed in more detail in the succeeding section.

3:4:4 Scatter Plates and Metal Mesh Reflection Filters

3:4:4:1 Problems Associated with Measurement of Reflectance

Since the instrument was designed as an absorption spectrometer, quantitative measurements on transmission filters, such as those described in the previous section, present no difficulties. Measurements on reflection filters do, however, present some problems unless the spectrometer has been designed with such measurements in view. Moller, for example, (28) constructed a sample cell in which three reflection

filters could be precisely positioned and adjusted, in this way it is possible to make quantitative comparisons of the reflectances of different filters. In this instrument the only plane mirrors occurring in one beam and not the other are M_{15} and M_{24} and the reflection filters must be substituted for one or other of these mirrors. This poses a number of problems:

a) These mirrors were not designed to be easily replaceable without disturbing the optical alignment. Consequently after the insertion of a reflection filter its position must be adjusted until the optical alignment is restored.

b) Considerable difficulty has been experienced in operating this instrument at low frequencies unevacuated: this is associated with air turbulence in the detector drum caused by the rotating beam switching chopper which disrupts either the ballasting facility or the thermal equilibrium of the detector. The only method of aligning the reflection filters is, therefore, to make a slight adjustment in their position, evacuate the instrument and observe the effect on the signal. This is a tedious and difficult operation and in the graphs to be presented, therefore, there is some uncertainty in the absolute value of the reflectances reported.

c) The angle of incidence at these mirrors is large, 46^{o}, and from the discussion in Section 1:5:9 we would expect the mesh reflection filters to show severe diffraction effects at this angle of incidence. It does not appear that the scatter plates will be affected by this large angle of incidence since in the original instrument (5) they were used at an angle of incidence greater than 45^{o}.

3:4:4:2 Reflectances of Three Types of Filter

The reflectances of three types of filter were measured and the results are shown in Figure 3:12.

The fine and coarse scatter plates are as used in the Perkin Elmer 301

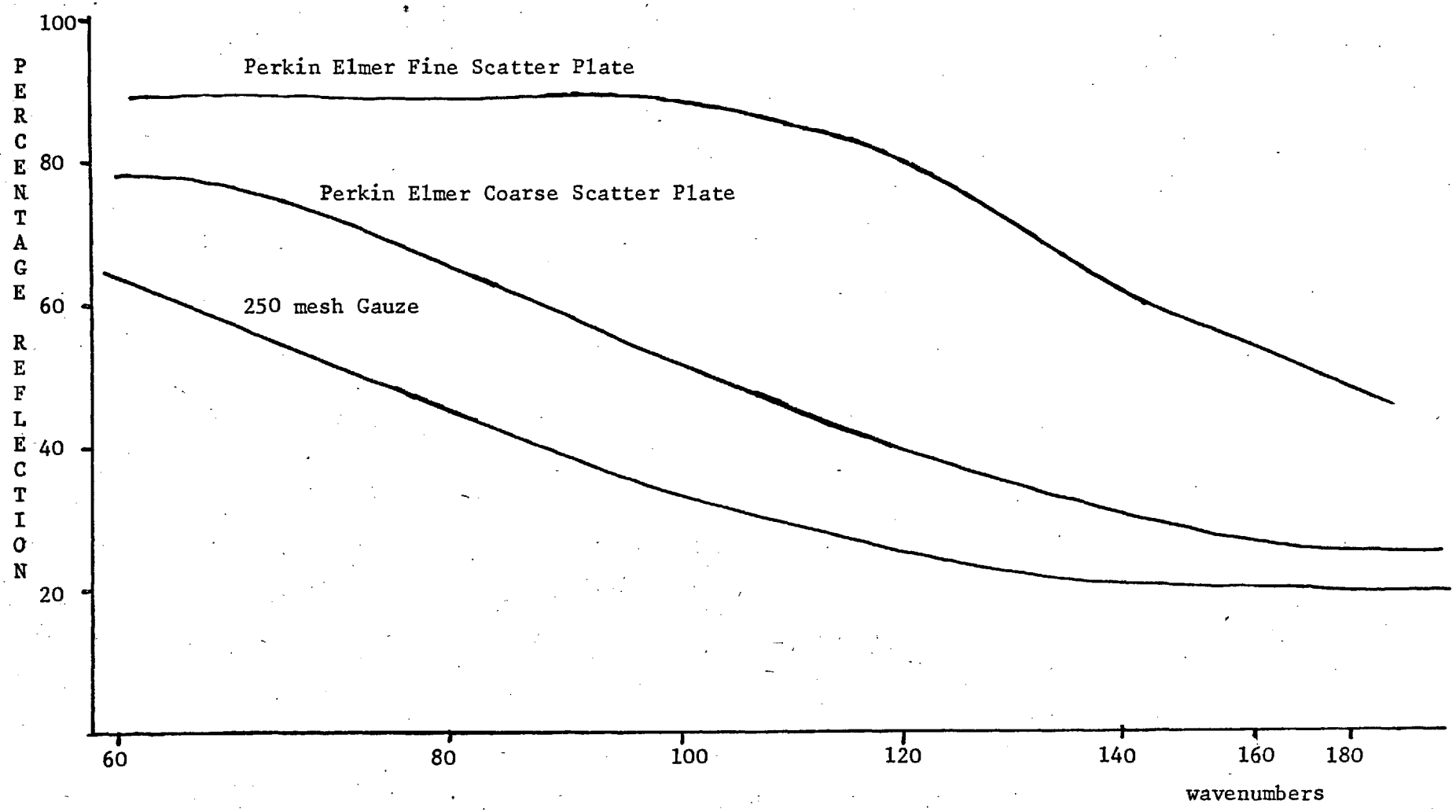

Figure 3:12 The Reflectances of two scatter plates and a brass backed wire mesh

far infra-red spectrometer (Part Number 301:0112). The wire mesh reflection filter was a sample of 250 guage, 100 wires to the centimetre, stainless steel wire mesh woven from 48 guage wire, diameter of the wires 40.6 microns, and obtained from Messrs. R. Cadisch, 36, Orsman Street, London, N.1. In this experiment the wire mesh was held flat by being stuck to a brass former with collodion in an analagous manner to that suggested by Genzel (56) for the production of beam splitters for a Fabry-Perot interferometer.

The sharpness of the cut-on of the scatter plates is not impressive. Apart from some experiments in the 150 to 180 cm^{-1} region which showed that neither the rejection of higher order radiation nor the reflectance of first order light was as favourable as that obtained from a KCl reststrahlen reflection filter, no further experiments were made on scatter plates. From the reflectances presented in Figure 3:12 the selectivity of wire meshes appears scarcely more promising than that of scatter plates. This is almost certainly due to the unfavourable circumstances of their use, which is not a contributory factor in the case of scatter plates. Firstly the mesh was mounted directly on a brass plate which probably accounts for the residual 15% reflectance at high frequencies and, secondly, the angle of incidence may have given rise to diffraction effects. The first of these problems was eliminated by an alternative method of mounting the mesh to keep it flat: the backing plate was eliminated by stretching the mesh across a brass frame. To avoid the high angle of incidence the mesh filter was inserted in place of mirror M_{27} where the angle of incidence is only 21^{o}. Since this mirror is common to both beams no quantitative reflectance measurements such as those in Figure 3:12 are possible, its filtering effect may be seen qualitatively, however.

Figure 3:13 shows the background obtained with the coarsest grating available, about 8 lines.cm^{-1}, with two brass backed mesh reflection filters and 45^{o} angle of incidence and a Manley 'G' transmission filter.

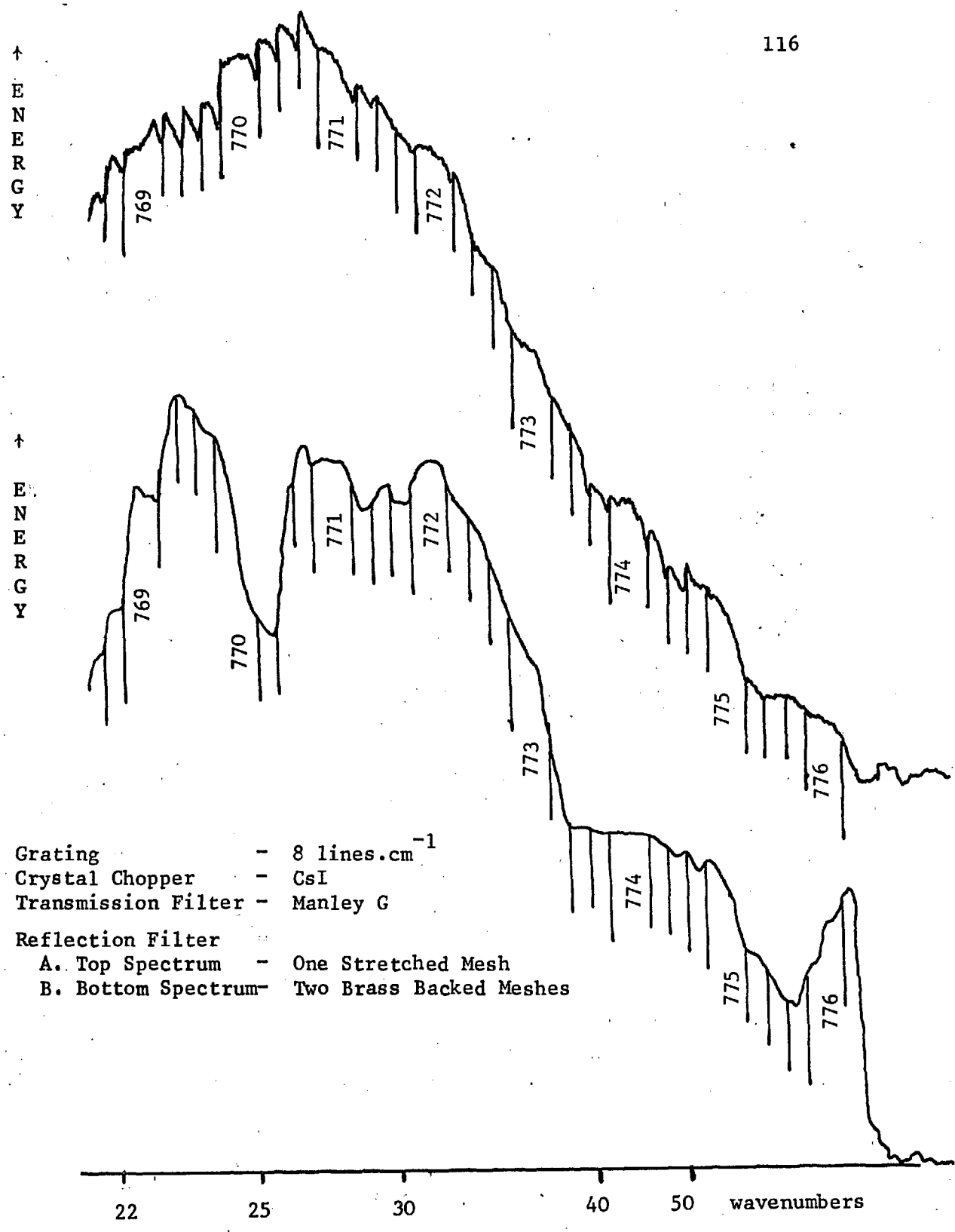

Figure 3:13 Comparison of Mesh Reflection Filters

The dip in the background at around 25 cm^{-1}, which corresponds to the blaze frequency of the grating, is caused by overcompensation of the optical chopper and illustrates the presence of higher order radiation. The rise in the background above 55 cm^{-1} is also attributable to higher order radiation probably being scattered into the light beam as the grating approaches its specular position.

Figure 3:13 shows the background for the same grating but with two mirrors in the reststrahlen holders and M_{27} replaced by a stretched gauze reflection filter. The differences between the two spectra represent, therefore, the effect of replacing two brass backed reflection filters at 45^{o} angle of incidence by a single stretched mesh reflection filter at 21^{o} angle of incidence. It will be seen that both of the features in the first spectra representing higher order radiation have been eliminated in the second case and it may be concluded, therefore, that a single stretched mesh reflection filter at a low angle of incidence is considerably more efficient in removing higher order radiation than two brass backed mesh filters at a higher angle of incidence. This conclusion must be viewed in relation to the fact that the signal to noise ratio in the second spectrum is about an order of magnitude greater than that obtained in the first, which illustrates the difficulties associated with stretching and aligning mesh reflection filters that are not provided with a firm substrate, such as a brass backing plate.

3:5 Sample Spectra

The capabilities of the instrument will be illustrated with a selected number of sample spectra.

Figure 3:14 shows a routine high frequency water vapour calibration run in the 250 to 400 cm^{-1} region with the instrument operating in the double 'single' beam mode of operation.

Figure 3:15 shows the resolution obtainable in the 75 to 80 cm^{-1} region. Bands 0.75 cm^{-1} apart are readily resolved. It should be noted that the

instrument is again working in its double 'single' beam mode in that each trace represents the energy throughput in its respective beam. It is not possible in this case to operate the instrument in its double beam mode as the whole instrument is filled with atmospheric water vapour at low pressure to avoid pressure broadening of the lines, the double beam ratio is, therefore, unity at all points. This is in distinction to most published spectra designed to show the resolution achievable where single beam operation is used to double the signal to noise ratio.

Figure 3:16 shows the low frequency performance in a routine hydrogen cyanide calibration run in the double beam mode of operation.

Although the spectrum shows no second order bands this is proof of high spectral purity only in the 30 cm^{-1} region since at 50 cm^{-1} the second order bands are too weak to be observed. Comparison of this spectrum with that of Williams (102) shows that although the most intense absorption would be expected for the J = 16 band at 50.2 cm^{-1} it is observed for the J = 8 band at 26.6 cm^{-1}.

At first this was thought to be evidence of low spectral purity in the 50 cm^{-1} region. Observation of the water vapour spectrum in the same region, however, showed complete absence of any absorption at 44 or 50cm^{-1} that could be attributed to the second order of the extremely intense water vapour absorptions at 88 and 99 cm^{-1}. In addition, observation of the HCN spectrum at 20 cm^{-1} under identical filtering conditions but with a grating possessing 8 lines.cm^{-1} (Figure 3:17) failed to show any second order bands whatsoever but still showed this apparent increase in intensity with decreasing frequency. This apparent increase in intensity at low frequencies would appear, therefore, to reflect not the low spectral purity at high frequency but the increasing resolution at low frequencies on account of both the decreasing spectral slit width and the decreasing rate of scan with frequency. In the example in Figure 3:16 the rate of scan is 1.1 $cm^{-1}.min^{-1}$ at 50 cm^{-1} and 0.37 $cm^{-1}.min^{-1}$ at

25 cm^{-1} while the spectral slit width has decreased from 3.7 cm^{-1} at 50 cm^{-1} to 0.86 cm^{-1} at 25 cm^{-1}.

Figure 3:17 shows the low frequency performance in the 14 to 20 cm^{-1} region on double beam operation. This spectrum was, in fact, taken with the 8 line.cm^{-1} grating but an equivalent signal to noise ratio is obtainable in this region of the spectrum with the 20 line.cm^{-1} grating which shows the comparatively low reflectivity that has been obtained from the grating ruled in the college workshop compared to that ruled by the Royal Radar Establishment, Malvern. The 8 line.cm^{-1} grating was milled from a brass blank and used unaluminised. A slight increase in reflectivity might be obtained, therefore, on aluminisation but this is likely to have only a marginal effect at these frequencies.

Figure 3:18 shows the linearity of the 100% transmission line, in the 60 to 200 cm^{-1} region, despite the undulatory nature of the background as the reststrahlen filters are changed.

Figure 3:19 shows the author operating the instrument.

Figure 3:19 The Author Operating the Spectrometer

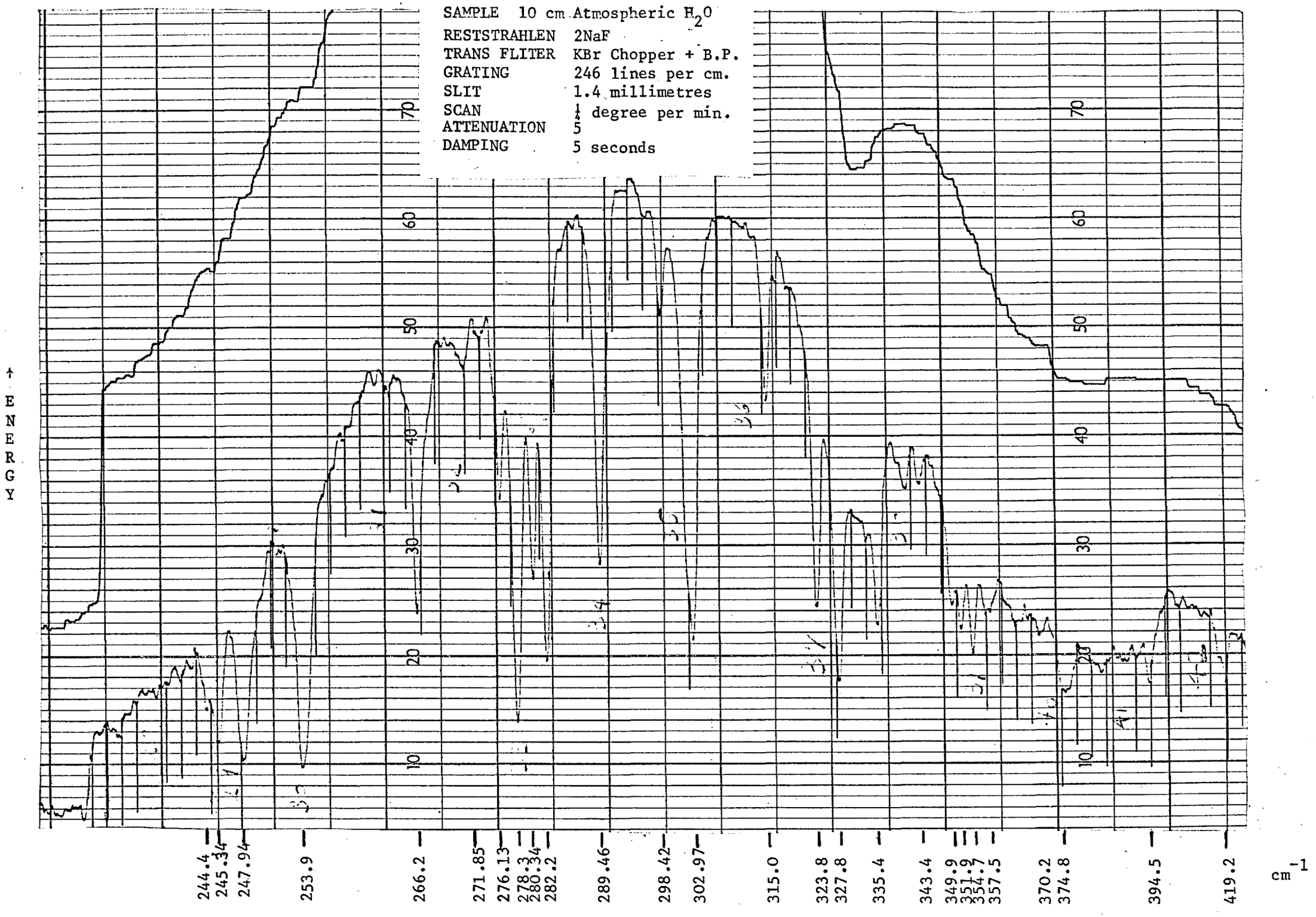

Figure 3:14 Calibration run in the 240 to 420 Wavenumber Region

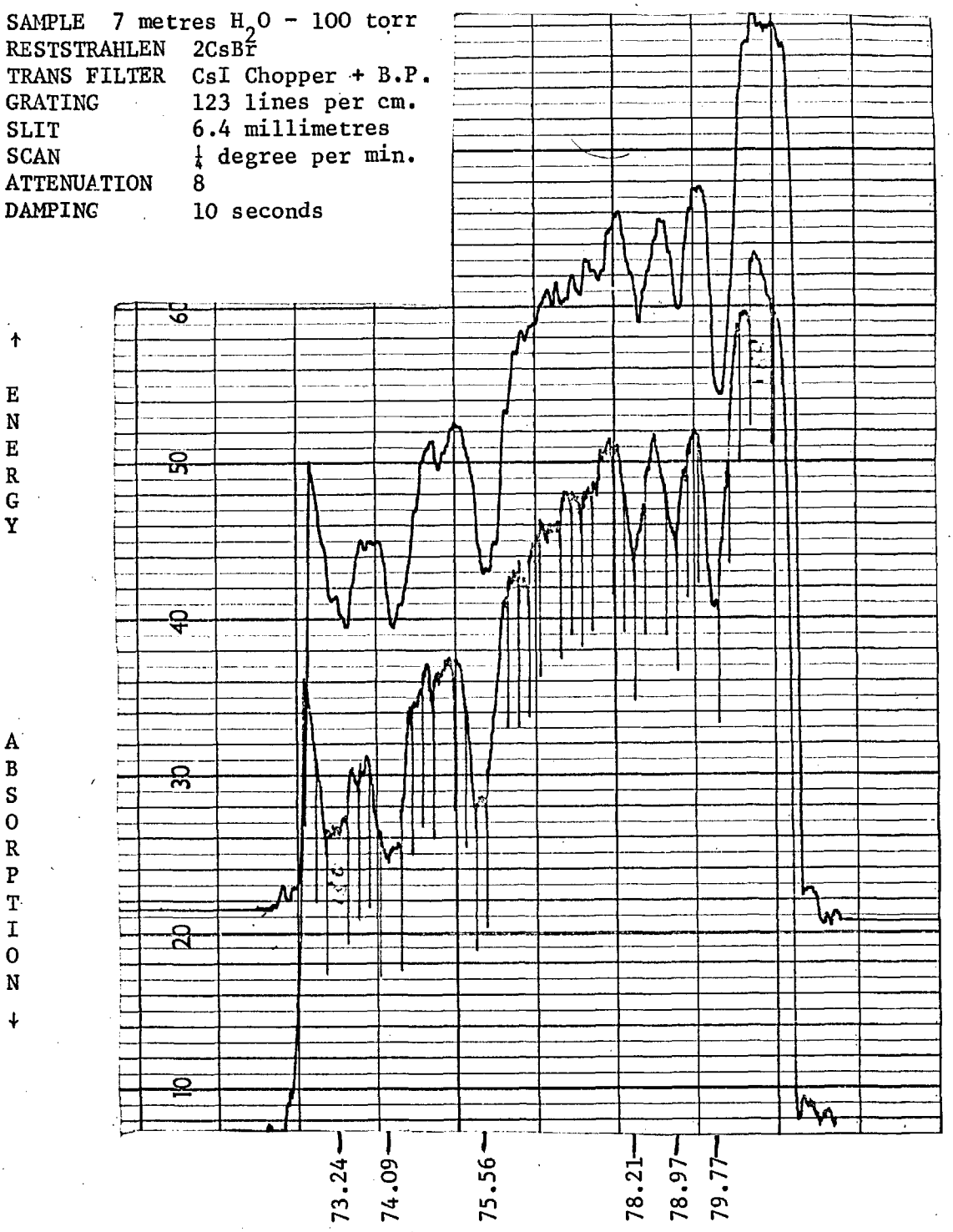

Figure 3:15 Resolution Obtainable in the 73 to 80 Wavenumber Region

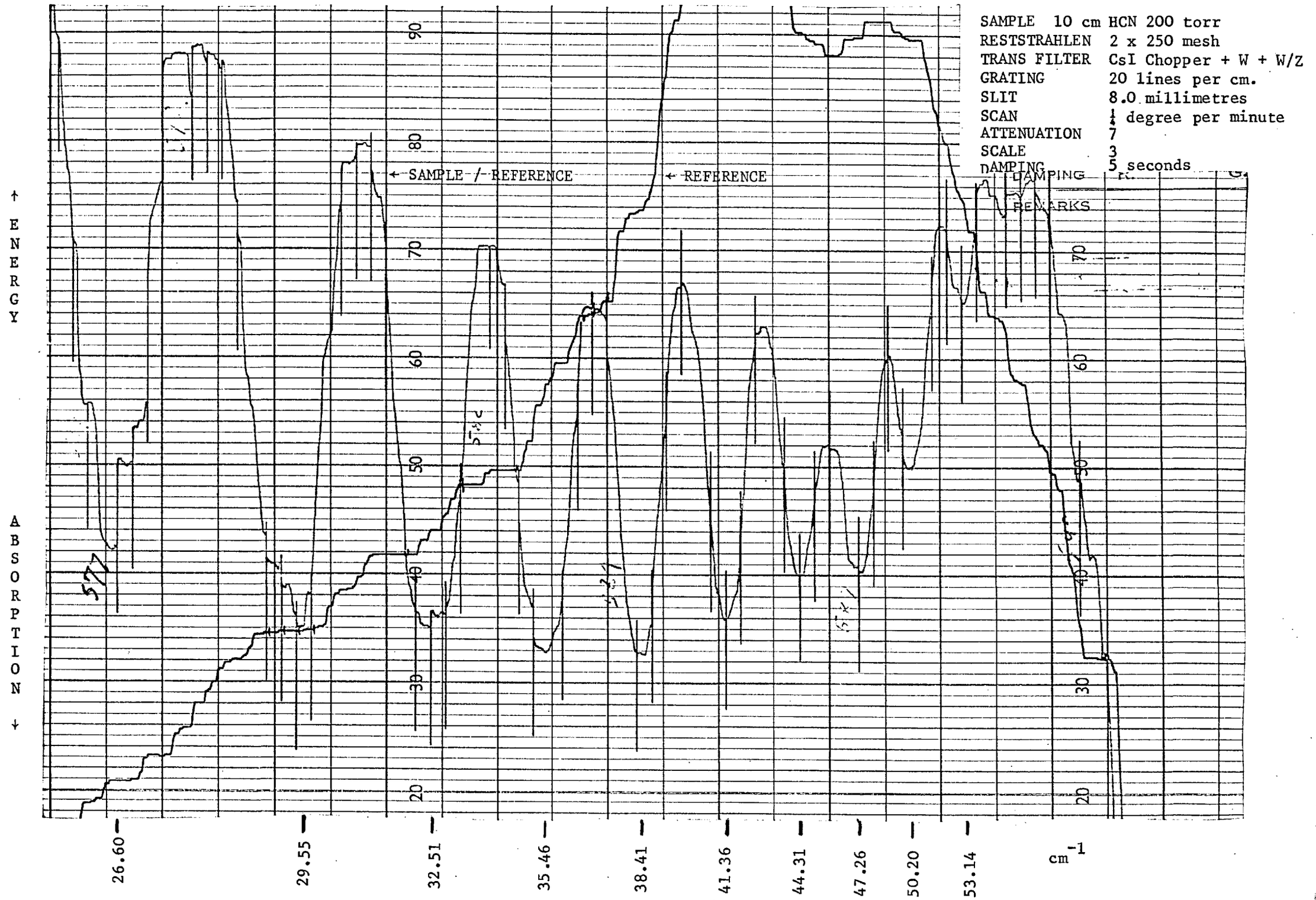

Figure 3:16 Calibration Run in the 25 to 55 Wavenumber Region

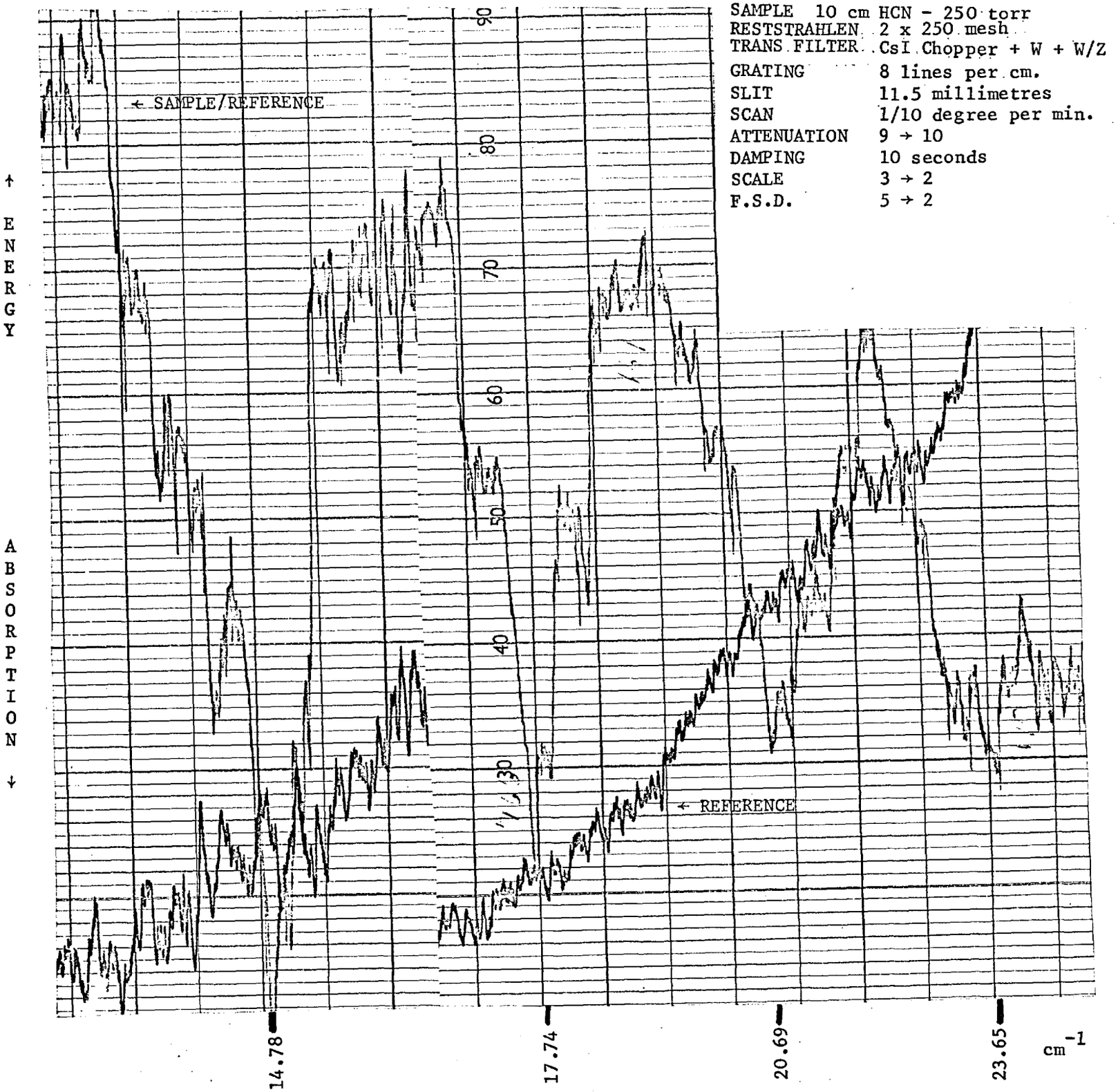

Figure 3:17 Low Frequency Performance in the 14 to 25 cm^{-1} Region

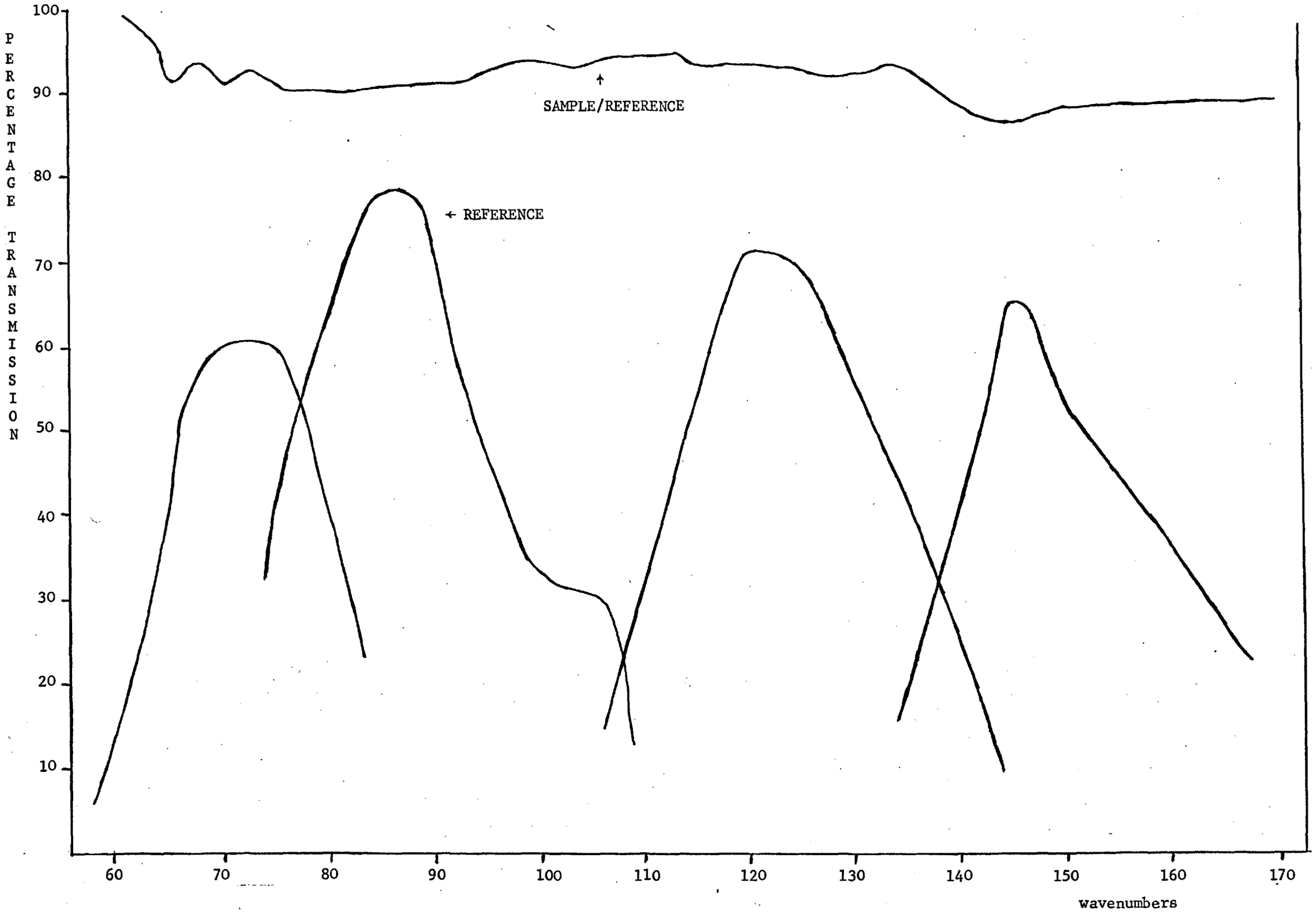

Figure 3:18 Linearity of the 100% Transmission Ratio in the 60 to 170 Wavenumber Region

4) LOW FREQUENCY INTERMOLECULAR AND INTERIONIC VIBRATIONS

4:1 INTRODUCTION

It has been noted that the far infra-red spectrometer described in the preceding pages was designed with the specific intention of permitting the observation of broad, weak absorption bands in the far infra-red.

A suitable system for study appeared to be the interionic interaction of dissolved ions in a polar solvent first reported by Evans and Lo (10). These authors observed, in a study of a series of tetra-alkyl ammonium halides in benzene, a number of broad, bandwidth about 80 cm^{-1}, absorptions in the 80 to 120 cm^{-1} region, the exact band centre being dependent on the nature of the halide anion. These absorptions were assigned, on the basis of their proximity to the lattice modes of the solids, to an ion pair interaction.

A comparable series of absorptions was observed by Edgell, Watts, Lyford and Risen (103) for the alkali metal pentacarbonyl-manganese and tetra-carbonyl-cobalt salts in tetrahydrofuran. In this case the assignment to an ion pair interaction was supported by electrical conductivity and near infra-red measurements (104).

The electrical conductivity of dilute aqueous solutions of strong electrolytes is well understood by the Debye-Huckel-Onsager equations(105) which consider the effect on the potential energy of a free ion of the oppositely charged ions in its neighbourhood. It was first recognised by Bjerrum (106) that in solutions of weak electrolytes, especially in solvents of low dielectric constant and at high concentrations, the ions will tend to associate into electrically neutral cation-anion pairs. This phenomenon leads to a reduction in the electrical conductivity of the solution compared to that of free ions and consequently this phenomenon has been extensively studied conductiometrically and has been placed on a quantitative basis by Fuoss and Kraus (107). The ion pair concept in general has been reviewed by Kraus (108).

The association of ion pairs into higher aggregates such as triplets, quadrupoles and hexapoles in concentrated solutions of low dielectric constant is generally accepted (109). However, the formation of ion quadrupoles and hexapoles from ion pairs involves no change in the conductivity of the solution and consequently the phenomenon has received far less attention than the formation of ion pairs from free ions. It is interesting to note that in a recent review of ions, ion pairs and their agglomerates (110) Szwarc devotes thirty-six pages to ions and ion pairs and one page to higher aggregates.

The further association of ion pairs may be studies thermodynamically (109) and these results confirm those obtained conductiometrically (111) that charged species such as ion triplets and ion quintuplets are relatively unimportant and the predominant association is between ion pairs, ion quadrupoles and ion hexapoles. The only experimental data available on higher aggregates is thermodynamic and it can be expected that far infra-red spectroscopy of the ion pair interaction in solution will provide valuable additional information on the equilibria established between ion pairs and their higher aggregates in solution.

4:2 EXPERIMENTAL

4:2:1 Spectra

The high frequency spectra, 10,000 to 400 cm^{-1}, were taken on a Grubb-Parsons potassium bromide prism-grating spectrometer. A few of the medium frequency spectra, especially in the 350 to 500 cm^{-1} region, were taken on a Grubb-Parsons DM-4 caesium iodide prism-grating spectrometer which operates in the 200 to 500 cm^{-1} region. Due to the low solubilities of many of the salts, rendering it necessary to use exceptionally thick samples, solvent attenuation was so severe that few useful spectra were obtained using this instrument. The low frequency spectra, 60 to 350 cm^{-1}, were taken on the double beam far infra-red spectrometer described in

the previous sections.

Solid samples were examined in nujol or hexachlorobutadiene mulls. In order to entirely eliminate differential absorption due to the solvent, solutions were examined in modified Research and Industrial Instrument Co. variable path length, 0 to 5 mm, liquid cells type P.E.-01. These cells are supplied with potassium bromide windows for use in the 400 to 10,000 cm^{-1} region and the initial modification was to replace the potassium bromide windows with crystal quartz ones for use below 250 cm^{-1}. This posed two problems:

1) Due to relatively strong absorption in the 100 to 250 cm^{-1} region it is only possible to use about 1 mm thickness for the cell window if attenuation of the signal is to be limited to 50%. Consequently, in order to avoid severe interference effects at approximately 2 cm^{-1} intervals, it is necessary to use wedge-shaped windows, the thickness tapering from 1 mm to 0.9 mm across a diameter. Even this is insufficient to prevent some interference bands being apparent below 100 cm^{-1} and it raises the problem that the two windows of the cell are no longer parallel. Consequently neither is the exact cell thickness known, nor is it possible to bring the windows together to zero thickness. This makes it impossible to measure extinction coefficients quantitatively.

2) Crystal quartz has an extremely intense absorption at 128 cm^{-1} associated with a polar optic vibrational mode of the crystal (112). Even though this absorption is very narrow, bandwidth about 6 cm^{-1}, it renders spectroscopy in the 120 to 140 cm^{-1} region very difficult with quartz windowed cells.

These problems could only be overcome by modifying the cells to accept polythene windows. Of the several methods attempted the most satisfactory appeared to be the use of stepped windows individually machined from 4.5 mm high density polythene sheet (Vitrathene, Stanley Smith Ltd., Worple Road, Isleworth, Middx.). The use of such a thick polythene

window prevented distortion and consequent alteration in the path length of the cell and also eliminated interference effects since the band spacing, 0.75 cm^{-1}, was appreciably less than the spectral slit width normally employed. The use of high density polythene reduced the possibility of absorption of the solvent by the polymer and the consequent observation of spurious bands which had been noted in the case of low density polythene, especially in association with pyridine. This effect was entirely avoided by discarding the windows after five to ten runs and whenever the solvent was changed.

4:2:2 Solvents

It was found necessary to dry the solvents extremely carefully, small quantities of water in the solvents were sufficient to cause large changes in the solubilities of the salts and in the intensities of the absorption bands observed, although no change in the band frequency was observable. The ethers, tetrahydrofuran (Hopkins and Williams Reagent Grade) and 1:4 dioxane (May and Baker), were distilled under reflux with hydrochloric acid, separated and dried with potassium hydroxide pellets, as recommended by Weissberger (113) to remove peroxides. The ethers were then distilled over sodium wire and the middle fraction collected and stored over further sodium. The amines, pyridine and piperidine (Hopkins and Williams Reagent Grade), were dried over barium oxide and distilled just before use. Benzene (May and Baker pure recrystallisable) was dried over phosphorous pentoxide and distilled as required.

In order to avoid ascribing absorption bands of the solvent to solute absorptions it is necessary to investigate the spectrum of the pure solvent. Dioxane was examined at a 2.0 mm path length in the range 225 to 60 cm^{-1} and an unexpectedly and relatively strong band was observed at 148 cm^{-1}. The far infra-red spectra, below 250 cm^{-1}, of dioxane does not appear to have been published but a complete vibrational assignment has been made by Malherbe and Bernstein (114) where the lowest fundamentals given are the infra-red active ν_{19} and ν_{28} ring

bending modes at 273 and 283 cm^{-1} respectively. In a recent discussion of the assignments of cyclohexane, dioxane and trioxane, Ward (115) does not call into question the dioxane assignment of Malherbe and Bernstein and assigns the ring bending modes in all three molecules to the 200 to 300 cm^{-1} region. Nevertheless, the bands at 273 and 283 cm^{-1} are extremely weak and would appear to be overtones of the fundamental frequencies at around 140 cm^{-1}. In the present experiment the wide spectral slit width and the fast scan might account for the failure to resolve the two fundamentals.

Pyridine shows strong absorption at 406 cm^{-1} and weaker bands at 367 and 208 cm^{-1} due to vibrational fundamentals (116). Increasing absorption below 140 cm^{-1} is observed which has been ascribed by Jakobsen and Brasch (9) to dipolar interactions.

Piperidine shows two weak absorptions in the 100 to 200 cm^{-1} region not reported in the literature (117) at 124 and 146 cm^{-1}. Tetrahydrofuran shows no distinct bands in the 250 to 150 cm^{-1} region but shows increasing absorption with decreasing frequency in the whole region due to dipolar absorption.

4:2:3 Salts

The starting material for all the salts was sodium tetraphenylboron (Hopkins and Williams Reagent Grade) which was used without further purification. The potassium and ammonium salts were prepared metathetically from the sodium salt and the respective chloride, as recommended by Szwarc et al. (118). The insoluble potassium and ammonium salts were filtered, washed and recrystallised twice from aqueous acetone and dried under vacuum.

The lithium salt cannot be prepared metathetically in aqueous solution as it is soluble in water. It can, however, be prepared in an analagous manner in tetrahydrofuran in which sodium chloride is only sparingly soluble. After centrifuging the sodium chloride off the lithium tetraphenylboron is recovered by evaporation of the solvent as described by

Szwarc. The crude lithium tetraphenylboron is then dissolved in excess 1:2 dichloroethylene, the excess lithium chloride removed by centrifugation and the lithium tetraphenylboron recovered by precipitation on the slow addition of cyclohexane. This removal of the lithium chloride was repeated to give a pure specimen of lithium tetraphenylboron which was then dried under vacuum.

ND_4BPh_4 was prepared metathetically from ND_4Cl (Ciba: isotopic purity greater than 99%) and sodium tetraphenylboron in D_2O solution. In order to prevent isotopic exchange with the filter paper the insoluble ND_4BPh_4 was centrifuged: despite thorough wetting of the precipitate, however, the D_2O layer persistently centrifuged to the bottom of the tube. It was removed by a long needled syringe and the precipitate washed twice more with D_2O to remove the sodium chloride. As the sodium chloride was removed the density of the D_2O decreased until on the fourth addition of D_2O centrifugation at 5,000 r.p.m. for 15 minutes failed to separate the precipitate. Further washing was, therefore, impossible and the ND_4BPh_4 was dried under vacuum. The isotopic purity was checked by observation of the relative intensities of the N-H and the phenyl C-H stretching vibrations of the solids in hexachlorobutadiene mulls in the near infra-red. This established a minimum isotopic purity for the ND_4^+ salt of 84%. In view of the difficulties encountered in its preparation this appears to be a satisfactory value: a higher isotopic purity might have been obtained if the separation of the insoluble ND_4BPh_4 from the soluble sodium chloride had been effected on a filter paper that had been previously allowed to exchange with D_2O rather than by centrifugation.

In view of the fact that the ND_4^+ salt was to be used in solution in polar solvents possessing C-H groups in five and six membered rings, it was necessary to establish the rate of isotopic exchange in such a solvent. A 0.1 M solution of the ND_4^+ salt in pyridine was prepared and after allowing the solution to stand for a prescribed time the salt was recovered by evaporation of the pyridine: the isotopic purity was then measured by the

method outlined above. No decrease was detectable in a solution which had been allowed to stand for one hour, the approximate time taken to observe a typical spectrum. In a solution that had been standing for 90 hours the isotopic purity had fallen from 84% to 60% so that the rate of exchange is relatively slow and can present no problems in this research.

4:2:4 Measurement of extinction coefficients

The absorbance, A, of a sample is given by:

$$A = \log_{10} I_o / I = \varepsilon c l$$

where ε = extinction coefficient

c = concentration of solution

l = path length of solution.

The measurement of extinction coefficient requires, therefore, a plot of absorbance against the product of concentration and path length. The latter was measured to within $\pm$ 0.01 mm by using the variable path length cells, described in Section 4:2:1, fitted with 4.5 mm high density polythene windows. Zero path length may then be accurately established by closing the cell until the windows are in contact, a procedure that cannot be adopted with crystal quartz or potassium bromide windowed cells. The cell was then opened to the desired path length.

The solutions were prepared volumetrically which probably places a limit of about $\pm$ 1% on the reported concentrations.

Since the variations of transmission efficiency with frequency of the two beams may not be constant and also in order to eliminate systematic differences of path length between the two cells, the pure solvent and the solutions were ratioed against a common reference, usually the pure solvent, and the solute absorbance derived from these results.

If for the first comparison, R, is the reference and, S, the pure solvent in the sample beam, then

$$\text{Ln } I_R = \text{Ln } I_{OR} - K_R$$

$$\text{Ln } I_S = \text{Ln } I_{OS} - K_S$$

where I_O = intensity incident on the cells in each beam

I_R+ I_S = intensity incident on detector from each beam

K = reflection losses from the cell windows and absorption caused by the liquids in the cells.

$$\text{Ln } (I_R/I_S) = \text{Ln } (I_{OR}/I_{OS}) - (K_R - K_S) \qquad \text{EQUATION 4:1}$$

If for the second comparison the same reference, R , is used and a solution,N, placed in the sample beam, then

$$\text{Ln } I_{R'} = \text{Ln } I_{OR}\, C - K_R$$

$$\text{Ln } I_N = \text{Ln } I_{OS}\, C - K_S - E_N$$

WHERE c = constant representing the change in source energy

E_N = absorbance of the solution less absorbance caused by the solvent.

$$\text{Ln } (I_{R'}/I_N) = \text{Ln } (I_{OR}/I_{OS}) - (K_R - K_S) - E_N$$

$$= \text{Ln } (I_R/I_S) - E_N \qquad \text{EQUATION 4:2}$$

Therefore, from Equations 4:1 and 4:2

$$E_N = \text{Ln } \frac{(I_R/I_S)}{(I_{R'}/I_N)} \qquad \text{EQUATION 4:3}$$

Both the sample and reference signals could be determined to about ± half a division of the recorder chart paper. This represents an uncertainty in the absorbance of about 2% if the absorbance is 0.7 (sample absorption 50%) but this rises to an uncertainty of about 4% if the absorbance rises above 1.0 or falls below 0.1 corresponding to 80% and 20% sample absorption respectively. For this reason the sample absorption was kept between 20% and 80% while measuring the extinction coefficients whenever possible. At least three measurements were made at each concentration with an overall reproductability of better than 5%. The extinction coefficients were determined from at least four concentration points and this enabled the extinction coefficients to be evaluated to a similar accuracy of about ± 5%. The measurement of a single extinction coefficient normally occupied about eight hours. A solution of the sodium salt in pyridine was examined, therefore, to see whether any deterioration of the solution occurred within this period if the solution was allowed to stand on the bench in a stoppered flask. No change in extinction coefficient was detectable over a period of twenty-four hours under these conditions and it was concluded that no special precautions were necessary to prevent deterioration of the solutions providing the measurements were made on the same day as the solutions were prepared.

The extinction coefficients were, with the exception of the sodium salt, measured at the frequency of maximum absorption. The sodium salt measurements were made at 185 or 164 cm^{-1} whereas the band centre is at 175 cm^{-1}. In the 160 to 190 cm^{-1} region strong water bands are centred at 157.6, 166.8, 170.4, 173.5, 176.1, 177.6, 181.5 and 188.3 (see Figure 3:1). The spectral slit widths used were of the order of four to five wavenumbers, consequently, if the absorption coefficients measured are not to be critically dependent on the amount of water vapour in the cell, measurements can only be made at 164 or 185 cm^{-1}. (Although the sample cell is dessicated with phosphorous pentoxide up to one hour is needed between each removal of the cell to ensure complete dryness and if

measurements were made close to water vapour absorption lines considerable delay would be experienced while waiting for the cell to dry.) The extinction coefficients measured at 164 and 185 cm^{-1} were found to be equal to within the limits of experimental error, $\pm$ 5%, and it is estimated that these values are not more than 5% below the maximum value at 175 cm^{-1}.

4:3 RESULTS AND DISCUSSION

4:3:1 Evidence for the basic interaction that gives rise to low frequency absorption of dissolved ions in polar solvents

It has been suggested by Evans and Lo (10) that the broad, low frequency absorption observed in a series of tetra n-alkyl ammonium halides in benzene resulted from an interionic interaction between the two ions in solution. The exact absorption maxima was dependent on the nature of the anion present, and it was noted that the absorption maxima was closely correlated to the reciprocal of the root of the reduced mass of the ion pair system, which suggests a two particle vibration. As further evidence to support the assignment to an interionic vibration it was noted that the absorption maxima were close to the lattice modes in the solid state which can, with certainty, be ascribed to an interionic interaction.

A similar dependence of absorption frequency on the reduced mass of the ion pair system was observed by Edgell, Watts, Lyford and Risen (103) for the broad, low frequency absorption of alkali metal pentacarbonyl manganese and tetracarbonyl-cobalt salts in tetrahydrofuran. In this case the assignment to an interionic interaction was further supported by conductiometric and near infra-red measurements which showed that ion pairs were the predominant species present in these solutions in the concentration ranges investigated.

It will be noted that both sets of authors relied, presumably due to experimental difficulties, on measurements in a single solvent. None of

the evidence presented by these authors completely eliminated the possibility that the absorption was arising as a result of an ion solvent interaction. It appeared necessary as a first step, therefore, to establish the role of the solvent in the absorption by attempting to observe the absorption of a single salt in a range of polar solvents.

Tetra alkyl-ammonium halides are noted for their solubility in benzene (119) but their solubility in other solvents appears, in general, to be low (108) and it was decided to investigate the alkali metal tetraphenylboron salts for which a limited amount of low concentration conductiometric data is available (118).

A comparable absorption to that observed by Evans and by Edgell was first observed for sodium tetraphenylboron in 1:4 dioxane which showed weak absorption in the 100 to 225 cm^{-1} region with the absorption maxima at about 175 cm^{-1}. As has been noted (Section 4:2:2) dioxane has a strong vibration fundamental centred on 148 cm^{-1}: by using the variable path length cells described in Section 4:2:1, however, it was possible to compensate almost exactly for this absorption, albeit with a marked decrease in the energy throughput in the 120 to 170 cm^{-1} region, so that the observation of the broad, weak band in a 2.0 mm path length of 0.025 molar sodium tetraphenylboron in dioxane was unambiguous. Due to the extreme broadness of the band, bandwidth about 80 cm^{-1}, location of the band centre was not precise, a series of four runs all placed it at 175 ± 3 cm^{-1}. The absorption in the 60 to 220 cm^{-1} region as compounded from a number of experimental runs is illustrated in Figure 4:1.

Having thus established the presence of a broad absorption for sodium tetraphenylboron in dioxane, similar to that observed by Evans and by Edgell for entirely different systems, a critical experiment was to see whether a similar absorption could be observed for the same salt in a second solvent and, if so, at what frequency. The solvent chosen was pyridine on account of its known transparency in the 350 to 130 cm^{-1}

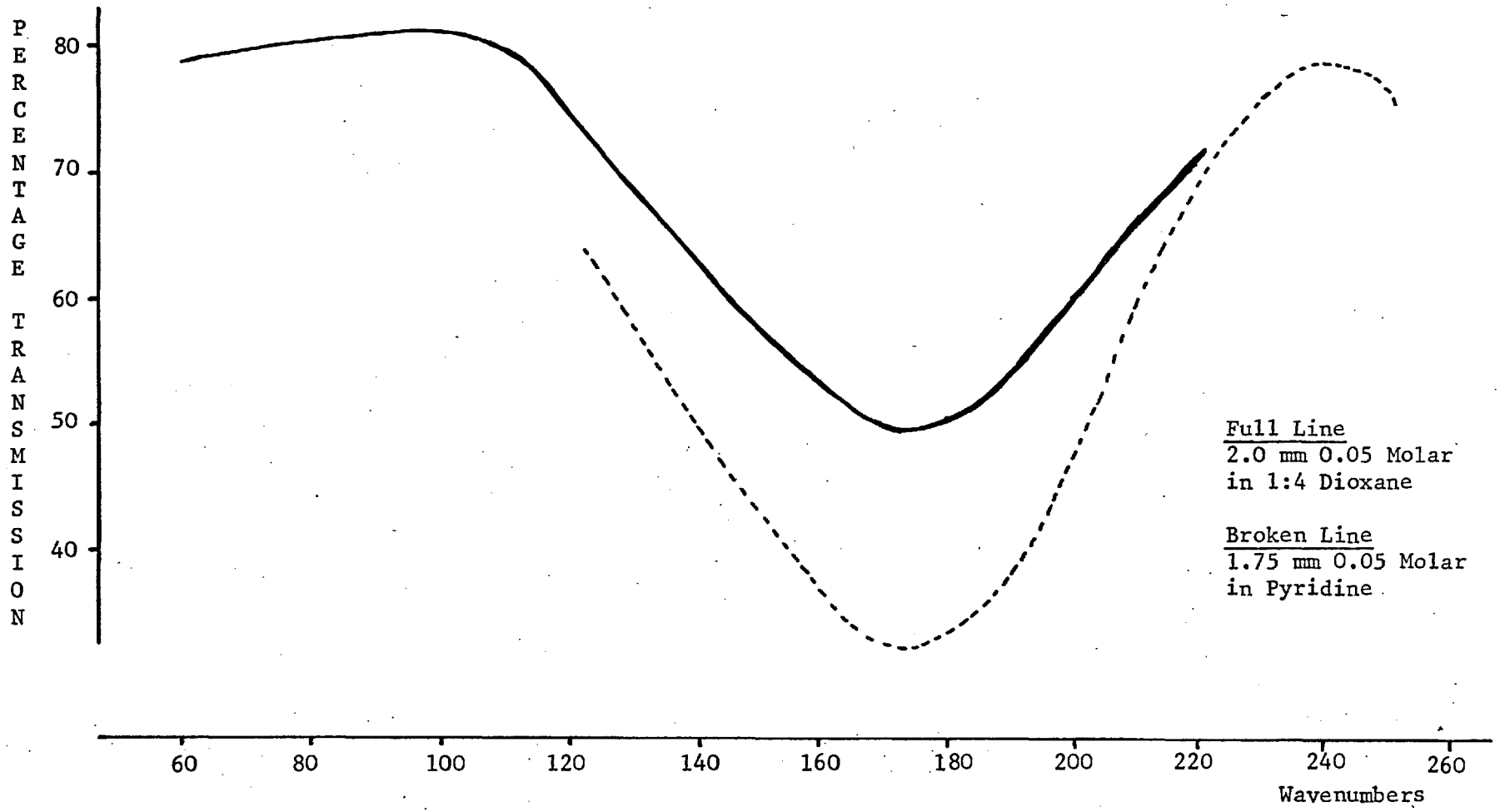

Figure 4:1 Compounded Spectrum Of the Interionic Vibration of Sodium Tetraphenylboron

region, apart from a sharp band at 208 cm^{-1} (see Section 4:2:2) and its highly polar nature compared to the small dielectric constant of dioxane. A 0.1 molar solution of sodium tetraphenylboron in pyridine at 2.0 mm path length showed a similar, but much more intense, band to that observed in dioxane. Once again, due to the extreme broadness of the band, about 80 cm^{-1}, it was not possible to locate the band centre with great precision but in a series of four runs no change from that observed in dioxane, 175 $\pm$ 3 cm^{-1}, was detected.

Sodium tetraphenylboron proved to be insoluble, that is, it is not possible to prepare a solution having a molarity greater than 10^{-3}, in all the remaining solvents normally employed in far infra-red spectroscopy, whose transmissivity in the 100 to 200 cm^{-1} region approaches that of benzene. Among the solvents tried were benzene, hexane, cyclohexane, chloroform, carbon tetrachloride, tetrachloroethylene, tetrachloroethane, dichloromethane, chlorobenzene, ethyl bromide, carbon disulphide, triethylamine, diphenyl ether, anisole and furan.

The solvents in which sodium tetraphenylboron is readily soluble, such as alcohols, ketones, amides and nitriles, have extremely low or negligible transmissivities in the far infra-red, less than 2% that of benzene, due to either hydrogen bonding or to dipolar interaction. The only solvents in which sodium tetraphenylboron was soluble and which appeared to offer any possibilities of use on the basis of their transmissivities at 170 cm^{-1} were dimethyl sulphoxide, nitrobenzene, piperidine, tetrahydrofuran and substituted pyridines such as 4-methylpyridine and quinoline. Since the dielectric constants of substituted pyridines are similar to that of pyridine it was felt that little further information on possible ion-solvent interaction would be gained by their use and attention was confined to the remaining solvents.

A 0.1 molar solution of sodium tetraphenylboron in piperidine at 1.0 mm path length was found to have a broad, bandwidth about 80 cm^{-1}, absorption centred on 175 $\pm$ 3 cm^{-1} and of about the same intensity as that observed in dioxane. Tetrahydrofuran shows increasing absorption below 120 cm^{-1}

due to dipolar interaction and although overall attenuation in the 120 to 180 cm^{-1} region is high, restricting sample thicknesses to 0.5 mm, measurements on the sodium salt were possible. A 0.1 molar solution of sodium tetraphenylboron in tetrahydrofuran at 0.5 mm path length showed a broad absorption, similar to that observed in the other three solvents, whose band centre could not be located to better than 175 $\pm$ 3 cm^{-1}. The intensity appeared to be intermediate to that observed in pyridine and that in dioxane.

Nitrobenzene has a strong vibration fundamental centred on 179 cm^{-1} (120) and absorbs strongly below 140 cm^{-1} due to dipolar interactions. Although it would be desirable to perform some experiments in nitrobenzene on account of its very high dielectric constant, 34.8 Debye, this did not prove possible either on the sodium potassium or ammonium salts as the expected absorptions of all (Section 4:3:2:1) correspond to intense nitrobenzene absorption. Dimethyl sulphoxide also has an extremely high dielectric constant making it an attractive solvent but in this case the onset of dipolar absorption occurs at 180 cm^{-1} rendering measurements on the sodium salt impractical.

A broad absorption has, therefore, been observed for sodium tetraphenylboron in four solvents, dioxane, piperidine, tetrahydrofuran and pyridine and within the accuracy imposed by the extreme bandwidth the absorption maxima were identical in all four solvents at 175 $\pm$ 3 cm^{-1}. A very significant difference in relative intensities was, however, observed in the four solvents and this will be considered further in Section 4:3:3.

The constancy of the absorption frequency in four solvents as diverse as pyridine, tetrahydrofuran, piperidine and dioxane is good evidence that the absorption does not arise as a result of ion-solvent interaction. If the absorption were caused in this way the very different nature of the donor oxygen and nitrogen atoms in the different solvent molecules could not fail to alter the force constant of the interaction and this would

be manifested by a change in the absorption frequency.

This is the first experimental justification for eliminating ion-solvent interaction as a cause for the low frequency absorption of ions dissolved in polar solvents and taken in conjunction with the evidence of Evans and Edgell provides four grounds for attributing the absorption to an interionic interaction:

1) Proximity of bands to interionic vibration lattice bands in the solid state.
2) Correlation between frequency and reduced mass of the ion pair system.
3) Conductiometric and near infra-red measurements showing that at these concentrations it would be expected that a proportion of the ions of the dissolved salt would be present as contact ion pairs.
4) Absence of strong ion-solvent interaction.

Assuming, therefore, that the absorption arises from an interionic vibration between contact ion pairs, the evidence that this affords as to the form of the interionic potential will now be considered, returning to further evidence of the absence of strong ion-solvent interaction in Section 4:3:4.

4:3:2 The Interionic Potential

4:3:2:1 Force constant of interionic vibration

A knowledge of the magnitude of the vibrational force constant is of prime importance to an understanding of the form of the potential function of any vibrating system. The force constant of the interionic vibration may be calculated, to a first approximation, from that applicable to a simple harmonic oscillator where the energy levels are given by

$$E_v = (1/2\ c)\ (k/\mu)^{\frac{1}{2}}$$

where k = force constant
μ = reduced mass
v = vibrational quantum number.

The fundamental vibration frequency, ν, is, therefore, given by

$$\nu_o = E_1 - E_o = (1/2\pi c)\ (k/\mu)^{\frac{1}{2}} \qquad \text{EQUATION 4:4}$$

Both Edgell et al. and Evans and Lo observed an almost linear relationship between the absorption frequency and the reciprocal of the root of the reduced mass of the interionic system suggesting that the force constant was almost invariant over the range of systems studies by these authors. It was desired, therefore, to observe experimentally the relationship between the absorption frequency and the reduced mass for a series of tetraphenylboron salts to see whether any significant variation in the force constant between different salts was observed.

1) Sodium salt It was shown in Section 4:3:1 that the absorption maxima for this salt was centred on 175 $\pm$ 3 cm^{-1}.

2) Lithium salt 0.5 mm of 0.5 molar lithium tetraphenylboron in tetrahydrofuran showed a strong broad, bandwidth about 90 cm^{-1}, absorption centred on 410 $\pm$ 5 cm^{-1} (illustrated in Figure 4:2). It was not possible to use pyridine as a solvent due to the presence of a strong vibrational fundamental at 406 cm^{-1} (116) but from the results of Section 4:3:1 it will be seen that the absorption frequency is not critically dependent on the nature of the solvent.

3) Ammonium salt 2.0 mm of 0.1 molar ammonium tetraphenylboron in pyridine showed a broad, bandwidth about 80 cm^{-1}, absorption centred on 198 $\pm$ 3 cm^{-1} (illustrated in Figure 4:3). Although the position of the band centre was determined seven times it was not possible to locate the band centre to a greater accuracy than that given.

4) Ammonium D_4 salt 2.0 mm of 0.025 molar ammonium-D tetraphenylboron in pyridine showed a similar band centred on 183 $\pm$ 3 cm^{-1} (illustrated in Figure 4:4). Once again, five measurements of the band centre failed to locate it with any greater precision.

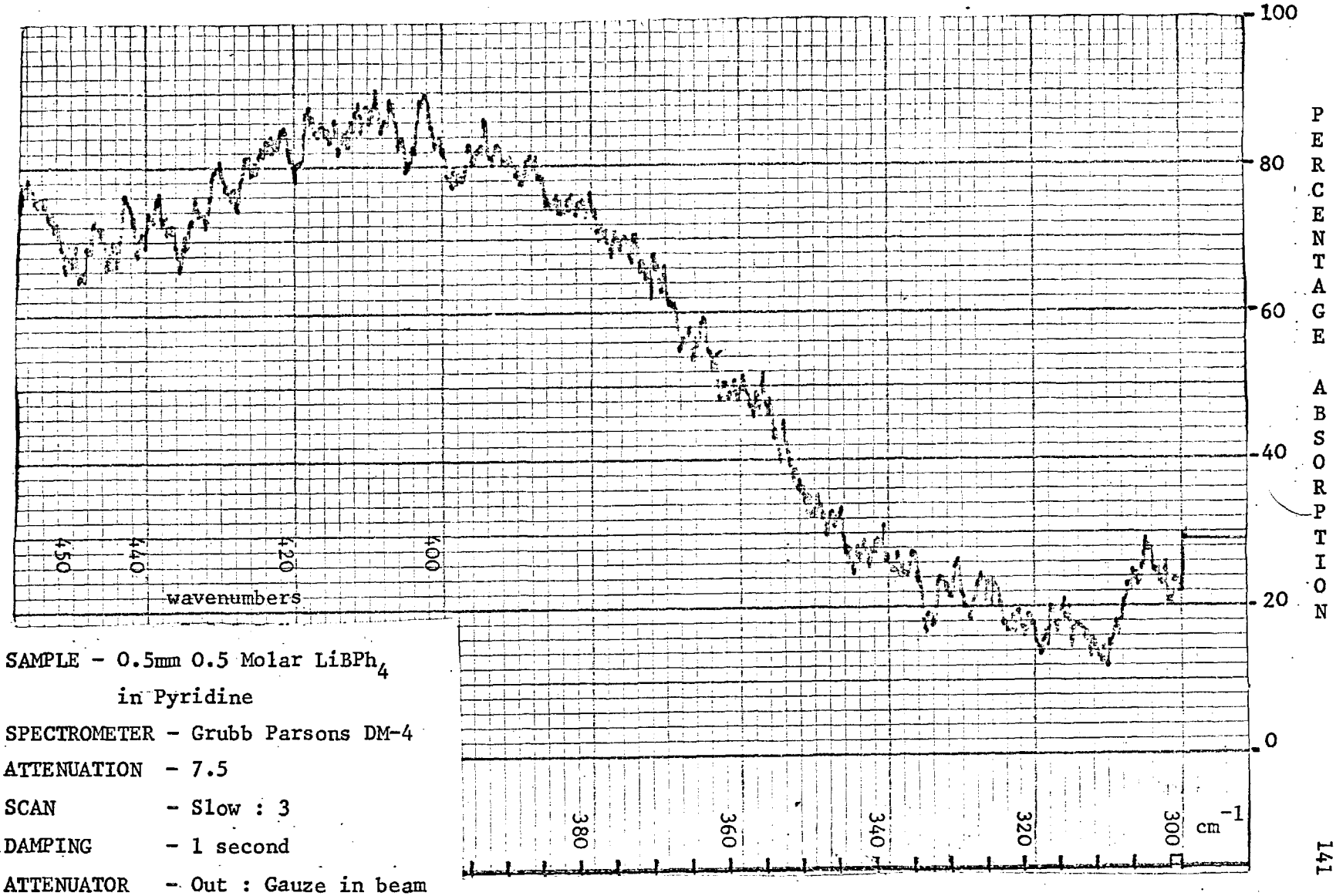

SAMPLE - 0.5mm 0.5 Molar $LiBPh_4$
in Pyridine
SPECTROMETER - Grubb Parsons DM-4
ATTENUATION - 7.5
SCAN - Slow : 3
DAMPING - 1 second
ATTENUATOR - Out : Gauze in beam

Figure 4:2 The Interionic Vibration of Lithium Tetraphenylboron

SAMPLE - 2.0 mm 0.01Molar NH_4BPh_4
in Pyridine
RESTSTRAHLEN 2 NaCl
TRANS FILTER KBr Chopper and B.P.
GRATING 246 lines per cm.
SLIT 8mm
SCAN 1 degree per minute
ATTENUATION 6
SCALE 3

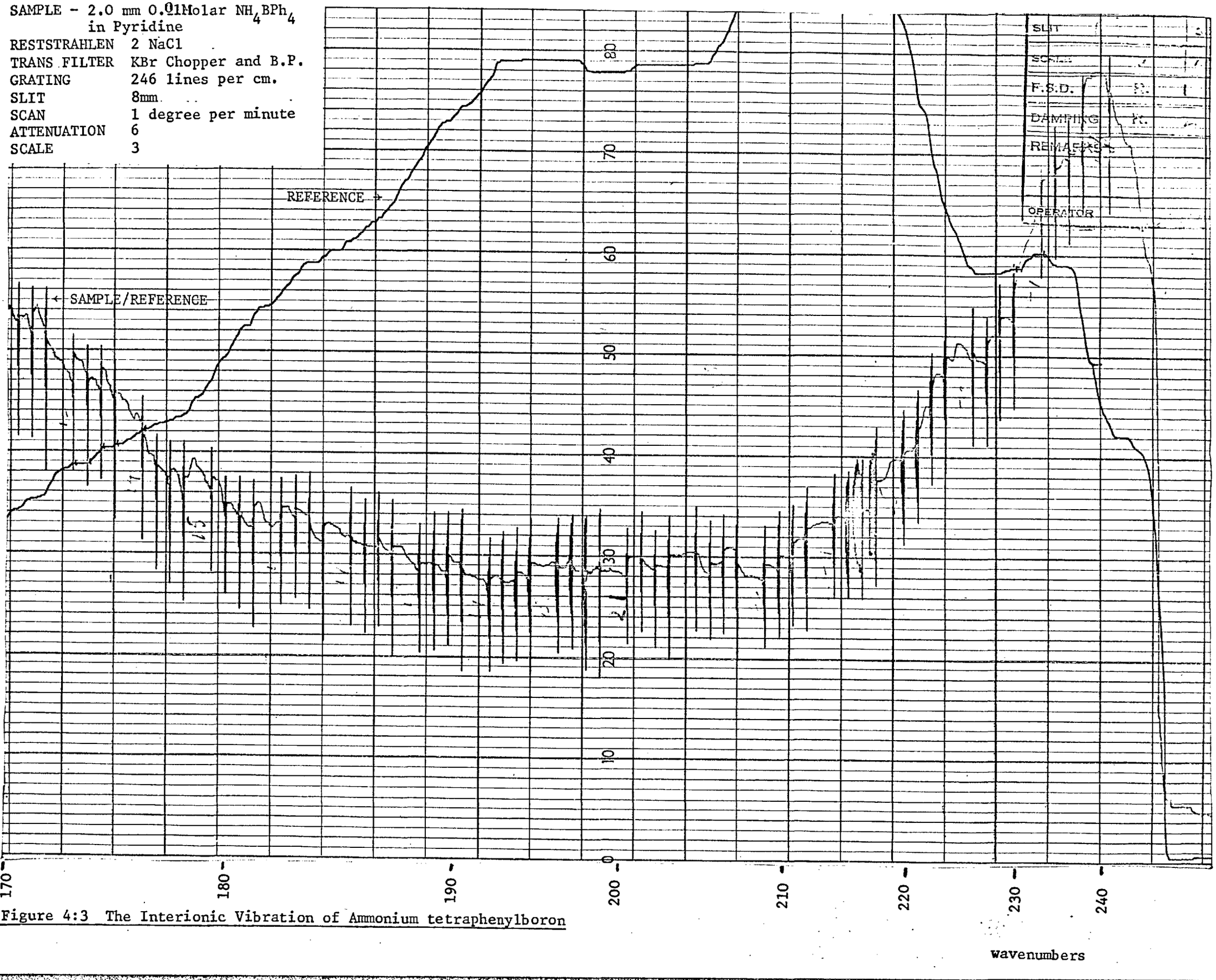

Figure 4:3 The Interionic Vibration of Ammonium tetraphenylboron

SAMPLE - 2.0mm 0.025 Molar ND_4BPh_4

in Pyridine

RESTSTRAHLEN	2NaCl
TRANS FILTER	KBr Chopper and B.P.
GRATING	246 lines per cm.
SLIT	11.5 mm
SCAN	1 degree per minute
ATTENUATION	6 SCALE 2

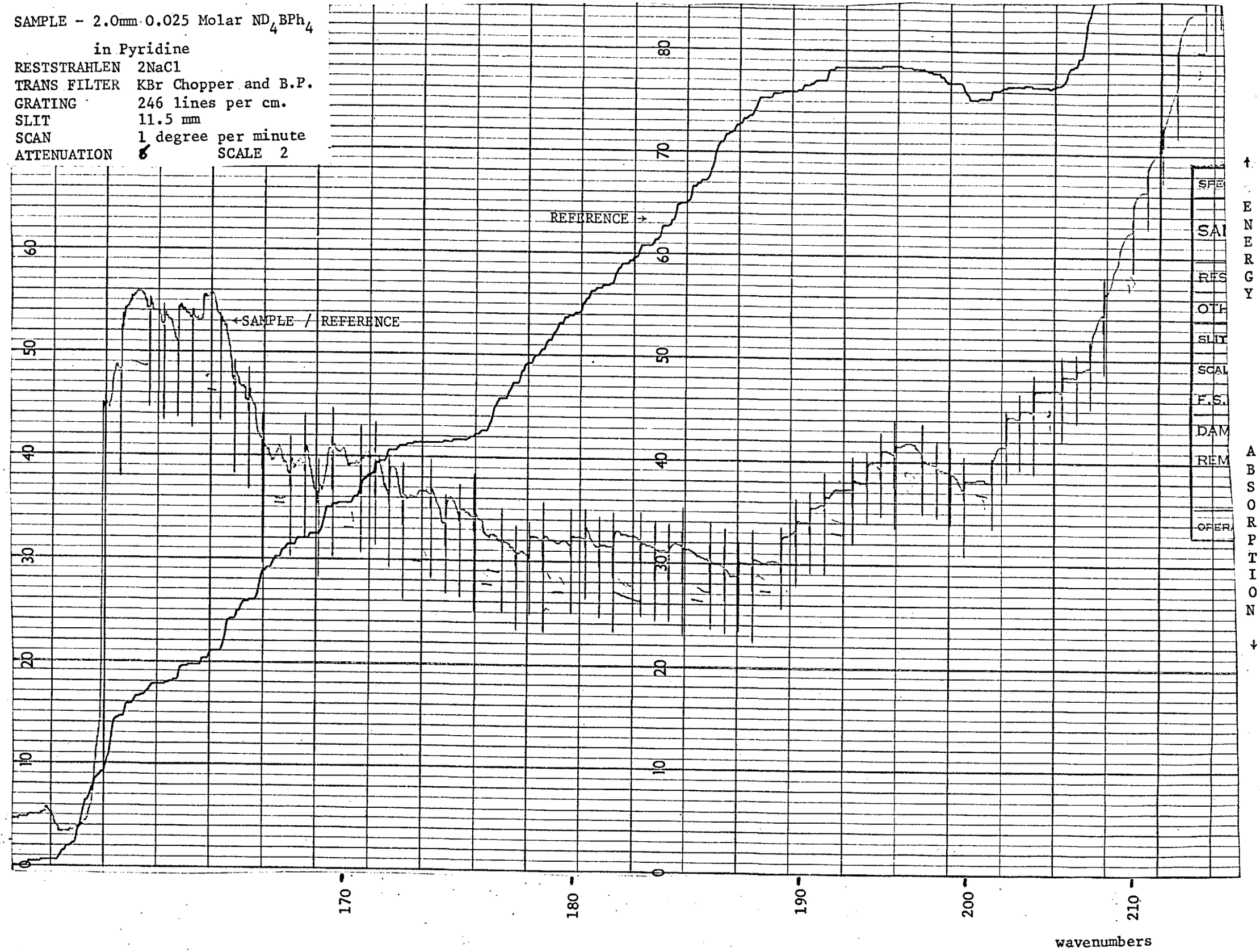

Figure 4:4 The Interionic Vibration of Ammonium D_4 Tetraphenylboron

5) Potassium Salt Increased absorption in the 130 to 140 wavenumber region does certainly occur with the potassium salt in polar solvents but great difficulty has been experienced in attempting to locate the exact band centre. Of the four solvents used for the measurements on the sodium salt, a saturated soltuion of the potassium salt in dioxane, piperidine or tetrahydrofuran is certainly less than 10^{-3} molar. From the expected extinction coefficients in these solvents (Section 4:3:3:3) a path length of at least 10 cm would be required at this concentration to observe the band which is quite impractical in this region of the spectrum.

In a polar solvent such as pyridine, where the solubility of the potassium salt is high, 0.1 M. solutions are possible, the solvent transmission at 133 cm^{-1} is extremely low on account of increasing absorption caused by dipolar interactions. It would be expected that the extinction coefficient of the potassium salt would be appreciably less than that of the sodium salt (Section 4:3:3:5) and therefore a path length of one to two millimetres would be required in order to observe the band. Solvent attenuation leads to low energy throughput and consequently a high noise level, making location of the band centre difficult. This is aggravated by the steeply rising solvent absorption as the frequency decreases. 0.1 molar solutions were used at 1.0, 1.75 and 2.0 mm and in each case the band centre was located at 136 $\pm$ 3 cm^{-1} although no estimates of the bandwidths were possible. Attempts were made to use the substituted pyridines 4-methyl pyridine and quinoline but these did not prove to have any greater transmission at 136 cm^{-1} than pyridine itself.

6) Other salts In view of the difficulties encountered with the potassium salt, no measurements were attempted on the rubidium, caesium, thallium or tetra n-butyl ammonium salts as their absorption frequencies were predicted on the basis of their reduced masses to be below that of the potassium salt. In addition, their solubilities in water (121) and tetrahydrofuran (118) have been reported to be even lower than that of the

potassium salt.

It was seen in Equation 4:4 that the fundamental absorption frequency was given by

$$\nu = (1/2\pi c)\ (k/\mu)^{\frac{1}{2}}$$

Therefore

$$k = 4\pi^2 \mu\ c^2 \nu^2$$

The force constants may be calculated, therefore, from the experimentally observed absorption frequencies and the reduced masses. This is shown in Table 4:1.

TABLE 4:1 VIBRATION FREQUENCIES, REDUCED MASSES AND FORCE CONSTANTS OF SOME TETRAPHENYLBORON SALTS

Cation	μ A.M.U.	$1/\mu^{\frac{1}{2}}$	ν C.M.$^{-1}$	K x 10^4 DYNE CM^{-1}
Li^+	6,79	0.384	410 $\pm$ 5	6.72
NH_4^+	17.04	0.242	198 3	3.94
ND_4^+	20.06	0.223	183 3	3.96
Na^+	21.45	0.216	175 3	3.87
K^+	34.84	0.169	136 3	3.80

The reduced mass of the ND_4^+ is calculated for 85% ND_4^+ and 15% NH_4^+.

It will be observed that the calculated force constants for the sodium, potassium, ammonium and ammonium D_4 salts are almost identical and a rather larger value is obtained for the lithium salt. The variation of

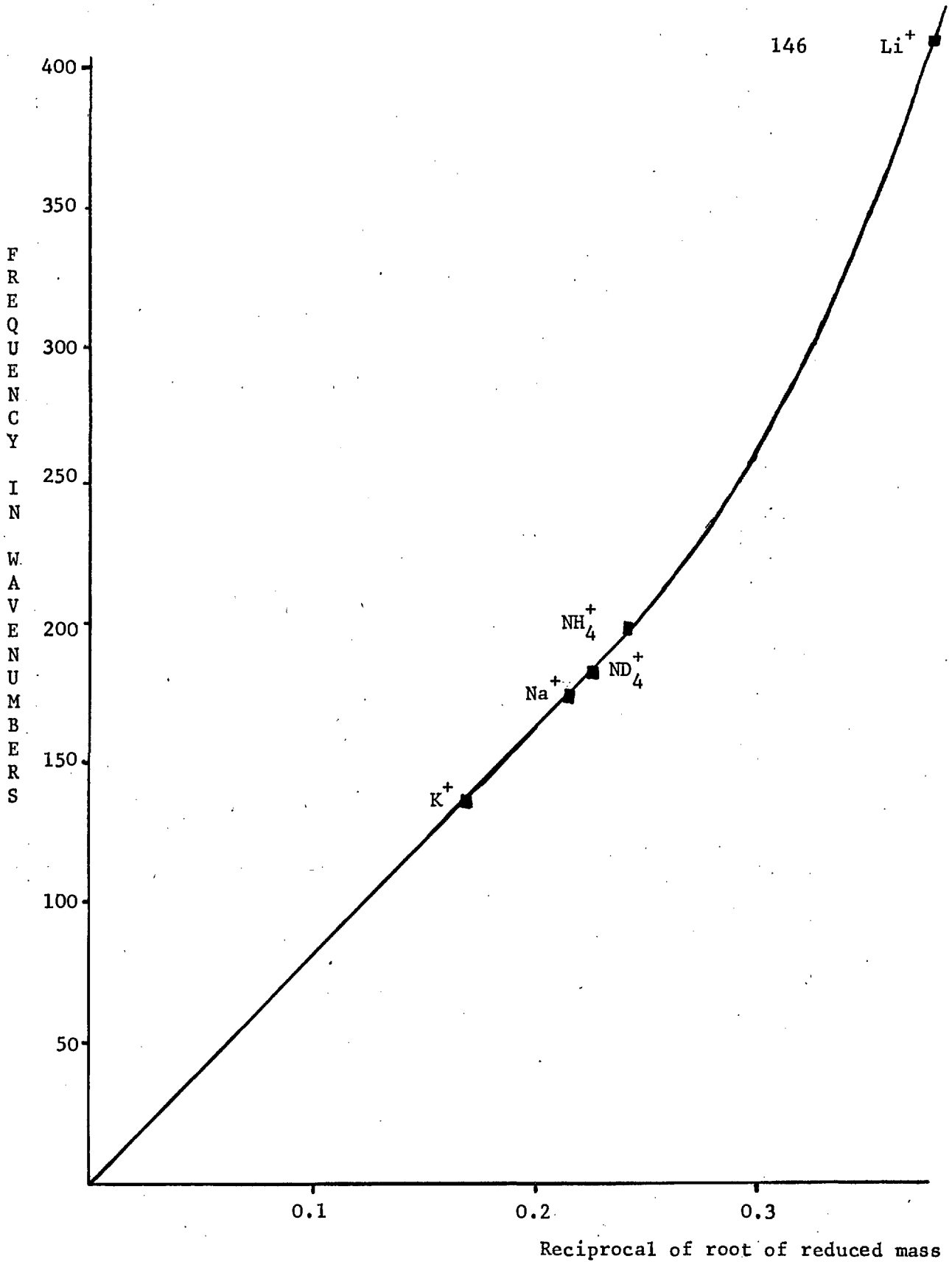

Figure 4:5 Variation of Force Constant for some Tetraphenylboron salts

force constant in the different salts is also shown graphically in Figure 4:5 where the absorption frequency is plotted against the reciprocal of the root of the reduced mass of the interionic system. The linearity observed for the potassium to ammonium salts indicates a largely invariant force constant with a higher value for the lithium salt.

4:3:2:2 Anharmonicity of the interionic vibration

A second feature of the interionic vibration that it might be possible to observe experiementally and which provides information on the form of the potential function is the frequency of the first overtone and its intensity relative to the fundamental. It will be shown below that it did not prove experimentally possible; nevertheless the absence of an intense overtone permits some conclusions to be drawn as to the probable limits of anharmonicity of the fundamental vibrations.

The sodium and lithium salts were carefully examined to see whether the position of the first overtone could be established. From the fundamental frequencies it would appear that the first overtone for the sodium salt would be expected in the 250 to 350 cm^{-1} region and in the 700 to 800 cm^{-1} region for the lithium salt.

A 0.25 molar solution of the sodium salt in pyridine was examined at the relatively long path length of 2.0 mm in the 200 to 350 cm^{-1} region. No absorption was observed in the 350 to 300 cm^{-1} region but increasing absorption at lower frequencies due to the fundamental already observed at 175 cm^{-1} was noted. A sharp,bandwidth about 10 cm^{-1}, absorption centred on 256 cm^{-1} was also present but as this had already been observed as a doublet at 248 and 260 cm^{-1} in a nujol mull of the solid it may be confidently ascribed to an anion vibration fundamental. No measurements in the 350 to 400 cm^{-1} region were possible due to the presence of vibration fundamentals. In a further attempt to locate the overtone a 0.5 molar solution of sodium tetraphenylboron in tetrahydrofuran was

investigated at 0.5 mm path length in the 300 to 400 cm^{-1} region. No absorption attributable to the overtone was detected. This places a maximum limit of around 5% on the intensity of the overtone relative to that of the fundamental.

It appeared probable that the greatest anharmonic influences would be present in the potential of the small lithium ion and 0.25 molar solutions of lithium tetraphenylboron in both tetrahydrofuran and pyridine were examined in the 1,000 to 400 cm^{-1} range. Increasing absorption below 480 cm^{-1} was observed due to the fundamental already located at 410 cm^{-1} and it was possible to demonstrate the complete absence of absorption, apart from anion and solvent bands, in the range 480 to 600 cm^{-1}. Unfortunately at higher frequencies solvent absorption rendered the solution almost totally opaque and no useful measurements were possible.

Since the intensity of the overtones relative to the fundamental is dependent on the anharmonicity of the potential well the placing of an upper limit of 5% on the intensity of the overtone of the sodium tetraphenylboron interionic vibration relative to the fundamental permits us to place an upper limit on the anharmonicity of the potential function.

The anharmonicity may arise either as a result of mechanical anharmonicity due to the higher order terms in the potential energy function, or electrical anharmonicity due to higher order terms in the dipole moment expansion. A rigorous derivation of the relative intensities of the fundamental and its overtones in relation to the anharmonicity coefficients in the potential energy and dipole moment expansions has been given by Crawford and Dinsmore (122). In the case of the interionic vibration of tetraphenylboron salts, however, these coefficients are not known with sufficient accuracy to permit a rigorous calculation of the relative intensities.

A qualitative comparison of the relative intensities of the first overtone and the fundamental of the tetraphenylboron salts and a molecule of known anharmonicity is, however, feasible. For example, it is known that the

first overtone of the HCl vibration is about 2% of the intensity of the fundamental (123) and that the fundamental frequency is about 1/13 the dissociation energy and that the anharmonicity constant in the Morse Equation is about 1.73×10^{-2}. Anharmonicities greatly in excess of these values would not be expected, therefore, for an acceptable potential function of the interionic vibration.

4:3:2:3 The Interionic potential of Pettit and Bruckenstein

We have, therefore, two experimentally observed criteria on which to assess the applicability of any proposed interionic potential.

1) The potential function must be reasonably harmonic in the base of the potential well. As we have shown in the previous section, this condition cannot be placed on a rigorous basis since only qualitative comparisons with molecules of known harmonicities are possible. The condition would, for example, appear to eliminate a potential of the form:

$$V = \infty, r < r_e \qquad V = e^2/r \quad , \quad r > r_e$$

since such a potential would have a high anharmonicity in the base of the well.

2) The potential function must predict an approximately equal force constant for the potassium, sodium, ammonium and ammonium-D_4 salts and a slightly higher value for the lithium salt. In effect this means that the potential function must predict a force constant that is largely independent of the equilibrium internuclear separation since it would be expected that this would vary considerably between the sodium, potassium and ammonium ions.

The potential function of Pettit and Bruckenstein (109) which has proved reasonably successful in predicting the association constants for ion pair formation of the alkali metal halides and tetra n-alkyl ammonium halides will be considered first.

The most general expression for the potential energy, V, of an ion pair, AB, which allows for all possible interactions between the ions and their induced dipoles has been given by Pettit and Bruckenstein as

$$V = -(e^2/r + \mu_A/r^2 + \mu_B/r^2 + 2\mu_A\mu_B/r^3 - \mu_A^2/2\alpha_A - \mu_B^2/2\alpha_B - B/r^n)$$

where e^2/r = Coulombic attraction EQUATION 4:5

α = polarizability

and μ = induced dipole moments

B/r^n = summation of all other potential terms.

Induced dipole interactions contribute only a small part to the energy and the potential may be reduced to:

$$V = B/r^n - e^2/r$$

The parameter, n, was adjusted empirically by Pettit and Bruckenstein to give the best fit with the measured alkali halide ion pair potential energies and was evaluated to be 6.9 (about 7). Therefore:

$$dV/dr = -7Br^{-8} + e^2r^{-2}.$$

At the equilibrium internuclear separation:

$dV/dr = 0$ and $r = r_o$

Therefore, $B = e^2r^6/7$, and,

$$V = e^2(r_o^6/7r^7 - 1/r) \qquad \text{EQUATION 4:6}$$

The applicability of this potential to the interionic vibration may be tested by the two criteria mentioned above, the probable anharmonicity of the well and the variation of the force constant for different equilibrium internuclear separations.

1) Anharmonicity The probably degree of anharmonicity in the base of the well can be determined from the depth of the well in relation to the separation of the energy levels. The greater the number of energy levels

that may be accommodated in the well the greater the harmonicity of the base of the well.

It was seen in Section 4:3:2 that the separation of the E_o and E_1 energy levels, as given by the fundamental frequency, was, in the case of sodium tetraphenylboron, 175 cm^{-1}.

An approximate value for the depth of the potential well may be calculated from the work required to separate the two ions from their equilibrium internuclear separation to infinity. If it is assumed that the interionic potential at the equilibrium internuclear separation, r_o, is given by Equation 4:6 with $r = r_o$

$$V_o = -6\, e^2\, r_o \,/\, 7D$$

where D = the effective interionic dielectric constant

and that the interionic potential with the ions at infinity equals zero, then the work done to separate the ions to infinity, ΔF, is given by

$$\Delta F = 6\, e^2\, r_o \,/\, 7D \qquad \text{EQUATION 4:7}$$

The problem then arises as to what is the correct value for the interionic dielectric constant. The problem has been fully treated by Fuoss and Sadek (124) who propose that with the ions in contact it would be expected that the effective interionic dielectric constant would be unity, as was tacitly assumed in the derivation of Equation 4:6. As the ions are separated, however, the interionic space will remain empty, with D = 1, until there is just sufficient room to accommodate a single solvent molecule. At this point, where r equals r_s, the effective dielectric constant of the medium between the ions rises to the bulk dielectric constant of the solvent medium, D'.

The total work, F, from Equation 4:7 is therefore:

$$\Delta F = 6e^2/7D\,(\,1/r_o - 1/\{r_o + r_s\}) + 6e^2/\,7D'(\,1/\{r_o + r_s\}\,)$$

EQUATION 4:8

In order to apply Equation 4:8 to the sodium tetraphenylboron ion pair to calculate the effective depth of the potential well it is necessary to know the effective internuclear separation in the equilibrium configuration. It is normally considered that the effective internuclear separation is the sum of the bare anion and bare cation radii (125), but this assumption has been called into question by Bodenesch and Ramsey (126) who found evidence of lower interionic separations for ion pairs in solution than in the crystal lattice, and by Szwarc (127) who found that the best agreement between the calculated and observed heats of ionic dissociation for the alkali metal tetraphenylboron salts was observed if the sum of the bare ion radii was decreased by 10%. Following Szwarc the effective internuclear separation of a contact ion pair will be taken as 90% of the sum of the bare ion radii.

The bare ion radii of the alkali metal cations is taken to be their crystal radii (125) which in the case of the sodium ion is 0.95 A, for the lithium ion 0.60 A. and for the potassium ion 1.33A. (110). The bare ion radius of the tetraphenylboron can be deduced from conductiometric data where the system (i Am_3 - Bu)N^+ BPh_4^- has been extensively studied on account of the fact that the two large ions contribute equally to the conductance of the salt. Therefore

$$\Lambda^+ = \Lambda^-$$

where Λ = limiting conductance at infinite dilution

Λ^+ and Λ^- are related to the hydrodynamic Stokes radii of the corresponding ions by

$$R_+ = 0.8194 / \Lambda^+ \eta \qquad R_- = 0.8194 / \Lambda^- \eta$$

where η = viscosity of the solvent

R_- for the tetraphenylboron anion has been measured by Szwarc et al. (127) to be 3.95A. The Stokes radius is only equal to the bare ion

radius if specific interaction between the ion and the solvent does not occur. The dependence of the ion pair association constant with the dielectric constant of the solvent for the tetra-alkyl ammonium tetraphenylboron system has been extensively studied by Fuoss and Berns (128). In all solvents a linear relationship was found between the log of the association constant and the reciprocal of the dielectric constant which indicates the absence of specific solvation of either the cation or the anion. It may be assumed, therefore, that the Stokes radius approximates to the bare ion radius.

The sum of the bare ion radii for sodium tetraphenylboron is, therefore, 3.90 + 0.95 = 4.85A. The effective internuclear separation, r_o, may now be taken as 90% of the sum of the bare ion radii or 4.35 A.

The depth of the well may now be calculated from Equation 4:8, inserting the value of 4.35 A. for r_o and a value of, say, 2.0 A. for r_s. The most unfavourable case of solvent medium, i.e. that of pyridine where the high dielectric constant of 12.3 which will lead to the lowest value for the depth of the well will be considered.

$$F = 6\,e^2/7\ (\ 1/\ 4.35 - 1\ /\ 6.35\ ) + 6e^2\ /\ 86.1\ (\ 1/\ 6.35)$$

$$= (6\,e^2/7\ h\ c) \times 8.50 \times 10^{+2}\,cm^{-1}$$

$$= 8.46 \times 10^3\ cm^{-1}$$

If the energy level spacing throughout the well was constant at the 0→1 value of 175 cm^{-1} about 50 energy levels could be accommodated in the well. As the energy level spacing of the anharmonic oscillator decreases with increasing vibrational quantum number a greater number of levels than this can be expected to be present in the actual interionic well.

It has been shown in the case of the HCl molecule that the dissociation energy is 36,300 cm^{-1} in relation to a fundamental vibration frequency of 2,886 cm^{-1}. This represents the accommodation of many fewer levels in the HCl potential well than would appear to be present in the inter-

ionic well. Since the relative intensity of the first overtone to the fundamental in the case of HCl was only 2%, the harmonicity of the proposed interionic potential well would appear to be more than sufficient to account for the failure to observe the overtone of the interionic vibration.

2)Force Constants The force constant is given by the second derivative of the potential function at $r = r_e$, i.e.

$$k = (d^2V/dr^2),\ r = r_e$$

If the potential function is given by Equation 4:6

$$k = 6e^2/r_o^3 \qquad \text{EQUATION 4:9}$$

If it is assumed that each ion is carrying a full unit electronic charge and that the equilibrium interionic separation is given by the sum of the bare ions radii, then the values of the force constant may be calculated from Equation 4:9 and compared to those observed experimentally. This is shown in Table 4:2.

TABLE 4:2 COMPARISON OF FORCE CONSTANTS FOR INTERIONIC VIBRATION

Cation	K^+	Na^+	NH_4^+	ND_4^+	Li^+	
k obs.	3.80	3.87	3.96	3.94	6.72	x 10^4 dyne.cm^{-1}
r_o	5.63	4.35	5.74	5.74	4.05	Angstroms
$k_{\text{Eqn 4:9}}$	0.78	1.68	0.73	0.73	2.08	x 10^4 dyne.cm^{-1}
$\frac{k_{\text{Eqn 4:9}}}{k \text{ obs.}}$	0.21	0.43	0.18	0.19	0.31	

It can be seen from Table 4:2 that the agreement between the observed force constants and those calculated from the potential function is not good, the correlation is unsatisfactory in two respects:

1) The observed force constants do not show the large dependence on the equilibrium internuclear separation predicted by the potential function. In the case of the ammonium salts the comparison may not be justified since there is no evidence to show that, for these ions, the bare ion radius of the cation in an ion pair approximates to the crystal radius. In the case of the sodium, potassium and lithium salts, however, this argument cannot be used and the ratio of the calculated and observed force constants range from 0.19 in the case of the potassium salt to 0.43 for the sodium salt.

2) The calculated force constants are too small by a factor varying between two and a half and five. Although the calculation is only approximate, the assumptions made all lead to the highest possible value for the force constant. For example, if the effective charge on the ion was assumed to be less than the charge on the electron or if the effective dielectric constant of the interionic medium was assumed to be greater than unity due to the effect of the solvent, then in either case the calculated force constants would be even lower. The only way in which the calculated force constants could be reconciled with the observed values is by reduction in the equilibrium internuclear separation. In the case of the potassium salt, for example, it would require a value of r_o equal to 3.2 Angstroms in order to predict the experimentally observed value of the force constant. As this is considerably less than the bare ion radius of the tetraphenylboron anion alone this does not appear probable.

The interionic potential of Pettit and Bruckenstein appears to fail therefore on the grounds of predicting a large dependence of the force constant on the equilibrium internuclear separation which is not observed experimentally and in predicting force constants that are in the region of one quarter the observed values.

4:3:2:4 The Morse Potential

Another equation for the internuclear potential that has found widespread

use in vibrational and electronic spectroscopy is the Morse equation (129) and it was decided to attempt to apply this equation to the interionic vibration.

The Morse equation is given by:

$$V = (1 - \exp - a\{r - r_e\})^2 \qquad \text{EQUATION 4:10}$$

where D = dissociation energy

a = variable parameter governing curvature of well

r = internuclear separation

r_e = equilibrium internuclear separation

The energy levels of the Morse oscillator may be rigorously evaluated (130) as:

$$E_v = (a\{Dh/2\pi c^2\mu\}^{\frac{1}{2}})(v + \tfrac{1}{2}) - (ha^2/8\pi^2 c\mu)(v + \tfrac{1}{2})^2$$

If this is compared to the normal form of the equation for the anharmonic oscillator resulting from the consideration of a cubic term in the potential energy equation (131)

$$E_v = \nu_e (v + \tfrac{1}{2}) - x\nu_e (v + \tfrac{1}{2})^2$$

then it is seen that the fundamental frequency and the anharmonic coefficient of the Morse equation are given by:

$$\nu_e = a(Dh/2\pi^2 c\mu)^{\frac{1}{2}} \qquad \text{EQUATION 4:11}$$

$$x = ha^2/8\pi^2 c\mu\nu_e = h\nu_e/4D \qquad \text{EQUATION 4:12}$$

Comparison of Equation 4:11 with that obtained from the S.H.O. shows that the force constant of the Morse equation, k_M, is given by:

$$k_M = 4\pi^2 c^2\mu\nu^2 = 2Da^2$$

Equation 4:11 and Equation 4:12 show that the three experimentally observable features of a vibration; the fundamental frequency, the anharmonicity coefficient and the dissociation energy are interrelated by the Morse equation so that a knowledge of any two of them permits the third to be calculated. In the case of the interionic vibration of the tetraphenylboron salts only the fundamental vibration frequency is known. It was shown (Section 4:3:2:2) that it was not possible experimentally to observe the first overtone frequency from which the anharmonicity coefficient might have been calculated and direct spectroscopic observation of the dissociation energy of the interionic interaction is clearly not possible in the way that dissociation energies of molecules can be determined from their electronic spectra. If any progress is to be made, therefore, in the application of the Morse equation to the interionic vibration a calculated value of the dissociation energy must be used. Although the potential of Pettit and Bruckenstein fails to represent adequately the interionic potential close to the equilibrium internuclear separation, as discussed in Section 4:3:2:3, the potential has been successfully applied by Pettit and Bruckenstein to the calculation of the potential energy change that occurs when an ion pair is formed from two ions initially separate at infinity. It does not appear unreasonable, therefore, to use this equation, as modified to take into account the effective dielectric constant of the interionic medium, to obtain an estimate of the dissociation energy of the ion pair.

The dissociation energies of the sodium, potassium and lithium salts were calculated from Equation 4:8 and the values obtained were used in association with the experimentally observed vibration frequencies to calculate the curvature of the Morse well, a, and the anharmonicity coefficient, x, for these salts. In view of the uncertainty of the effective radius of the ammonium cation this procedure was not extended to the tetraphenylboron salts of these ions. The results of these calculations are presented in Table 4:3.

TABLE 4:3 THE CURVATURE OF THE MORSE WELL AND THE ANHARMONICITY COEFFICIENTS OF SOME TETRAPHENYLBORON SALTS

Cation	K^+	Na^+	Li^+		
ν	136	175	410		cm^{-1}
D - Eqn. 4:8	5.69	8.46	9.46	$\times 10^3$	$dyne.cm^{-1}$
a - Eqn. 4:11	1.30	1.07	1.34	$\times 10^8$	cm^{-1}
x - Eqn. 4:12	5.95	5.10	10.75	$\times 10^{-3}$	

The small variations in the calculated curvature of the Morse well, a, between the different salts could reflect an actual change in the form of the interionic potential in the different salts. This appears unlikely as the differences in curvature do not correlate with the increase in cation radius between the salts: although a change in the potential function between the salts may indeed be present, it appears probable that the differences in curvature of the well noted in Table 4:3 reflect the shortcomings of the equation used to calculate the dissociation energies rather than any positive evidence for a change in the interionic potential.

The calculated anharmonicity coefficients are of the same order of magnitude as that for HCl, 1.73×10^{-2}, and this is in accord with the failure to observe the overtone vibrations.

The Morse equation, therefore, satisfactorily accounts for the two observed features of the interionic vibration, its low anharmonicity and the changes in absorption frequency with the reduced mass of the interionic system.

4:3:3 Ionic Association

4:3:3:1 Introduction

It has been shown in the previous sections that the low frequency absorption of ions dissolved in polar solvents may be ascribed to an interionic interaction between the two ions of an ion pair. It was found experimentally that the force constants for the interionic vibration of the potassium, sodium, ammonium and ammonium D-4 tetraphenylboron salts are almost equal with a slightly higher value for the lithium salt. A simple two term potential function representing the Coulombic attraction, e^2/r, and a repulsion term, B/r^7, is inadequate in that it predicts that the force constant should be heavily dependent on the equilibrium interionic separation. The observed invariance of the force constant for the potassium to ammonium series may be rationalised on the basis of a Morse type potential function where the force constant may be independent of the equilibrium interionic separation.

In the previous sections, therefore, the variation of absorption frequency with the reduced mass of the interionic system has been discussed. A second feature of the absorption that was noted at an early stage of the experimental investigation was that, although the absorption frequency for a single salt in a range of solvents was constant, a wide variation in intensity was observed. Although it will be placed on a more quantitative basis below, it was readily apparent that the most intense absorption occurred in pyridine and the weakest in piperidine and dioxane, with the intensity in tetrahydrofuran in an intermediate position. This could be a reflection of either of two effects:

1) A variation of the extinction coefficient per ion pair system in the different solvents due either to the polarizability of the bulk solvent or to small solvent induced changes in the form of the potential function. The absorption intensity being very sensitive to the precise form of the potential function.

2) A variation of the proportion of the dissolved ions present as ion pairs in the different solvents.

These possibilities will be explored in the succeeding sections.

4:3:3:2 Possible Variation of Extinction Coefficient Per Ion Pair System in Different Solvents on Account of Polarization Effects

Using the S.H.O. approximation the integrated absorption intensity, I, for an absorption at a given frequency, including the contribution from hot bands may be shown to be (132)

$$I = \int \kappa d\nu = (N\pi/3c)\,(\{\mu_x^k\}^2 + \{\mu_y^k\}^2 + \{\mu_z^k\}^2) \qquad \text{EQUATION 4:13}$$

where $\mu_x^k = (\,d\mu_x/dQ_k\,)_o$

For an interionic vibration along the x axis,

$(\,d\mu_y/dQ_k)_o = 0$, and $(\,d\mu_z/dQ_k)_o = 0$, therefore,

$$\mu_x = e\Delta r/D \qquad \text{EQUATION 4:14}$$

where Δr = Change in internuclear separation

D = Effective interionic dielectric constant

If the extinction coefficient per ion pair system is dependent on the solvent then this may result from a variation of the effective dielectric constant for the interionic vibration, as given in Equation 4:14, with solvent. The dielectric constant of the solvent is related to its total molar polarizability, P, by

$$P = (\{D - 1\}/\{D + 2\})\,(M/\rho) \qquad \text{EQUATION 4:15}$$

where M = Molecular weight

ρ = Density

The total molar polarizability, P, is the summation of three polarizabilities, the electron polarizability, P_e,

$$P_e = (\{\eta^2 - 1\}/\{\eta^2 + 2\})\,(M/\rho) \qquad \text{EQUATION 4:16}$$

where η= visible refractive index.

the atomic polarizability, P_a, due to the normal vibrations of the molecule and the orientational polarization, P_o, given by the Debye Equation

$$P_o = (4\pi N/9K)\ (\mu^2/T) \qquad \text{EQUATION 4:16a}$$

where μ = dipole moment.

At frequencies of 10^{13}Hz. such as those encountered in the interionic vibration the electron polarizability will predominate with possibly a small contribution from the atomic polarizability. P_a is not readily accessible experimentally as it requires measurements of the refractive index in the far infra-red and it is customary (133) to take P_a as 10% of P_e. Its magnitude is, therefore, small compared to P_e and since its contribution to the total polarizability at 10^{13}Hz. is also small it may be neglected without undue error. Therefore:

$$P = P_e$$

Comparison of Equations 4:15 and 4:16 shows that the effective dielectric constant at optical frequencies is given by

$$D = \eta^2 \qquad \text{EQUATION 4:17}$$

If the variation of intensity of the interionic vibration with the solvent is due to the influence of the dielectric constant of the solvent medium, then the magnitude of the effect must be related to the effective dielectric constant of the solvent at frequencies in the region of 10^{13}Hz.

Equations 4:14 and 4:17 show

$$\mu_x = e\Delta r/\eta^2$$

and $$d\mu_x/dQ = e\ /\ \eta^2\ \mu^{\frac{1}{2}}$$

where Q = normal co-ordinate

μ = reduced mass

The integrated absorption intensity in Equation 4:13 is, therefore given

by

$$I = N\pi e^2 / 3c\, \eta^4 \mu \qquad \text{EQUATION 4:18}$$

If the observed differences in intensity of the interionic vibration with solvent result from a change in the extinction coefficient per system in different solvents on account of polarization effects then Equation 4:18 predicts that the integrated absorption intensity should vary with $1/\eta^4$ of the solvent.

It has been shown in Section 4:3:1 that no observable change in the bandwidth of the absorption was detectable in different solvents, the integrated absorption intensity is, therefore, proportional to the extinction coefficient at a given frequency and Equation 4:18 therefore predicts:

$\varepsilon \propto 1/\eta^4$

This may be tested experimentally by measuring the extinction coefficients of a single salt at the same frequency and in the same concentration range in a series of solvents and comparing the values of the extinction coefficient to $1/\eta^4$. This was performed for the sodium salt in a series of solvents.

The experimental procedures for measuring the extinction coefficients has been outlined in Section 4:2:4 when it was noted that the experimental error rose appreciably if the absorbance being measured fell below 0.1 or rose above 1.0. The experimental absorbances are, therefore, kept in this range by varying the path length and concentration of the absorbing solution. Unfortunately, attenuation caused by the solvent limits the maximum path length of tetrahydrofuran that can be used to 0.5 mm, consequently, although the dioxane, piperidine and pyridine measurements can be made in the same concentration range, 5×10^{-3} to 2.5×10^{-2} molar, the THF measurements had to be made in a concentration range of an order of magnitude greater. The value of the extinction coefficient in THF,

therefore, is of slightly less value in the comparison between extinction coefficients and refractive index although the effect is likely to be small, see Section 4:3:3:3.

A tentative value for the extinction coefficient in piperidine is shown. Extreme difficulty was encountered in measurements with piperidine due to precipitation of colourless crystals occurring about one hour after preparing the solution. As each series of measurements of extinction coefficients normally occupied about eight hours, the degree of accuracy obtained with the other solvents was not possible in the case of piperidine.

The results of the measurements of extinction coefficients and the values of $1/\eta^4$ (134) for the solvents are compared in Table 4:4.

TABLE 4:4

Solvent	Pyridine	THF	Piperidine	Dioxane
η	1.51	1.41	1.45	1.42
$1/\eta^4$	0.193	0.253	0.226	0.246
ε	66 $\pm$ 3	30 $\pm$ 2	15 - 22	21.4 $\pm$ 2

The potential influence on the intensities due to the polarizabilities of the solvent molecules, as represented by $1/\eta^4$, is, therefore, small and quite inadequate to account for the very large changes in intensity observed and, in general, the experimental trend is in the opposite direction to that predicted from the polarizability of the solvent molecules. Because the expected differences in the extinction coefficient per ion pair system caused by the polarization of the solvent are so small it is not possible to eliminate on the basis of these experiments the possibility that ion solvent interaction is occurring and this problem will be returned to in Section 4:3:4.

It is necessary, however, to look for an alternative explanation of the wide variation of intensities observed in different solvents and we will turn to the second possible explanation offered above, namely that the proportion of the dissolved ions that are present as ion pairs is dependent on the nature of the solvent.

4:3:3:3 Variation of the proportion of ions present as ion pairs with the dielectric constant of the solvent medium

As has been mentioned in Section 4:1, conductance measurements provide considerable information on the equilibrium established between ion pairs and solvated free ions. This is on account of the fact that the formation of ion pairs reduces the conductivity of the solution under investigation. On the other hand, conductiometric measurements afford no information on the equilibrium established between ion pairs and ion quadrupoles and hexapoles since the formation of these entities does not alter the conductivity of the solution.

The ion pair-ion quadrupole equilibrium has been approached from the thermodynamic standpoint by Pettit and Bruckenstein (109) following the thermodynamic treatment of the free ion-ion pair equilibrium of Dennison and Ramsey (135). The latter considered the free energy of formation of the ion pair in solution in the following cycle:

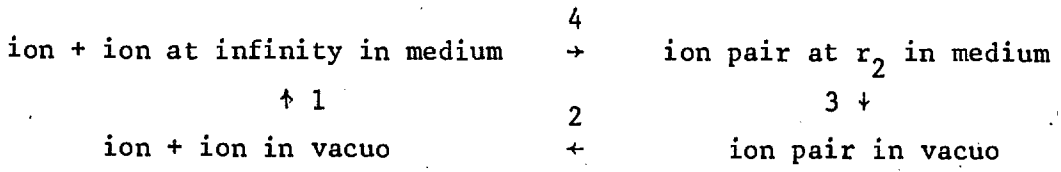

If $\Delta F_1 = -\Delta F_3$, then $\Delta F_4 = -\Delta F_2$

and it may be shown that,

$$\Delta F_4 = N \Delta V_2 / D$$

Where N = Avogadro Number

ΔV_2 = Change in Potential Energy in step 2

D = Dielectric constant

ΔF_4 is related to the Gibbs Free energy, ΔG_4 , by

$$\Delta G_4 = \Delta F_4 - T\Delta S_4$$

and the ion pair association constant, K_2 , is given by

$$\text{Ln } K_2 = N\Delta V_2 / DRT - \Delta S / R \qquad \text{EQUATION 4 : 19}$$

The association constant can, therefore, be calculated providing ΔS_2 and ΔV_2 are known. ΔS may be calculated from the relevant derivative of the partition function and an equation, such as 4:5, may be set up to give ΔV_2. Pettit and Bruckenstein observed that the basic approach of Dennison and Ramsey was equally valid to ion quadrupole and hexapole formation providing that the assumptions regarding solvation energies, $\Delta F_1 = -\Delta F_3$, was still valid.

Association of ions in solution will occur in a stepwise manner as the concentration increases and Pettit and Bruckenstein considered all aggregates up to hexapoles. It will be seen from equation 4:19 that the resultant stepwise association constants will be dependent on the changes in potential energy, ΔV_2, and the entropy, ΔS_2, which occur on the formation of ion aggregates. Calculation of ΔV_2 requires a potential energy function, such as equation 4:5, which is dependent on the equilibrium internuclear separation, r_o, and the calculation of ΔS_2 not only a knowledge of the translational, rotational and vibrational partition functions of the ion pair but also the gas phase entropy of the free ions. Pettit and Bruckenstein performed these calculations for a series of alkali metal halides and derived a set of step-wise association constants for the ionic equilibrium. Neglecting polarizabilities, taking r_o = 4 A and assuming average values for the entropy changes on ion aggregate formation their step-wise association constants may be reduced to

$$\text{Log } \beta_2 = 52.1/D - 3.7 \qquad \text{Log } \beta_3 = 75.1/D - 6.9$$

$$\text{Log } \beta_4 = 121.3/D - 7.5 \qquad \text{Log } \beta_6 = 193.2/D - 12.0$$

Where $\beta = |AB| / |A||B|$ $\quad | \; |$ = Concentrations

For the equilibrium $A + B \rightleftarrows AB$

Using these equations the variation in the proportion of the ions in the various ionic aggregates with dielectric constant and concentration may be evaluated.

A typical set of values from the work of Pettit and Bruckenstein for 10^{-5} and 10^{-3} molar solutions is shown in Figure 4:6.

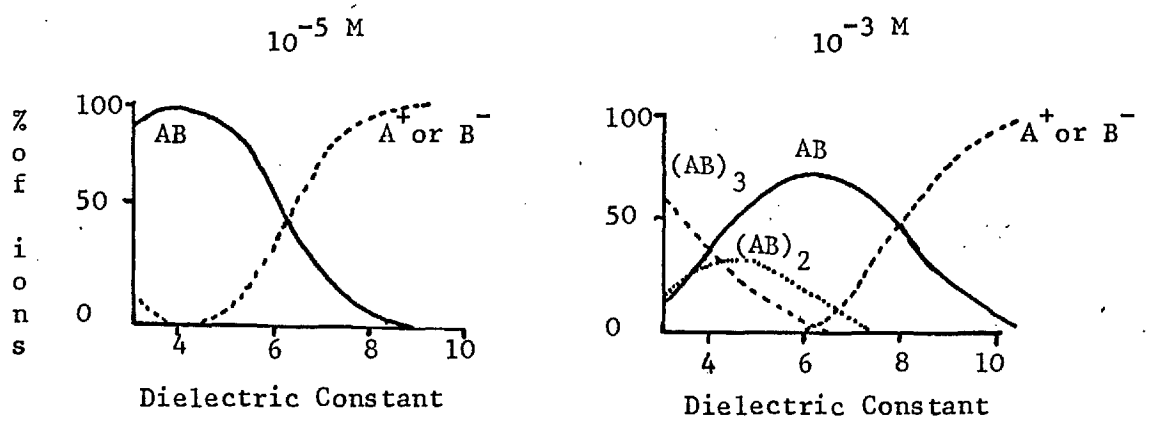

Figure 4:6 Relative Proportions of Associated Species in ionic Solution

Figure 4:7 illustrates diagrammatically the result of varying two of the parameters simultaneously, for example, the dielectric constant of the solvent and the total ion concentration.

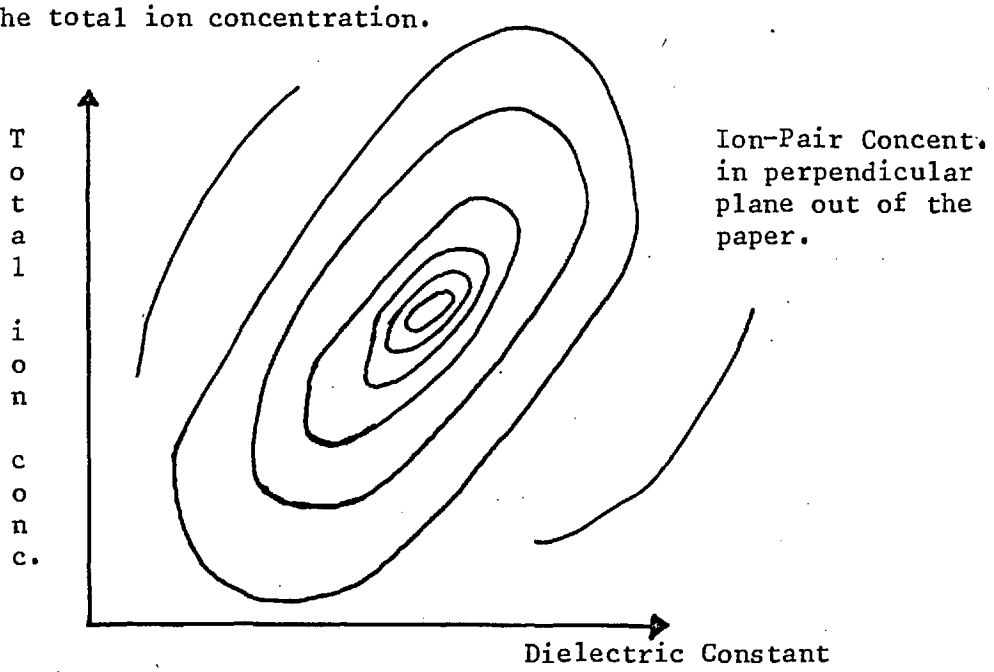

Figure 4:7 Diagramatic Representation of Changes in Ion Pair Concentration

From the outline given of the procedure of Pettit and Bruckenstein it will be seen that the method requires a large number of assumptions to be made before any results can be obtained. It was felt, therefore, that no useful purpose would be served by attempting a similar calculation for the tetraphenylboron salts, particularly as the values of the polarizabilities and gas phase entropies of the free ions were not available in the literature as had been the case for the alkali metal halides. The results of Pettit and Bruckenstein do, however, provide a qualitative picture of the type of equilibria which are established in ionic solutions and the probable variations that may be expected in the proportion of the dissolved ions that are present as ion pairs as the concentration, dielectric constant and the ease of solvation of the cation by the solvent are varied.

Returning to the variation in intensity of the interionic vibration in different solvents, it has been shown in Section 4:3:3:2 that the observed variation in intensity could not be explained on the basis of the polarizability of the solvent. A second possibility was that variation in intensity might reflect, even in solutions of the same molarity, an actual variation in the concentration of ion pairs present with solvent. It was seen in the analysis of Pettit and Bruckenstein that in any solution the ion pairs are in equilibrium with the ion quadrupoles and with free ions and that the positions of the equilibria which govern the ion pair concentration will be altered by changes in the total concentration of the ions, the dielectric constant of the solvent, the temperature of the solution and by the ability of the solvent to solvate the free ions. The variation in the position of the equilibrium with the dielectric constant of the solvent, thus altering the proportion of the dissolved ions that are present as ion pairs, might provide an explanation, therefore, of the observed variation of intensity of the interionic vibration in different solvents.

If the variation of dielectric constant of the solvent is varying the

proportion of dissolved ions that are actually present as ion pairs then two limiting cases may be distinguished:

1) If the distribution of the ions in solution between the various associated species is being dominated by the ion pair-ion quadrupole equilibrium, then:

$$2\ AB \overset{\rightarrow}{\leftarrow} (AB)_2 \qquad \text{and} \qquad \beta_4 = |(AB)_2| / |AB|^2$$

From equation 4:19,

$$\text{Log}\ \beta_4 = N\Delta V_4 / DRT - T\Delta S_4$$

That is, a decrease in dielectric constant would promote the formation of ion quadrupoles at the expense of the ion pairs and lead to a reduction in the proportion of ions that were present as ion pairs. A decrease in dielectric constant of the solvent would lead, therefore, to a decrease in the molar extinction coefficient.

2)If the distribution of the ions in solution is being dominated by the free ion-ion pair equilibrium, then:

$$A + B \overset{\rightarrow}{\leftarrow} AB \qquad \text{and} \qquad \beta_2 = |AB| / |A||B|$$

From equation 4:19

$$\text{Log}\ \beta_2 = N\Delta V_2 / DRT - T\Delta S_2$$

That is, a decrease in dielectric constant will promote the formation of ion pairs at the expense of free ions and lead to an increase in the proportion of the ions that are present as ion pairs. A decrease in dielectric constant of the solvent would lead, therefore, to an increase in the molar extinction coefficient.

If the variation of extinction coefficient for the sodium tetraphenylboron interionic vibration in solvents of different dielectric constant is attributable to the variation in the proportion of the dissolved ions that are present as ion pairs, then the experimental determination of whether the extinction coefficient is increasing or decreasing with increasing dielectric constant will permit us to determine which is the

dominant equilibrium and whether the predominant species in the solvent of highest dielectric constant is ion pairs or free ions.

The experimentally observed values for the extinction coefficient of sodium tetraphenylboron in different solvents have been given in Table 4:4 and these are plotted against the dielectric constant of the solvent in Figure 4:8.

It will be observed that the extinction coefficient is unmistakably increasing with dielectric constant, which is consistent with the variation in dielectric constant affecting predominantly the position of the ion pair-ion quadrupole equilibrium, an increase in dielectric constant promoting the formation of ion pairs at the expense of ion quadrupoles. It would appear, therefore, that in the concentration range 5×10^{-3} to 2.5×10^{-2} molar the proportion of ion pairs present in pyridine is greater than that in solvents of lower dielectric constant and that this would account for the variation in intensity of the inter-ionic vibration in different solvents.

This effect is sufficient to account for the observed variation in extinction coefficient in the different solvents investigated whereas it was shown in Section 4:3:3:2 that the possible variation of extinction coefficient due to the polarization of the solvent was not. It was not possible to test experimentally the suggestion that the variation in intensity resulted from solvent induced changes in the form of the potential function so that neither this nor a possible variation in the extinction coefficient on account of the polarization of the solvent can be eliminated on the basis of the experimental results presented: nevertheless, it is not necessary to postulate their occurrence since the variation in the proportion of the dissolved ions present as ion pairs does provide an adequate explanation of the variations in intensity observed.

The extinction coefficient obtained for dioxane, 21.4 ± 2, appears to be

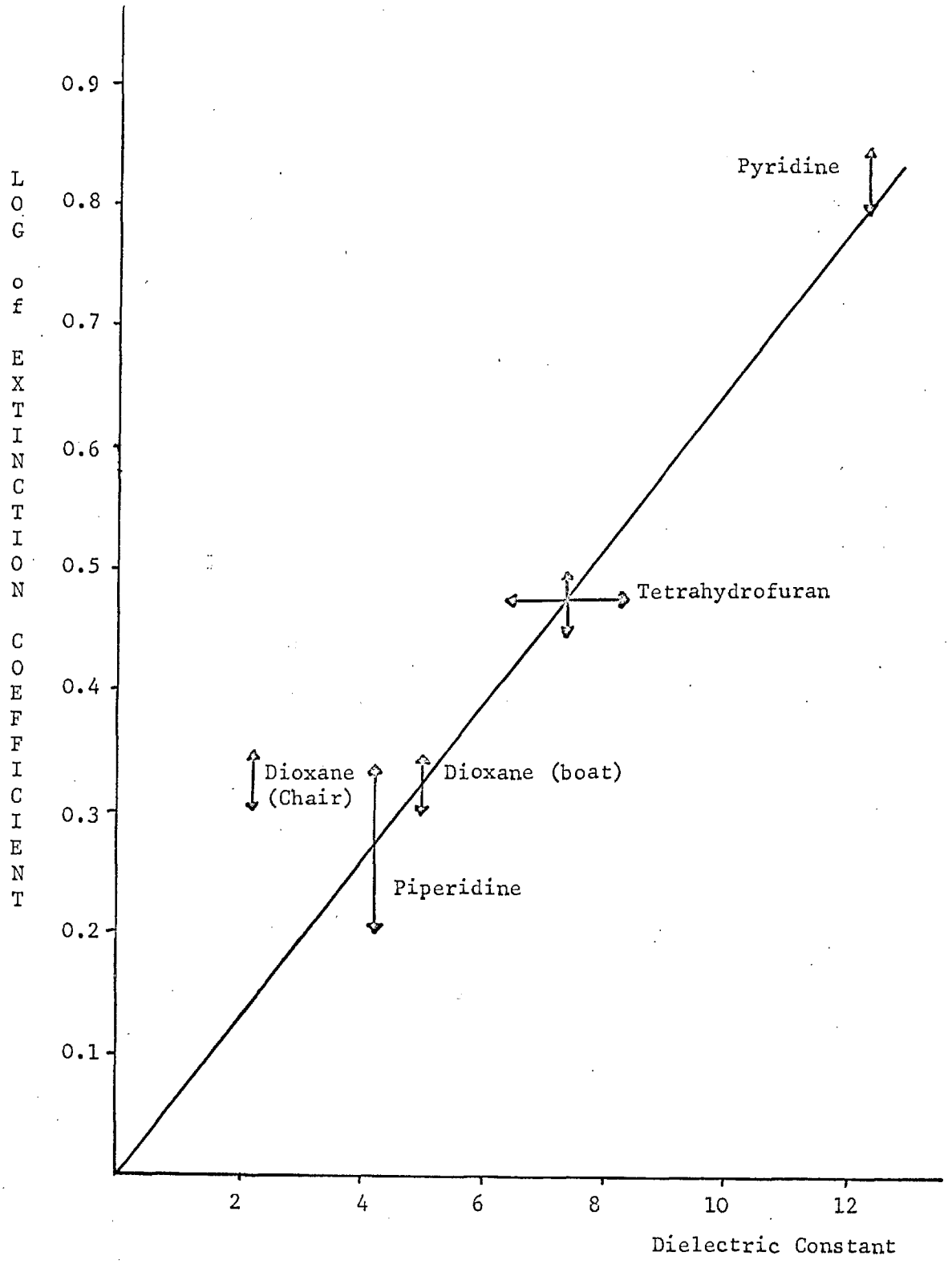

Figure 4:8 Variation of Extinction Coefficient with Dielectric Constant

anomalously high for the bulk dielectric constant of dioxane, 2.24, and the discrepancy, 7 litres.mole^{-1}.cm^{-1} well outside the experimental error. It was thought that this higher value might result from the atmospheric oxidation of the dioxane but extensive purification did not alter the measured extinction coefficient. It is suggested, therefore, that the effective dielectric constant of dioxane in the ion pair-ion quadrupole equilibrium of sodium tetraphenylboron is in the region of 5.0. Support for this is found in the work of Hyne (136) who observed in a study of the association of tetrabutyl ammonium bromide in a series of pure and mixed solvents, a deviation from linearity of the log K_A against 1/D plot for dioxane-water mixtures which was not observed in pure solvents. This was interpreted by Hyne as evidence for the specific solvation of the Bu_4NBr ions by the dioxane. In the pure liquid the dioxane is, from energetic considerations, mainly in the chair form where opposing oxygen dipoles account for the low dielectric constant of the pure liquid, 2.21. On the addition of a salt to the dioxane the solvent assumes the boat configuration due to interaction between the salt and the dioxane molecule. This is illustrated in Figure 4:9:

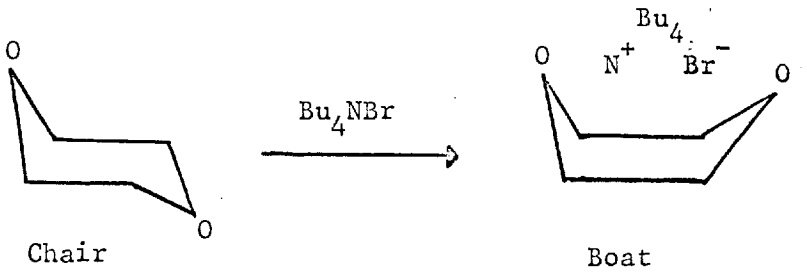

Figure 4:9 Possible Cause of Anomalous Dielectric Constant of 1:4 Dioxane

Although no specific value was given by Hyne for the effective dielectric constant of the boat configuration, a value of about 5 can be deduced from the values of the dissociation constant in different dioxane-water mixtures presented by Fuoss (137). This is in accordance with the value suggested above from the measurements of the extinction coefficient of sodium tetraphenylboron in dioxane. This analysis might be tested by

the measurement of the extinction coefficient in 1:3 dioxane where an analagous increase in effective dielectric constant would not be possible.

4:3:3:4 Variation of the proportion of ions present as ion pairs with the total ion concentration

It was suggested in the previous section that the observed decrease in molar extinction coefficient of the interionic vibration of sodium tetraphenylboron with a decrease in the dielectric constant of the solvent could be interpreted on the basis of the changing position of the ion pair-ion quadrupole equilibrium with dielectric constant of the solvent, although it was not possible to draw any conclusions on the relative proportions of ion pairs and ion quadrupoles present. The measurements of extinction coefficient referred to in the previous section were made over a small concentration range, in order to reduce the experimental error, and no variation in the extinction coefficient was observed in the concentration range normally employed: 5×10^{-3} to 2.5×10^{-2} molar for dioxane, pyridine and piperidine and an order of magnitude greater for tetrahydrofuran. In this limited concentration range, therefore, it appears that the proportions of the dissolved salt that were present as ion pairs in each solvent was constant within the accuracy imposed by the experimental conditions.

In order to obtain some experimental data on the relative proportions of ion pairs and ion quadrupoles present it is necessary to measure the extinction coefficient of a single salt in a single solvent over as wide a concentration range as possible in the hope of detecting a concentration range in which the molar extinction coefficient reaches a maximum denoting the concentration range at which the proportion of the dissolved salt which is actually present as ion pairs reaches a maximum.

The extinction coefficient of ammonium tetraphenylboron was measured at concentrations ranging from 5×10^{-4} molar at 6mm path length to 0.25 molar at 0.2 mm path length. The experimental procedure is described in Section

4:2:4 and the results are summarised in Table 4:5.

Log 1/s(log I_o/I) , where s equals path length, is plotted against log c in Figure 4:10.

TABLE 4:5

$c \times 10^4$	log I_o/I	s	(1/s)(log I_o/I)
5	0.039	6 mm	0.065
10	0.079	6 mm	0.132
20	0.182	6 mm	0.303
50	0.339	6 mm	0.506
20	0.063	2 mm	0.315
50	0.104	2 mm	0.519
100	0.239	2 mm	1.19
166	0.376	2 mm	1.88
250	0.546	2 mm	2.73
500	0.071	0.2 mm	3.54
1000	0.184	0.2 mm	9.19
2500	0.385	0.2 mm	17.24

It will be observed that Figure 4:10 is essentially linear over the concentration range 5×10^{-4} to 2.5×10^{-2} molar but shows a pronounced decrease in 1/s (log I_o/I) above 2.5×10^{-2} molar up to the most concentrated solution investigated 0.25 molar.

The linearity of Figure 4:10 in the concentration range 5×10^{-4} to 2.5×10^{-2} molar shows that the molar extinction coefficient remains unchanged in this concentration range and this implies that the proportion of the dissolved salt that is actually present as ion pairs must also

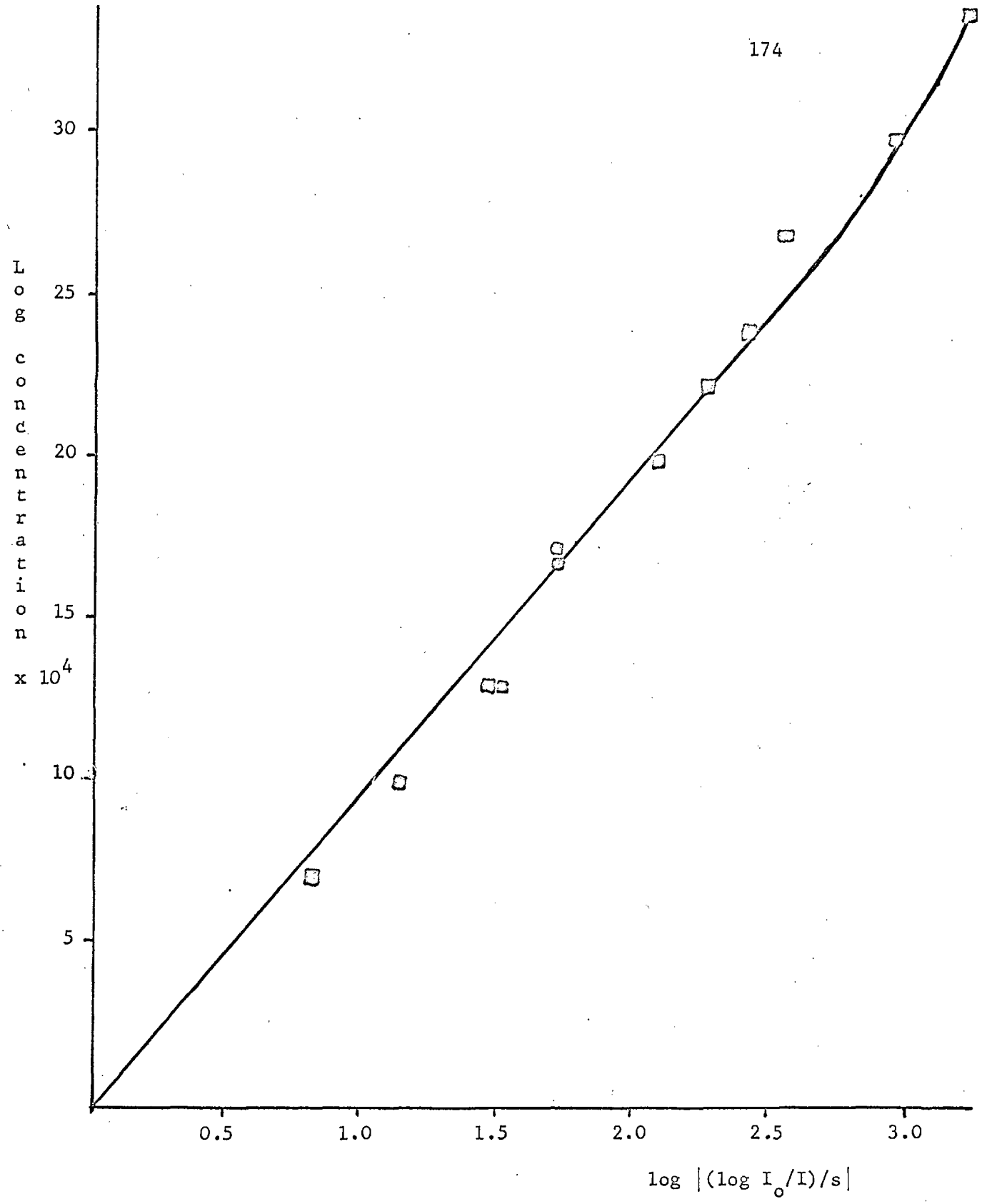

Figure 4:10 Variation of Molar Extinction Coefficient with Total Ion Concentration

remain constant in the concentration range. Reference to Figure 4:7 shows that this only occurs when the proportion of the dissolved salt that is present as ion pairs is at a maximum or a minimum. The possibility that the ion pair concentration might be a minimum may be excluded in the case of pyridine since it has been suggested in the previous section in the discussion of the variation of intensity of the interionic absorption in different solvents that the observed results might be interpreted as showing a smaller proportion of ion pairs in dioxane, piperidine and tetrahydrofuran than in pyridine. If this explanation is correct the proportion in pyridine cannot be a t a minimum. The concentration range, 5×10^{-4} to 2.5×10^{-2} molar represents in pyridine, therefore, the concentration range in which the proportion of dissolved ammonium tetraphenylboron that is actually present as ion pairs is at a maximum.

It will be shown in the following section that the integrated absorption intensity of the sodium salt in pyridine in the concentration range 5×10^{-4} to 2.5×10^{-2} molar is only slightly less than that for the ammonium salt. It may be concluded, therefore, that in these concentration ranges the proportion of sodium tetraphenylboron that is actually present as ion pairs in pyridine is also at, or very close to, a maximum. The results of Section 4:3:3:3 on the variation of the extinction coefficient of the sodium salt with the dielectric constant of the solvent may now be interpreted, therefore, as showing that in pyridine solution the proportion if ions present as ion pairs is at, or very close to, a maximum and that in the other solvents the proportion is less than the maximum on account of the promotion of ion quadrupole formation.

If the proportion of ions present as ion pairs in ammonium tetraphenylboron is a maximum up to 2.5×10^{-2} molar then a decrease in the proportion at some concentration above this figure would be expected on account of the formation of an increasing proportion of ion quadrupoles. It can be seen from Figure 4:10 that a decrease in the molar extinction coefficient

from 120 litres.mole.$^{-1}$cm^{-1} at 2.5 x 10^{-2}M to around 70 litres.mole.$^{-1}$cm^{-1} at 0.25 molar is observed experimentally. As was shown in Section 4:3:3:2 this may either reflect a decrease in the proportion of the dissolved ions that are present as ion pairs or it may represent a decrease in the extinction coefficient per ion pair system on account of the polarizability of the solvent molecules or a solvent induced change in the form of the potential curve. Clearly, a change in the proportion of the dissolved ions present as ion pairs offers a satisfactory explanation of the decrease in molar extinction coefficient with the total ion concentration and is in line with the explanation offered for the observed variations of intensity with dielectric constant of the solvent. Just as was the case with those measurements so with the variation of intensity with the total ion concentration the effect of the polarizability of the solvent and solvent induced changes in the form of the interionic potential appear to be too small to account for the experimentally observed changes and it is necessary to postulate that the actual proportion of ions present as ion pairs is altered. At the same time there is insufficient experimental evidence to positively eliminate polarization and potential function changes as contributory factors to the observed variations of intensity.

Three further experiments, which unfortunately did not prove experimentally feasible, were attempted to support the suggestion that the proportion of ion pairs in pyridine in the concentration range 5 x 10^{-4} to 2.5 x 10^{-3} is at a maximum and that at higher concentrations the proportion decreases due to ion quadrupole formation.

1) If measurements were possible in solvents of higher dielectric constant, and unfortunately no suitable solvent has yet been found, then a lower value for the extinction coefficient than that found in pyridine would be expected. In other words, Figure 4:8 should not be a straight line but should be parabolic returning, in solvents of extremely high dielectric constant, e.g. water, to the X axis.

2) The molar extinction coefficient of the ammonium salt in pyridine should decrease at some point below 5×10^{-4} molar due to the formation of increasing proportions of free ions. The presence of free solvated ions has been observed by Szwarc et al. (118) for sodium tetraphenylboron in tetrahydrofuran, dielectric constant 7.38, in the concentration range 10^{-6} to 10^{-4} molar. Consequently in the higher dielectric constant solvent pyridine, D equals 12.3, it might be expected that the onset of appreciably free ion formation might occur at a molarity in the region of 10^{-3} molar. It did not prove possible to undertake any measurements in pyridine at molarities less than 5×10^{-4} as the absorbance at this concentration even at a 6 mm path length was only 0.04. Increasing the path length above 6 mm did not prove possible due to the absence of a suitable cell and even if one had been available it is doubtful whether useful results could have been obtained due to the very high attenuation of the radiation by the long path length of the solvent.

3) If it is correct to assume that the constant value obtained for the extinction coefficient of the ammonium salt in pyridine in the concentration range 5×10^{-4} to 2.5×10^{-2} molar can be interpreted on the basis that the proportion of dissolved ions present as ion pairs is at a maximum and that the results for dioxane, piperidine and tetrahydrofuran reflect the lower proportion of ion pairs present as a result of the promotion of ion quadrupole formation, then a plot of extinction coefficient against concentration for these solvents, such as that shown for pyridine in Figure 4:10, should show marked non-linearity.

It has already been shown that the experimental technique with piperidine was complicated by the precipitation of colourless crystals after a short period and attempts to measure extinction coefficients over wide concentration ranges were confined to dioxane and tetrahydrofuran. These were frustrated by the low transmission of tetrahydrofuran, limiting the maximum path length usable to 0.5 mm, and the low solubility of the salts in dioxane, saturated solution of the sodium salt was 0.025 molar at room

temperatures. Consequently measurements were only feasible in the concentration range 10^{-2} to 0.5 molar in tetrahydrofuran and 5×10^{-3} to 2.5×10^{-2} molar in dioxane and no changes in the molar extinction coefficient in either solvent were detected in these concentration ranges.

4:3:3:5 Variation of the proportion of ions present as ion pairs with the radius of the cation

It has been suggested in the previous section that in pyridine in the concentration range 5×10^{-4} to 2.5×10^{-2} molar the proportion of dissolved ammonium tetraphenylboron ions which are present as ion pairs is at a maximum. It has been shown that for the same system it would be expected that the molar extinction coefficient would decrease at concentrations above 2.5×10^{-2} molar and below 5×10^{-4} molar due to an increase in proportion of the dissolved salt being present as ion quadrupoles and free ions respectively. It was shown in Section 4:3:3:3 that the variation of absorption intensity with dielectric constant of the solvent for the sodium salt may be interpreted as showing that with this ion, too, the proportion of ions present as ion pairs is at, or very close to, a maximum in pyridine and decreases in solvents of lower dielectric constant due to the more favourable conditions for the formation of ion quadrupoles.

It was also shown in Section 4:3:3:3 that in addition to concentration and dielectric constant of the solvent, two further factors influenced the proportion of dissolved ions that are present as ion pairs, namely temperature and the ability of the solvent to solvate the cation. Unfortunately, measurements were not feasible at temperatures other than ambient with the apparatus available but investigations were undertaken on the effect of the solvability of the cation.

Clearly, the smaller the cation, the more readily it will be solvated by the solvent molecules on account of its higher surface charge density.

The smaller the cation radius, therefore, the more the position of the equilibria will lie in favour of the free ions. The obvious starting point for an investigation of this phenomenon is the fact that in the concentration range 5×10^{-4} to 2.5×10^{-2} molar the proportion of ammonium ions in pyridine which are present as ion pairs appears to be at a maximum. For smaller ions than ammonium the proportion present as ion pairs in pyridine will decrease due to the formation of a greater proportion of free ions and for larger ions than ammonium the proportion present as ion pairs in pyridine will also decrease due to the formation of a greater proportion of ion quadrupoles.

The drawback of this approach has already been foreseen in Section 4:3:2:4. Although there is good evidence that the crystal radii of the alkali metal ions give a fair representation of the bare ion radii it was shown that the crystal radius of ammonium, 1.48A, which makes it isostructural with rubidium, does not appear to correlate with its effective bare ion radius in the interionic vibration. There is no basis, therefore, for a comparison of the effective radii of the alkali metal cations and the ammonium ions. Nevertheless, some qualitative conclusions can be drawn from the experimental molar extinction coefficients for the sodium, ammonium and ammonium-D_4 ions in pyridine.

For different ions the ratio of the molar extinction coefficient does not give the ratio of ion pairs present directly since it was shown in Equation 4:18 that the integrated absorption intensities, and consequently the extinction coefficients if the band widths are constant, are proportional to $1/\mu$, the reciprocal of the reduced mass. The product, $e\mu$ is, therefore, a measure of the relative proportions of different ions present as ion pairs since no differences in the band widths could be detected experimentally (Section 4:3:2:1). The extinction coefficients of the sodium ammonium and ammonium-D_4 salts were measured in pyridine solution in the concentration range 5×10^{-3} to 2.5×10^{-2} molar and at path lengths of 2.00 mm. The results are collected in Table 4:6.

TABLE 4:6

Cation	Na^+	ND_4^+	NH_4^+
Extinction coefficient	66 ± 3	120 ± 5	115 ± 5
Reduced mass	21.45	20.06	17.04
e x μ	1416	2407	1959

Although the extinction coefficients of the ammonium and ammonium-D_4 salts are identical, within experimental error, the more meaningful comparison, the eμ product is not. Of the three explanations offered in Section 4:3:3:1 for variations of intensity, namely a variation of extinction coefficient on account of polarization by the solvent, a variation in the proportion of the dissolved ions present as ion pairs and changes in the form of the potential function, only the last would appear to be available to explain the variation in eμ product of the ammonium and ammonium-D_4 salts. It was seen (Section 4:3:2:1) that the differences in the potential function were insufficient to cause any appreciable change in the interionic vibrational force constant but it is well known that intensities are more sensitive to changes in the form of the potential function than are force constants (122). Further clarification of the problem might result if measurements were made of the two extinction coefficients in a series of solvents.

Despite the difficulty of interpretation of the results for the ammonium and ammonium-D_4 salts the position of these two salts relative to the sodium salt is clear. In the absence of changes in the potential function the proportion of sodium ions that are present as ion pairs appears to be less than the proportion in either ammonium salt, and on the basis of the eμ product of the sodium and ammonium salts it would appear that the

proportion in the sodium salt is about 70% of that in the ammonium salt. This could be interpreted as evidence that the effective radius of the ammonium ion in the interionic vibration is somewhat less than that of sodium ion; the smaller radius of the ammonium ion promoting the formation of ion pairs at the expense of ion quadrupoles.

In order to provide further experimental data the extinction coefficients were measured in tetrahydrofuran in order that a comparison between the sodium, ammonium and lithium salts could be made. (Pyridine is opaque at the absorption frequency of the lithium salt.) A 2.0 mm path length in the concentration range 2.5×10^{-3} to 10^{-1} molar was used and the measured extinction coefficients are collected in Table 4:7.

TABLE 4:7

cation	Li^+	NH_4^+	Na^+
ε	132 ± 10	52 ± 5	30 ± 2
μ	6.79	17.04	21.44
$\varepsilon \times \mu$	896	886	644

The results in tetrahydrofuran confirm those obtained in pyridine, that the proportion of the ions present as ion pairs in the sodium salt appears to be about 70% of the proportion present as ion pairs in the ammonium salt. The figures in tetrahydrofuran provide a comparison between the ability of tetrahydrofuran to solvate the ammonium ion relative to its ability to solvate the lithium ion and it is seen that these measurements suggest that the effective radius of the bare ammonium ion in the interionic vibration occupies a position between the bare sodium ion radius and the bare lithium ion radius.

4:3:4 Ion-Solvent Interaction

4:3:4:1 Introduction

The model proposed, of a contact ion pair immersed in solvent consisting

of polar molecules, suggests the possibility of an interaction arising between the ions and the induced dipoles of the solvent molecules. This possibility has been mentioned on several occasions in the above sections and the evidence as regards its importance will not be collected together for assessment.

1) The constancy of the interionic vibration frequency in different polar solvents, Section 4:3:1, suggests that strong ion solvent interaction cannot be present since the very different nature of the possible solvent donor atoms could not fail to alter the force constant of the interionic interaction and this would manifest itself as a change in the absorption frequency.

2) It was shown in Section 4:3:3:2 that it was not necessary to postulate an ion solvent interaction to account for the variation of the molar extinction coefficient in different solvents.

3) Similarly, it was seen in Section 4:3:3:3 that it was not necessary to postulate an ion solvent interaction to account for the variation of molar extinction coefficient with concentration.

4) The effective ionic charge may be calculated from the integrated absorption intensity as given in Equation 4:18.

$$I = N\pi e^2 / 3\, c\mu$$

The theoretical intensity, assuming that the total dissolved ion concentration is present as ion pairs and that a full electronic charge is present on each nucleus, is, for the ammonium ion

$$\int k\, d\upsilon = 1.71 \times 10^{14}\ cm^{-1} sec^{-1}$$

It has been shown in Section 4:3:3:3 that the molar extinction coefficient for the ammonium ion in pyridine, in the concentration range 5×10^{-4} to 2.5×10^{-2} molar is 115 litres.mole.$^{-1}$cm^{-1} and the experimentally observed bandwidth at half height is 70 cm^{-1}. It is reasonable to consider the ammonium salt since it is believed that the proportion of

ions present as ion pairs is at a maximum for this salt in pyridine in the concentration range considered.

The experimental integrated absorption intensity is

$$\int k\, d\nu = 115 \times 2.303 \times 3 \times 10^{10} \times 70\ cm^{-1}.sec^{-1}$$
$$= 5.5 \times 10^{14}\ cm^{-1}sec^{-1}.$$

It will be noted that the experimental value exceeds the calculated intensity. In addition, the calculated intensity is too high by a factor representing the percentage of the dissolved ions that are present as ion pairs even when this percentage is at a maximum. It appears from Figure 4:3 that this percentage will not exceed 75%. Any further lowering of the calculated absorption intensity by reduction of the effective ionic charge by ion solvent interaction can only make the correlation between the calculated and experimental integrated absorption intensities poorer. Nevertheless, the observed correlation between the calculated and observed absolute intensities is very satisfactory: in view of the complex ion-solvent dipole and ion-induced ion dipole interactions that might be present (138) the fact that the observed and calculated intensities differ only by a factor of four strongly supports the suggestion that the absorption results from an interionic interaction.

4:3:4:2 Selective Solvation

The variation of extinction coefficient with the dielectric constant of the solvent presented a method of determining whether, in mixed solvents, the ion pair was preferentially solvated by one of the species of solvent molecules or whether the extinction coefficient varied linearly with the mole fraction of one of the solvent species as, of course, does the bulk dielectric constant.

The system investigated was 0.025 molar solution of the sodium salt in benzene-pyridine mixtures, the mole percent of benzene varying from 0 to 90%. The extinction coefficient was measured at 164 cm^{-1} in a 2.5 mm

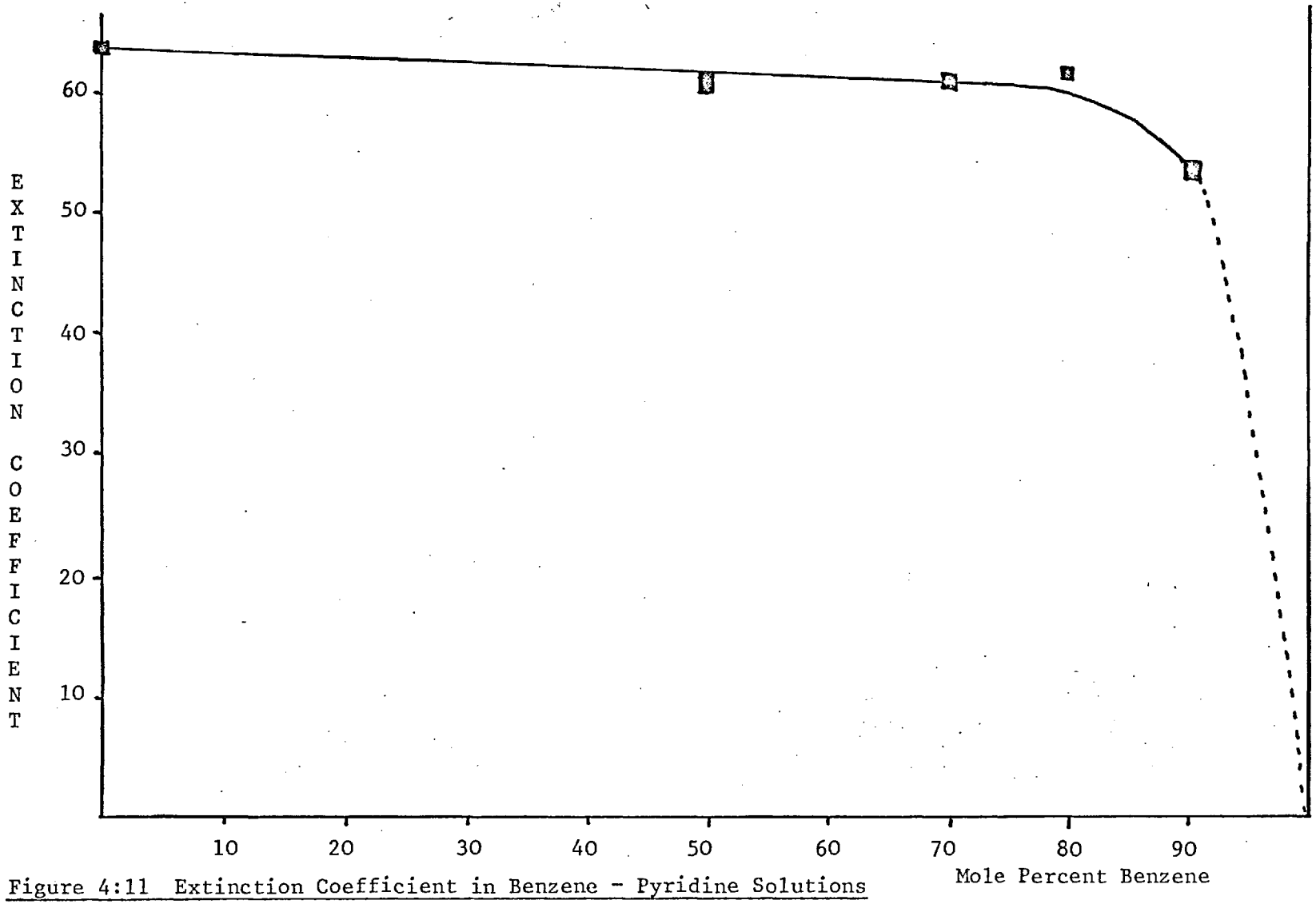

Figure 4:11 Extinction Coefficient in Benzene - Pyridine Solutions

path length cell and the results are shown in Figure 4:11.

This shows that the extinction coefficient is effectively constant at the value for pure pyridine up to 80 mole percent benzene and then decreases rapidly. At 90 percent benzene the ratio of pyridine molecules to sodium tetraphenylboron molecules is only about 40:1 so that this indicates not only that the ionic species is strongly preferentially solvated by the pyridine molecules but also that this preferential solvation continues even to relatively low ion pair to solvent molecule ratios.

It was not possible to complete the graph above 90% benzene on account of the insolubility of the salt in pure benzene.

This observation of selective solvation is in agreement with measurements that have been made conductiometrically and by means of reaction kinetics.(139, 140, 141.)

4:4 CONCLUSIONS

A series of broad absorption bands have been observed in solutions of lithium, sodium, potassium, ammonium and ammonium-D_4 tetraphenylboron salts in a range of polar solvents.

The absorption frequency is not sensitive to the nature of the solvent, pyridine, piperidine, tetrahydrofuran and dioxane were investigated and this is adduced as evidence that the absorption results from an interionic interaction between the dissolved ions in solution.

The observed vibration frequencies of the potassium, sodium, ammonium and ammonium-D_4 salts shows that the force constant for the interionic vibration is almost equal for these four salts and that the value is slightly increased for the lithium salt. A simple two term interionic potential function, which considers only a Coulombic attraction and a single repulsion term predicts a strong dependence of the force constant

on the interionic separation: the observed invariance of the force constant for the potassium, sodium, ammonium and ammonium-D_4 salts and its slightly higher value for the lithium salt is rationalised on the basis of a Morse type potential function. No evidence was found for high anharmonicity in the base of the potential well.

The variation of the molar extinction coefficient with dielectric constant of the solvent of a single salt can be explained on the basis of the ion pair-ion quadrupole equilibrium lying further in favour of quadrupoles in solvents of low dielectric constant. The invariance of the molar extinction coefficient for the ammonium salt in pyridine in the concentration range 5×10^{-4} to 2.5×10^{-2} molar is adduced as evidence that the proportion of the dissolved ions that are actually present as ion pairs is a maximum under these conditions. The decrease in molar extinction coefficient in solutions whose molarities exceed 2.5×10^{-2} molar is then due to the formation of a higher proportion of ion quadrupoles than at lower concentrations. Experimental difficulties prevented any results relating to the ion pair-free ion equilibrium being obtained. The variation of molar extinction coefficient with cation is also explained on the basis of the postion of the equilibrium between ion pair and ion quadrupoles being influenced by the greater ability of the solvent to solvate the smaller cations with higher surface charge density.

No direct evidence was found to indicate the presence of ion solvent interaction and this is believed to be largely absent. In mixed solvents, evidence of preferential solvation by the solvent of higher dielectric constant was observed. No direct evidence was found, either in frequency or intensity measurements, to indicate the magnitude of any differences in the interionic potential function between the various ions studied. It is suggested, however, that the changes are small and it is possible that this might be confirmed by a study of the relative intensities of the interionic absorption in isotopically substituted ions.

These are the first measurements reported of the observation of interionic vibrations in a range of polar solvents and establish, for the first time, the role of the solvent in the interionic interaction. These measurements also provide considerable further information on the interionic potential. Measurements of extinction coefficient variation with dielectric constant of the solvent, concentration of the ions and cationic radius provide the first direct infra-red spectroscopic support for the thermodynamic calculations on the equilibria established in concentrated ionic solutions.

REFERENCES

1. E.D. Palik : A Far Infra-red Bibliography, National Bureau of Standards, Washington, D.C. 1963.
2. G.R. Wilkinson, S.A. Inglis and C. Smart : Spectroscopy p. 157, Institute of Petroleum, London. 1962.
3. J.L. Wood : Quarterly Review 17 362 1963
4. J.W. Brasch, Y. Mikawa and R.J. Jakobsen : To be published.
5. C.C. Helms, H.W. Jones, A.J. Russo and E.H. Siegler : Spectrochim. Acta 19 819 1963
6. Beckman : Technical Brochure on I.R. 11
7. H. Yoshinaga, S. Minami, I. Makino, I. Iwahashi, M. Inaba and K. Matsumoto: Applied Optics 3 1425 1964
8. F.K. Kneubuhl, J-F. Moser and H. Steffen : J. Opt. Soc. Amer. 56 760 1966
9. R.J. Jakobsen and J.W. Brasch : J. Amer. Chem. Soc. 86 3571 1964
10. J.C. Evans and G.Y-S. Lo : J. Phys. Chem. 69 3223 1965
11. W.J. Hurley : J. Chem. Educ. 43 236 1966
12. P.L. Richards : J. Opt. Soc. Amer. 54 1474 1964
13. P. Fellgett : J. Phys. Radium 19 187 1958
14. J.M. Dowling and R.T. Hall : J. Opt. Soc. Amer. 57 269 1967
15. F.K.Kneubuhl, J-F. Moser and H. Steffen : J. Opt. Soc. Amer. 57 271 1967
16. H.A. Gebbie, T. Store and R. Findlay : Nature 202 685 1964
17. M.D. Martin and E.L. Thomas : J. Quantum Electronics 2 196 1966
18. H. Brunet : J. Quantum Electronics 2 382 1966
19. E.K. Plyler, D.J.C. Yates and H.A. Gebbie : J. Opt. Soc. Amer. 52 859 1962
20. L. Genzel and W. Eckhardt : Z. Physik 139 578 1954
21. R. Papoular : Infra Red Physics 4 137 1964
22. R. Cano and M. Mattioli : Infra Red Physics 7 25 1967
23. J. Strong : J. Opt. Soc. Amer. 39 320 1949
24. T.K. McCubbin and W.M. Sinton : J.Opt. Soc. Amer. 42 113 1952
25. W.G. Fastie : J. Opt. Soc. Amer. 42 641 1952

26. M. Czerny and A.F. Turner : Z. Physik 61 792 1930
27. R.J. Bell, S.I. Drasky and W.L. Barnes : Infra Red Physics 7 57 1967
28. K.D. Moller, V.P. Tomaselli, L.R. Skube and B.K. McKenna : J. Opt. Soc. Amer. 55 1233 1965
29. S.W. Russell and H.L. Strauss : Applied Optics 4 1131 1965
30. R.H. Hunt, R.A. Leacock, C.W. Peters and K.T. Hect : J. Chem. Phys. 42 1931 1965
31. L.R. Blaine : J. Research Nat. Bur. Stand. 67c 207 1963
32. N.G. Iaroslavskii, B.A. Zheludov and A.E. Stanevich : Opt. i Spektroskopiya 1 507 1956
33. P.L. Richards : J. Opt. Soc. Amer. 54 1474 1964
34. W. Benesch and J. Strong : J. Opt. Soc. Amer. 41 252 1951
35. P. Taimsalu : Ph.D. Thesis, London, 1963 p. 45
36. H. Cary : Symposium on Molecular Spectroscopy, Ohio 1953
37. A. Savitzky and R.S. Halford : Rev. Sci. Inst 21 203 1950
38. R.A. Oetjen, W.H. Haynie, W.M. Ward, R.L. Hansler, H.E. Schauwecker and E.E. Bell : J. Opt. Soc. Amer. 42 559 1952
39. J.U. White : J. Opt. Soc. Amer. 37 713 1947
40. V.N. Murzin and A.I. Demshina : Opt. and Spectroscopy 13 467 1962
41. F.A. Firestone : Rev. Sci. Inst. 3 186 1932
42. R.J. Bell and S.I. Drasky : Infra Red Physics 5 137 1965
43. A. Mitsuishi, Y. Yamada and H. Yoshinaga : J. Opt. Soc. Amer. 52 14 1962
44. W. Sinton and W.C. Davis : J. Opt. Soc. Amer. 44 503 1954
45. A.F. Turner, L. Chang and T.P. Martin : Applied Optics 4 927 1965
46. E.F. Nichols : Phys. Rev. 4 297 1897
47. D.W. Berreman : Rev. Sci. Inst. 37 513 1966
48. Y. Yamada, A. Mitsuishi and H. Yoshinaga : J. Opt. Soc. Amer. 52 17 1962
49. T.R. Manley and D.A. Williams : Spectrochim. Acta 21 737 1965
50. H.E. Bennett and P. Porteous : J. Opt. Soc. Amer. 51 123 1961
51. H. Yoshinaga, S. Fujita, S. Minami, A. Mitsuishi, R.A. Oetjen and Y. Yamada : J. Opt. Soc. Amer. 48 315 1958

52. O.M. Stafsudd : Applied Optics 5 1951 1966
53. A. Hadni : Spectrochim. Acta 19 793 1963
54. K.D. Moller and R.V. McKnight : J. Opt. Soc. Amer. 53 760 1963
55. A. Mitsuishi, Y. Otsuka, S. Fujita and H. Yoshinaga : Japanese J. Applied Physics 2 574 1963
56. K.F. Renk and L.Genzel : Applied Optics 1 643 1962
57. P. Vogel and L. Genzel : Infra Red Physics 4 257 1964
58. G.M. Ressler and K.D. Moller : Applied Optics 6 893 1967
59. R. Ulrich : Infra Red Physics 7 37 1967
60. A. Hadni, J. Claudel, E. Decamps, X. Gerbaux and P. Strimer : Compte Rendu 255 1595 1962
61. G.M. Ressler and K.D. Moller : Applied Optics 5 877 1966
62. A. Hadni and E. Decamps : Compte Rendu 250 1827 1960
63. W. Wettling and L. Genzel : Infra Red Physics 4 253 1964
64. P.L. Richards : Pure and Applied Chem. 11 535 1965
65. D.H. Martin and D. Bloor : Cryogenics 1 159 1961
66. D. Bloor, T.J. Dean, G.O. Jones, D.H. Martin, P.A. Mawer and C.H. Perry : Proc. Royal Soc. A260 510 1961
67. W.S. Boyle and K.F. Rogers : J. Opt. Soc. Amer. 49 66 1959
68. F.J. Low : J. Opt. Soc. Amer. 51 1300 1961
69. R.A. Smith : Applied Optics 4 636 1965
70. R.G. Wheeler and J.C. Hill : J. Opt. Soc. Amer. 56 657 1966
71. W.J. Moore and H. Shenker : J. Applied Physics 35 2965 1965
72. H. Shenker, W.J. Moore and E.M. Swiggard : Infra Red Physics 5 99 1965
73. E.H. Putley : Applied Optics 4 649 1965
74. M.J.E. Golay : Rev Sci. Inst. 18 357 1947
75. M.J.E. Golay : Rev. Sci. Inst. 20 816 1949
76. A.E. Martin : Infra Red Instrumentation and Techniques : Elsevier, Amsterdam, 1966, p. 22
77. R.F. Potter and W.L. Eisenman : Applied Optics 1 571 1962
78. C.E. Jones, A.R. Hilton, J.B. Damrel and C.C. Helms : Applied Optics 4 683 1965
79. J.L. Wood : Private Communication.

80. J.E. Quarrington : Private Communication

81. M. Born and E. Wolfe : Principles of Optics, Pergamon, New York 1965 p. 188

82. M.P. Freeman and S. Katz : J. Opt. Soc. Amer. 53 1172 1963

83. J. Fischer and D.E. Weimar : Precious Metal Plating, Draper, Teddington, 1964

84. G. Sage and W. Klemperer : J. Chem. Phys. 39 371 1963

85. Reference 35 p. 42

86. K. Radcliffe : Ph.D. Thesis, London, 1966, p. 17

87. Reference 35 p. 49

88. D.E. Williamson : J. Opt. Soc. Amer. 42 712 1952

89. R.G. Greenler : J. Opt. Soc. Amer. 46 433 1956

90. Reference 35 p.52

91. D.M. Adams : Spectrochim. Acta 18 1039 1962

92. D.E. Collins : Rev. Sci. Inst. 36 850 1965

93. M.J.E. Golay : J. Opt.Soc. Amer. 46 422 1956

94. S. Minami, H. Yoshinaga and K. Matsunga : Applied Optics 4 1137 1965

95. D.F. Hornig, G.E. Hyde and W.A. Adcock : J. Opt. Soc. Amer. 40 497 1950

96. G.E.M.L. Campagnaro : Ph.D. Thesis, London 1967

97. K.N. Rao, R.V. deVore and E.K. Plyler : J. Res. N.B.S. 67A 351 1963

98. R.T. Hall, D. Vrabec and J.M. Dowling : Applied Optics 5 1147 1966

99. Reference 86 : p. 12

100. Reference 86 : p. 20

101. L. Genzel, H. Happ and R. Weber : Z. Physik 154 13 1959

102. T.H. Williams : J. Opt. Soc. Amer. 50 1159 1960

103. W.F. Edgell, A.T. Watts, J. Lyford and W.M. Risen : J. Amer. Chem. Soc. 88 1815 1966

104. W.F. Edgell, M.T. Yang and N. Koizumi : J. Amer. Chem. Soc. 87 2563 1965

105. R.A. Robinson and R.H. Stokes : Electrolyte Solutions, Academic Press New York, 1959

106. N. Bjerrum : Kgt. Danske Vidensk. Selsk. 7 9 1926

107. R.M. Fuoss and C.A. Kraus : J. Amer. Chem. Soc. 57 1 1935

108. C.A. Krauss : J. Phys. Chem 60 129 1956

109. L.D. Pettit and S. Bruckenstein : J. Amer. Chem. Soc. 88 4783 1966

110. M. Szwarc : Makromoleculare Chem. 89 44 1965

111. R.M. Fuoss and F. Accascina : Electrolytic Conductance Interscience, New York, 1959

112. W.G. Spitzer and D.A. Kleinman : Phys. Rev 121 1324 1961

113. A. Weissberger and E.S. Proskauer : Technique of Organic Chemistry, Vol. 7, Interscience, New York, 1955

114. F.E. Malherbe and H.J. Bernstein : J. Amer. Chem. Soc. 74 4408 1952

115. W.R. Ward : Spectrochim. Acta 21 1311 1965

116. H.R. Wyss, R.D. Werder and H.H. Gunthard : Spectrochim. Acta 20 576 1964

117. D.A. Crowder and D.W. Scott : U.S. Bureau of Mines, Report of Investigations 6630 1965

118. D.N. Bhattacharyya, C.L. Lee. J. Smid and M. Szwarc : J. Phys. Chem. 69 608 1965

119. E.D. Hughes, C.K. Ingold, S. Patai and Y. Pocker : J. Chem. Soc. 1206 1957

120. D.E.H. Jones and J.L. Wood : J. Chem. Soc. 1448 1966A

121. R.P. Flaum and L.C. Howick : Anal Chem 28 1542 1956

122. B.L. Crawford and H.L. Dinsmore : J. Chem. Phys. 18 983 1950

123. G. Herzberg : Molecular Spectra and Molecular Structure 1, Spectra of Diatomics, Van Nostrand, Princeton, 1950, p. 54

124. R.M. Fuoss and H. Sadek : J. Amer Chem. Soc. 76 5905 1954

125. R.H. Stokes : J. Amer. Chem. Soc. 86 979 1964

126. H.K. Bodenesch and J.B. Ramsey : J. Phys. Chem. 69 543 1965

127. C. Carvajal, K.J. Tolle, J. Smid and M. Szwarc : J. Amer. Chem. Soc. 87 5548 1965

128. R.M. Fuoss and D.S. Berns : J. Amer. Chem. Soc. 82 5585 1960

129. P.M. Morse : Phys. Rev. 34 57 1929

130. Reference 123 : p. 101

131. Reference 123 : p. 92

132. E.B. Wilson, J.C. Decius and P.C. Cross : Molecular Vibrations McGraw - Hill, New York, 1955, p. 165

133. A.L. McClellan : Tables of Experimental Dipole Moments, Freeman, San Francisco, 1963, p.2

134. Handbook of Chemistry and Physics, 46th Edition, The Chemical Rubber Co. Ltd., Cleveland, 1965

135. J.t. Denison and J.B. Ramsey : J. Amer Chem. Soc. 77 2615 1956

136. J.B. Hyne : J. Amer. Chem. Soc. 85 304 1963

137. R.M. Fuoss : Proc. Nat. Acad. Sci. U.S. 41 1033 1957

138. A.D. Buckingham : Disc. Faraday Soc. 24 151 1957

139. H.S. Harned and B.B. Owen : The Physical Chemistry of Electrolyte Solutions, Reinhold, New York, 1958, p.277

140. A.M. Fainberg and S. Winstein : J. Amer. Chem. Soc. 79 1597, 1602 and 1608 1958

141. E.R. Thornton : Solvolysis Mechanisms, Ronald Press, New York, 1964, p. 68